

The mechanism of organic-mediated zeolite crystallization

Citation for published version (APA):

Moor, de, P-PEA. (1998). *The mechanism of organic-mediated zeolite crystallization*. [Phd Thesis 1 (Research TU/e / Graduation TU/e), Chemical Engineering and Chemistry]. Technische Universiteit Eindhoven.
<https://doi.org/10.6100/IR513696>

DOI:

[10.6100/IR513696](https://doi.org/10.6100/IR513696)

Document status and date:

Published: 01/01/1998

Document Version:

Publisher's PDF, also known as Version of Record (includes final page, issue and volume numbers)

Please check the document version of this publication:

- A submitted manuscript is the version of the article upon submission and before peer-review. There can be important differences between the submitted version and the official published version of record. People interested in the research are advised to contact the author for the final version of the publication, or visit the DOI to the publisher's website.
- The final author version and the galley proof are versions of the publication after peer review.
- The final published version features the final layout of the paper including the volume, issue and page numbers.

[Link to publication](#)

General rights

Copyright and moral rights for the publications made accessible in the public portal are retained by the authors and/or other copyright owners and it is a condition of accessing publications that users recognise and abide by the legal requirements associated with these rights.

- Users may download and print one copy of any publication from the public portal for the purpose of private study or research.
- You may not further distribute the material or use it for any profit-making activity or commercial gain
- You may freely distribute the URL identifying the publication in the public portal.

If the publication is distributed under the terms of Article 25fa of the Dutch Copyright Act, indicated by the "Taverne" license above, please follow below link for the End User Agreement:

www.tue.nl/taverne

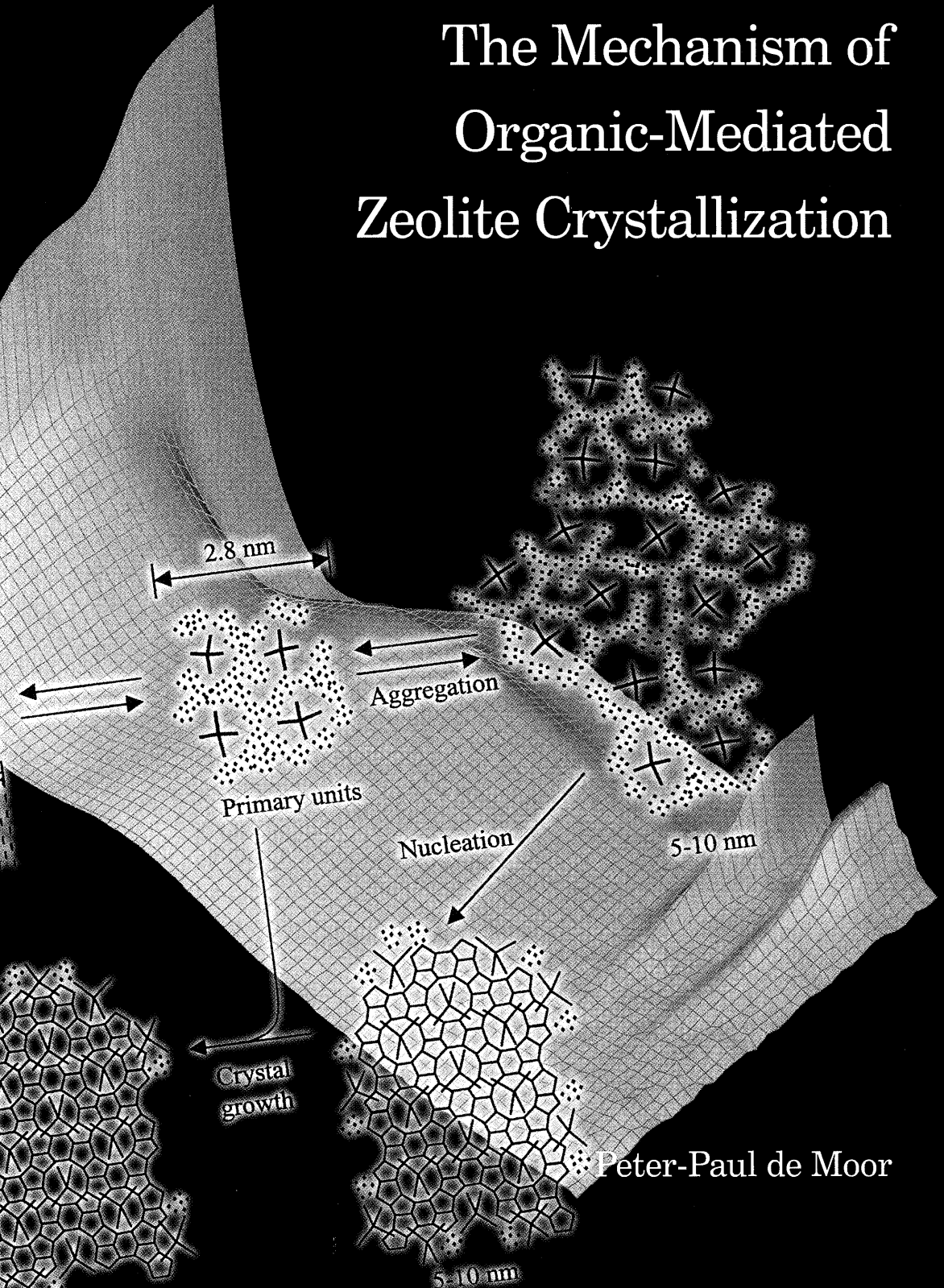
Take down policy

If you believe that this document breaches copyright please contact us at:

openaccess@tue.nl

providing details and we will investigate your claim.

The Mechanism of Organic-Mediated Zeolite Crystallization



Peter-Paul de Moor

The Mechanism of Organic-Mediated Zeolite Crystallization

Proefschrift

ter verkrijging van de graad van doctor aan de
Technische Universiteit Eindhoven, op gezag van de
Rector Magnificus, prof.dr. M. Rem, voor een
commissie aangewezen door het College voor
Promoties in het openbaar te verdedigen
op vrijdag 28 augustus 1998 om 16.00 uur

door

Peter-Paul Eugène Andrea de Moor

geboren te Hulst

Dit proefschrift is goedgekeurd door de promotoren:

prof.dr. R.A. van Santen
en
prof.dr.ir. W.J. Mortier

Copromotor: dr.ir. T.P.M. Beelen

The work described in this thesis has been carried out at the Schuit Institute of Catalysis (part of the Netherlands School for Catalysis Research), Laboratory of Inorganic Chemistry and Catalysis, Eindhoven University of Technology, The Netherlands

Printed at the *Universiteitsdrukkerij*, Eindhoven University of Technology

CIP-DATA LIBRARY TECHNISCHE UNIVERSITEIT EINDHOVEN

Moor, Peter-Paul E.A. de

The mechanism of organic-mediated zeolite crystallization
by Peter-Paul E.A. de Moor.

Eindhoven : Technische Universiteit Eindhoven, 1998.

Proefschrift.

ISBN 90-386-0548-X

NUGI 813

Trefwoorden: zeolieten

Subject headings: zeolites (synthetic) / x-ray scattering / self-assembly

Another problem solved!

*Voor mijn ouders
Aan Fulya*

Contents

1. Zeolites, their synthesis, and the scope of this thesis	1
2. SAXS/WAXS, USAXS and Si-TPA-MFI crystallization	7
3. Influence of aging and dilution on the crystallization of silicalite-1	29
4. Nucleation and crystal growth in Si-TPA-MFI synthesis	41
5. Gelating systems	65
6. The Assembly Process of Organic-Mediated Zeolite Synthesis	79
Summary	91
Samenvatting	95
Publications	99
Acknowledgement	101
Curriculum Vitae	103

Zeolites, their synthesis, and the scope of this thesis

Nature provides us with a broad range of complicated materials with exciting properties, both made by living organisms (e.g. bone and hair) as well as by spontaneous assembly processes (e.g. zeolites). The often very specific properties of these materials make them useful for many applications. However, new applications often require variations of the properties, and therefore a change in the synthesis of the materials is needed. Zeolites are typical examples of such materials. The zeolites found in nature do meet the properties needed for a large variety of applications, but for new processes inspired on existing ones, new (combinations) of characteristics are desired. To be able to assemble materials with the desired properties, one has to understand the rules which nature applies. This thesis deals with the understanding of the formation of zeolites, with coming closer to their rational design as underlying goal.

Zeolites are microporous, crystalline aluminosilicates, where the intracrystalline void spaces are accessible through rings consisting of 8 oxygen atoms or more^{1,2}. These crystalline materials contain three-dimensional frameworks of corner-linked TO_4 tetrahedra, where T is Si or Al. A three-dimensionally connected network without any defects with only silicon tetrahedrally coordinated will be electronically neutral. When a silicon atom is substituted by an aluminum atom, the +3 valence of aluminum will result in a net formal charge of -1, which will be balanced by a cation. The Löwenstein rule³ allows only the formation of zeolites having $\text{Si}/\text{Al} \geq 1$. According to the classification proposed by Liebau and co-workers^{1,2} a pure-silica microporous crystal is not a zeolite, but the term zeolite in the literature is often also used for the all-silica polymorphs and will be used here as such.

The main applications of zeolites are as molecular sieves in separation processes, as adsorbents, as (shape-selective) catalysts, and as ion exchange agents⁴. The vast majority by volume of the zeolites made is used as environmentally friendly replacement of the polyphosphates for ion exchange in detergents. The use of zeolites as catalysts has led to impressive commercial applications in petroleum

refining, petrochemicals and aromatics processing. Venuto⁵ has recently provided an exhaustive review on the catalysis of organic molecules over zeolite catalysts.

The oldest known written report on zeolites is by Axel Fredrick Cronstedt and dates from 1756 (Translated from the original Swedish text to English by Schlenker and Kühl⁶). Early efforts to synthesize zeolites centred around mimicking geological conditions ($T > 200^{\circ}\text{C}$, $p > 100$ bar)²⁰, and can be traced back to 1862⁷. Zeolite technology was initiated in the late 1940's, when large scale hydrothermal syntheses of zeolites using reactive alkali-metal aluminosilicate gels at low temperatures ($\approx 100^{\circ}\text{C}$) and autogeneous pressures were developed. This type of crystallization may involve the structure-directing effects of hydrated alkali-metal cations that organize zeolite structural sub-units and solution-mediated crystallization of the amorphous gel. At the same time Barrer for the first time synthesized a zeolitic material which did not have a natural counterpart⁸. In the early 1960's the use of organic molecules in zeolite synthesis started⁹. The use of ammonium salts led to the synthesis of many new high-silica zeolite types, of which ZSM-5 is the most famous one¹⁰ (recently, approximately 25 years after its first report, a natural counterpart of this zeolite was discovered in Antarctica¹¹). In the 1980's attention was drawn to microporous crystalline aluminophosphates, for which structures with pore sizes larger than for aluminosilicate based materials could be obtained¹². Unfortunately, the practical value of phosphate-based extra-large pore materials is limited by their poor thermal and hydrothermal stability compared to zeolites¹³. In the quest for large pore structures, there have been numerous disclosures of ordered, aluminosilicate mesoporous materials with pore sizes of 20-110 Å^{14,15} in the early 1990's. Because the inorganic portions of the mesoporous materials are not crystalline, they lack the acidity and the (hydro)thermal stability of high-silica zeolites¹⁶. Therefore there is an increasing interest to synthesize crystalline zeolitic materials with large pores. Recently^{17,18} there have been successes on the synthesis of so-called extra-large pore zeolites, which allow access to the intracrystalline voids by apertures of 14 oxygen-containing rings. In general, the continuing commercial successes of zeolite catalysts are largely due to the constant discovery of new materials that enables process improvements and the development of new technologies¹⁹. The control of zeolite properties involves the composition, the crystal morphology as well as molecular level manipulations of structural features, e.g., pore architecture and location of active sites²⁰. Therefore many efforts are being made to obtain understanding on the synthesis of zeolites, ultimately aiming for their design for specific applications.

Although zeolites can be prepared from non-aqueous synthesis mixtures^{21,22,23,24}, the synthesis of most zeolites is performed in an aqueous phase at elevated temperatures, where nucleation and crystal growth occur in a supersaturated solution^{25,26}. Because of experimental problems studying such systems, traditional investigations on the mechanism in the crystallization of zeolites are often based on correlations between the reactants, the process conditions, and the products formed. Some knowledge on the intermediate silicate species was obtained from ²⁹Si-NMR spectroscopy^{27,28}. However, it appeared that the silicate

structures present in solution could not be correlated to the structure of the zeolites formed²⁹.

New, advanced cross-polarization NMR techniques provided information on the non-bonded interaction between organic molecules and silicate species^{30,31}. It is not surprising for such interactions to occur, since the organic molecule acts as an agent which directs the synthesis to a certain crystalline SiO₂ topology and it is present in the voids of the final product. There are strong indications for these interactions to be present in the synthesis mixtures well before the formation of crystalline product. This implies that composite organic-inorganic entities are present in the solution or the gel phase before the formation of long range order. Apart from the organic and the silicate species being close together, no information was revealed on the structure of these entities.

To be able to understand the assembly mechanism of zeolites, information is needed on a nanometer length scale, considerably larger than the ions in solution (order Ångströms). Now a fundamental problem arises since most spectroscopic methods cannot be informative on such length scales. An additional, but very serious experimental problem is the vulnerability of the fragile intermediates in the supersaturated solution. Therefore it is preferable to probe the intermediates *in situ* under synthesis conditions. Furthermore, when studying transformations processes, time-resolved information is necessary.

The purpose of this thesis is to investigate the (trans)formations and the role of nanometer-scale precursors in the crystallization of zeolites with an organic structure-directing cation. To probe these large structures (compared to ions), we used small-angle scattering of X-rays (SAXS). By combining small- and wide-angle scattering (SAXS/WAXS), the (trans)formations of the precursors can be correlated with the presence of crystalline phases. By probing an extended range of length scales (examining X-ray scattering at ultra-small-angles, USAXS), information can be obtained on (very) large structures like gel phases and growing crystals. The use of high-brilliance synchrotron radiation allows us to use short data-acquisition times, and therefore to perform time-resolved experiments.

An introduction in the theory of small-angle X-ray scattering, the combined SAXS/WAXS and Bonse-Hart set-up, and in the interpretation of the data is presented in chapter 2. An extensive description of the Bonse-Hart set-up is outside the scope of this thesis, and is published elsewhere³². By combining the USAXS and SAXS data, information is obtained about growing crystals and aggregation processes. These methods have been applied for the crystallization of all-silica zeolite ZSM-5 (MFI structure) from a clear solution, using tetrapropylammonium (TPA) as template (Si-TPA-MFI). Based on SAXS/WAXS experiments, a provisional crystallization mechanism involving two aggregation steps was proposed previously for this synthesis³³. Our recent results show that no second aggregation step occurs. The first aggregation step (formation of ≈ 10 nm sized precursors) appears to be dependent on the alkalinity of the synthesis mixture.

In many zeolite syntheses, parameters like aging time at room temperature prior to heating, and the concentration of the reactants, have a pronounced influence on the crystallization process, and sometimes even on the zeolite structure formed. These parameters are therefore expected to influence the precursors involved in the crystal nucleation and growth. In chapter 3 we report on the influence of aging and dilution of Si-TPA-MFI synthesis mixtures on the formation of colloidal precursors for the crystallization.

By adapting the small-angle scattering set-up at station 8.2 of Daresbury Laboratory, we were able to obtain information on a continuous range of length scales spanning over four decades (0.17 - 6000 nm). In chapter 4 we demonstrate that for the crystallization of Si-TPA-MFI from a clear solution, two types of precursor particles are present: 2.8 nm sized primary units and aggregates (≈ 10 nm). Variation of the process conditions like the alkalinity of the synthesis mixture, the addition of seed crystals, and the reaction temperature revealed that the formation of aggregates of primary units is essential for zeolite nucleation, and that the primary units are consumed in the crystal growth process.

In the synthesis of zeolites, often a heterogeneous gel phase is formed after mixing of the reagents or when the synthesis mixture is brought to reaction temperature. In order to check the generality of the features observed for organic-mediated zeolite crystallization, the formation of precursors in the synthesis of Si-MFI from a clear solution is compared to gelating systems. Chapter 5 discusses the crystallization of Si-MFI, Si-BEA, and Si-MTW from synthesis mixtures containing bis-piperidinium compounds as structure-directing agents. Besides the presence of large gel structures, again the formation of nanometer sized primary units is observed. The results indicate that the primary units are specific for the zeolite topology formed.

In the concluding chapter a mechanism for the organic-mediated crystallization of zeolites is presented, and appropriate additional scattering experiments on zeolite synthesis mixtures using a broad variety of conditions and template molecules have been carried out to confirm our hypothesis. The proposed nucleation mechanism involves ordering first on the nanometer scale, after which order at larger length-scales is obtained from the order in the primary building units. The primary building units are specific for the crystalline structure formed. The sequential formation of order from small (primary units), to medium (nuclei), to large length-scales (crystals) is consistent with other assembly processes in nature, e.g. the construction of biological entities.

References

- ¹ Liebau, F. *Zeolites* 1983, **3**, 191-193
- ² Liebau, F.; Gies, J.; Gunawardane, R.P.; Marler, B. *Zeolites* 1986, **6**, 373-377
- ³ Löwenstein, W. *Am. Mineral.* 1954, **39**, 92-96
- ⁴ Van Bekkum, H.; Flanigen, E.M.; Jansen, J.C. *Introduction to zeolite science and practice*, Ed. Studies in surface science and catalysis, Elsevier, 1991, **58**
- ⁵ Venuto, P.B. *Microporous Mater.* 1994, **2**, 297-411

- ⁶ Cronstedt, A.F. translated by: Schlenker, J.L.; Kühl, G.H., In: proceedings of the 9th International Zeolite Conference, Montreal 1992, Ed. Von Ballmoos, R.; Higgins, J.B.; Treacy, M.M.J. Butterworth-Heinemann, 1993, pp. 3-9
- ⁷ Sainte-Claire-Deville, M.H. *Compt. Rend.* 1862, **54**, 324-327
- ⁸ Barrer, R.M. *J. Chem. Soc.*, 1948, 127-132
- ⁹ Barrer, R.M.; Denny, P.J. *J. Chem. Soc.* 1961, 971-982
- ¹⁰ Argauer, R.J.; Landolt, G.R. US Patent 3,702,886, 1972
- ¹¹ Galli, E.; Vezzalini, G.; Quartieri, S.; Alberti, A.; Franzini, M. *Zeolites* 1997, **19**, 318-322
- ¹² Davis, M.E.; Saldarriaga, C.; Montes, C.; Garces, J.P.; Crowder, C. *Nature* 1988, **311**, 698-699
- ¹³ Davis, M.E. *Chem. Eur. J.* 1997, **3**, 1745-1750
- ¹⁴ Kresge, C.T.; Leonowicz, M.E.; Roth, W.J.; Vartuli, J.C.; Beck, J.S. *Nature* 1992, **359**, 710-712
- ¹⁵ Tanev, P.T.; Pinnavaia, T.J. *Science* 1995, **267**, 865-867
- ¹⁶ Davis, M.E. *Nature* 1993, **364**, 391-393
- ¹⁷ Freyhardt, C.C.; Tsapatsis, M.; Lobo, R.F.; Balkus Jr, K.J.; Davis, M.E. *Nature* 1996, **331**, 295-298
- ¹⁸ Wagner, P.; Yoshikawa, M.; Lovallo, M.; Tsuji, K.; Taspatsis, M.; Davis, M.E. *Chem. Commun.* 1997, 2179-2180
- ¹⁹ Davis, M.E.; Katz, A.; Ahmad, W.R. *Chem. Mater.* 1996, **8**, 1820-1839
- ²⁰ Davis, M.E.; Lobo, R.F. *Chem. Mater.* 1992, **4**, 756-768
- ²¹ Fan, W.; Li, R.; Ma, J.; Fan, B.; Dou, T.; Cao, J. *Microporous Mater.* 1997, **8**, 131-140
- ²² Deforth, U.; Unger, K.K.; Schüth, F. *Microporous Mater.* 1997, **9**, 287-290
- ²³ Kikuchi, E.; Yamashita, K.; Hiromoto, S.; Ueyama, K.; Matsukata, M. *Microporous Mater.* 1997, **11**, 107-116
- ²⁴ Hari Prasad Rao, P.R.; Ueyama, K.; Matsukata, M. *Applied Catalysis A: General* 1998, **166**, 97-103
- ²⁵ Barrer, R.M.; *Hydrothermal Chemistry of Zeolites*, Academic Press, London, 1982
- ²⁶ Jacobs, P.A. In: Zeolite microporous solids: Synthesis, structure, and reactivity, Ed.: Derouane, E.G.; Lemos, F.; Naccache, C.; Ribeiro, F.R. Kluwer Academic Press, 1992, pp. 3-18
- ²⁷ Bell, A.T. In: Zeolite synthesis, Ed. Ocelli, M.L.; Robson, H.E. ACS Symp. Ser. 398, American Chemical Society, Washington DC, 1989, pp. 66-82
- ²⁸ Knight, C.T.G.; Harris, R.K. *Magn. Res. Chem.* 1986, **24**, 872-874
- ²⁹ Knight, C.T.G. *Zeolites* 1990, **10**, 140-144
- ³⁰ Burkett, S.L.; Davis, M.E. *J. Phys. Chem.* 1994, **98**, 4647-4653
- ³¹ Burkett, S.L.; Davis, M.E. *Chem. Mater.* 1995, **7**, 920-928
- ³² Diat, O.; Bösecke, P.; Lambard, J.; De Moor, P.-P.E.A. *J. Appl. Cryst.* 1997, **30**, 862-866
- ³³ Dokter, W.H.; Van Garderen, H.F.; Beelen, T.P.M.; Van Santen, R.A.; Bras, W. *Angew. Chem. Int. Ed. Engl.* 1995, **34**, 73-75

SAXS/WAXS, USAXS and Si-TPA-MFI crystallization*

An introduction in small-angle scattering and the synthesis of all-silica zeolite ZSM-5 (Si-MFI) from a clear solution will be given in this chapter. The mathematical description of small-angle scattering patterns of real systems often is very complex. The description of the theory and data interpretation given here, is restricted to the features necessary to understand the scattering patterns throughout this thesis. The equipment used at the Synchrotron Radiation Source (Daresbury Laboratory, United Kingdom) and the European Synchrotron Radiation Facility (Grenoble, France), as well as the specially designed sample cell for the in situ experiments will be discussed. The results presented here for the crystallization of all-silica zeolite ZSM-5 with tetrapropylammonium as structure-directing agent (Si-TPA-MFI) from a clear solution, illustrate the methods and the data interpretation. The alkalinity of the synthesis mixtures is a very important process parameter, and has an important influence on the formation of precursors in the crystallization process.

* The results presented here have been published: P.-P.E.A. de Moor, T.P.M. Beelen, B.U. Komanschek, O. Diat, R.A. van Santen, *In situ* investigation of Si-TPA-MFI crystallization using (ultra-) small- and wide-angle X-ray scattering, *J. Phys. Chem. B*, **101** (1997) 11077-11086

2.1 Introduction

The crystallization of zeolites is a self-assembly process in which small entities of molecular scale order to macroscopic crystals. The assembly of the complex crystalline structures of zeolites probably involves ordering first on the nanometer scale, after which order at larger length scales is obtained. Therefore, in the preparation of high-silica zeolites, it is very important to understand the role of the organic structure-directing agents^{1,2,3}. One of the key properties of an organic species is to direct the synthesis towards a certain microporous crystalline structure. In water solutions these organic molecules are hydrated, but the hydration is strongly depending on hydrophobic or hydrophilic properties. Successful structure-directing agents in zeolite synthesis are believed to have a hydrophobic hydration sphere⁴. A dissolved hydrophobic particle seems to increase the local water structure by enhanced hydrogen bonding between the water molecules⁵. Frequently it has been said, that dissolution of hydrophobic compounds in water causes a subtle shift in the water structure around the solute towards a more ice-like state, in which the water molecules possess less rotational and translational freedom than those in bulk water. The release of this 'ordered' water can provide a thermodynamic driving force for the assembly process, when it elicits interactions with hydrophobically hydrated silicates^{6,7}. Therefore, the organic structure-directing agent is believed to play an important role in the assembly process on a molecular scale.

Apart from information on a molecular scale an understanding about processes on larger length scales is indispensable, e.g. for the detection of long range order and to study the formation and transformations of an amorphous gel phase. While the presence of long range order of stable systems can easily be tested by *ex situ* X-ray diffraction, the characterisation of the amorphous gel is more difficult because the length scale to be probed does not allow the use of spectroscopic techniques. Moreover, the structures to be investigated are very fragile and therefore only *in situ* techniques can give reliable results. In this chapter it will be demonstrated that *in situ* time-resolved combined small- and wide-angle X-ray scattering can give valuable information on both the long range order and the formation of amorphous colloidal structures.

For the synthesis of Si-TPA-MFI from a clear solution Dokter *et al.*⁸ found the formation of amorphous colloidal aggregates (size ~7nm) prior to the onset of crystallization. As soon as the first signs of MFI-Bragg reflections appeared in the WAXS pattern, changes in the SAXS pattern showed the formation of particles larger than 50 nm. Since these patterns corresponded with the formation of mass fractal aggregates⁹, a provisional crystallization mechanism was described involving a second aggregation step with the colloidal aggregates as primary particles. In this chapter it will be demonstrated that the formation of colloidal aggregates depends on the alkalinity of the synthesis mixture, and that the crystallization of Si-TPA-MFI is also possible without their clear presence at any stage during the reaction. However, the length scales needed to be probed to obtain information on the proposed second aggregation step⁸ as well as

information about the growing crystals cannot be obtained with the SAXS/WAXS set-up at station 8.2 of Daresbury Laboratory.

To extend *in situ* experiments to length scales between 50 nm and several micrometers, scattering with larger wavelengths can be applied, for example scattering with visible light^{10,11}. A disadvantage of visible light scattering for our system is that it cannot be used for turbid samples and, in the case of an aggregating system, the size of the individual particles cannot be determined. Therefore it can only be used *ex situ* at advanced stages of the crystallization process by diluting the samples and cannot be used for samples in which a heterogeneous gel phase is formed.

An alternative is to exploit scattering of X-rays at much smaller angles with a Bonse-Hart type of camera. The efficiency of this type of camera is low (crystal analyzer, zero-dimension detection which imposes a 2Θ scan), and therefore high-brilliance synchrotron radiation has to be used and only static experiments could be performed due to the long data acquisition times. Recently a Bonse-Hart camera has been developed^{12,13} at the high-brilliance beamline ID2/BL4^{14,15} of the European Synchrotron Radiation Facility (ESRF). The high-brilliance of the beam allows a USAXS pattern to be obtained every 15 minutes, which, to our knowledge, is unique in zeolite investigations.

In this chapter both simultaneous SAXS and WAXS experiments and USAXS experiments on the crystallization of Si-TPA-MFI from clear solutions with synthesis mixtures of different alkalinities will be discussed. By combining these results, information is obtained on a very broad range of scattering angles providing information about the amorphous precursors on a colloidal scale as well as the crystals formed. The presence and role of sub-colloidal precursors (size: few nanometers) will be discussed in later chapters.

2.2 Small-angle X-ray scattering

Small-angle scattering of X-rays is observed when electron density inhomogeneities on a colloidal scale exist in the sample¹⁶. The detected intensity as a function of the scattering angle Θ , described in terms of $Q=(4\cdot\pi/\lambda)\cdot\sin \Theta$, can be written as¹⁷:

$$I(Q) = \phi \cdot P(Q) \cdot S(Q) \quad (1)$$

ϕ is the number density of the particles or the individual scatterers in the sample. The form factor $P(Q)$ describes the relation between the geometry of the individual particles and their scattering. The structure factor $S(Q)$ contains information on the correlation of these particles.

The general mathematical description (using Debye approximation) of the form factor is¹⁸:

$$P(Q) = I_c N_c^2 \frac{\int_0^L g(r) \frac{\sin(Qr)}{Qr} r^2 dr}{\int_0^L g(r) r^2 dr} \quad (2)$$

where I_e = the scattered intensity per electron, N_e = the number of electrons per scatterer and $g(r)$ = the electron density correlation function. Using this formula in principle the form factor for all types of particles can be calculated, though only for a limited set of morphologies an analytical solution has been found¹⁹. The form factor for a homogeneous sphere with electron density ρ and radius R is given by:

$$P(Q) = V^2(\rho - \rho_0)^2 \left[3 \frac{\sin(QR) - QR \cos(QR)}{(QR)^3} \right]^2 \quad (3)$$

Here ρ_0 is the electron density of the medium surrounding the particle and V the volume of the scattering sphere with radius R . If we have a polydisperse system of homogeneous spheres with a particle size distribution $D(r)$ for which $\int_0^\infty D(r)dr = 1$, then the scattered intensity in the case of non-interacting particles is given by²⁰:

$$I(Q) = \phi \int_0^\infty D(r) \cdot P(Q, r) dr \quad (4)$$

Figure 1 shows the calculated intensities for populations of non-interacting particles with different normal number particle size distributions. Upon increasing polydispersity the maxima and minima are less pronounced, and in the $\log I \cdot Q^4$ vs. $\log Q$ plot one observes that their position shifts to smaller angles.

In almost all experiments, the concentration of the scattering entities is such that one has to account for the particle interference²¹, using the structure factor $S(Q)$. The scattering theory relates $S(Q)$ via a Fourier transform with the pair correlation function $g(r)$, describing the chance to find another particle within a distance r from a certain particle^{22,17}:

$$S(Q) = 1 + 4\pi\phi \int_0^\infty |g(r) - 1| r^2 \frac{\sin(Qr)}{Qr} dr \quad (5)$$

In some systems the individual scattering particles form aggregates with mass fractal properties²³. For such structures the pair correlation function can be related to the mass fractal dimension D_f , and substitution in equation (5) and solving the Fourier transformation leads to the following structure factor¹⁷:

$$S(Q) = 1 + \frac{D_f \Gamma(D_f - 1)}{(Qr_0)^{D_f} \left(1 + \frac{1}{Q^2 \xi^2} \right)^{(D_f - 1)/2}} \sin[(D_f - 1) \text{tg}^{-1}(Q\xi)] \quad (6)$$

Here $\Gamma(x)$ is the Gamma-function, r_0 is the size of the individual particles, and ξ corresponds to the size of the aggregate. In regions where this structure factor dominates the scattering intensity behaviour ($r_0 < Q^{-1} < \xi$), one finds $I(Q) \sim Q^{-D_f}$. This mass fractal dimension can give information about the mechanisms controlling the aggregation process and the transformations in the structures formed^{23,24}, and can have values between 1 and 3.

It has been shown^{25,26} that scattering from particles with surface fractal properties results in $I(Q) \sim Q^{-\alpha}$, with $\alpha = 6 - D_s$ (D_s = surface fractal dimension). Because D_s ranges from 2 (smooth) to 3 (extremely rough), α will vary between 3 and 4.

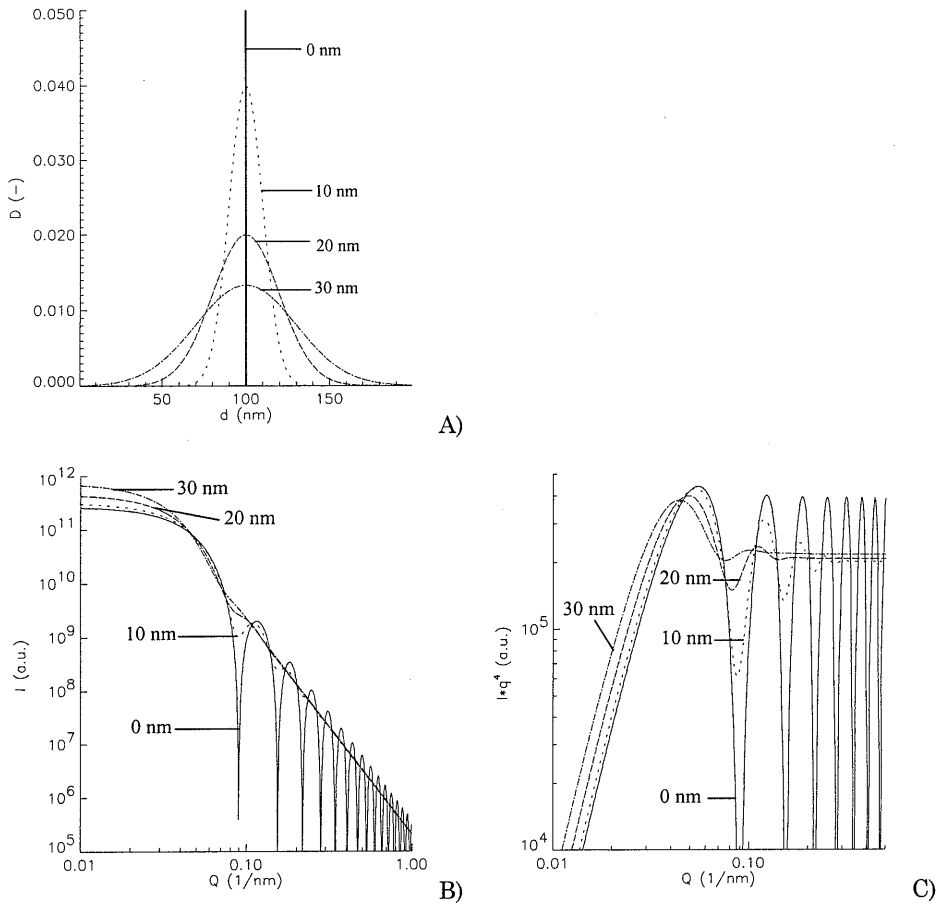


Figure 1: Normal particles size distributions (A) with mean diameter $\mu=100$ nm and standard deviation $\sigma=0, 10, 20$ and 30 nm (annotated at the curves), the corresponding calculated scattering patterns assuming non-interacting particles (B), and a plot of $\log I \cdot Q^4$ vs. $\log Q$ of the same data (C).

The relation between the scattering pattern and the structures responsible for the scattering is shown schematically in figure 2 for a system of aggregates of spherical particles with surface fractal properties. For very large d -spacings (very low Q -values), no density gradients are present in the sample, and homogeneous scattering is observed. At larger Q -values, the scattering at the aggregates is observed. In this region the scattering intensity is determined by the ordering of the small spheres, in other words, the structure factor $S(Q)$. In case of aggregates with a fractal distribution of mass, the slope in the $\log I$ vs. $\log Q$ plot corresponds with the mass fractal dimension. The cross-over between the homogeneous scattering at very low angles and the region where the structure factor dominates the scattered intensity, is a measure for the size of the aggregates. At larger angles, the scattering pattern is determined by the form factor $P(Q)$ of the individual particles. In case of perfectly smooth spheres (dimension of surface is 2), a slope of -4 will be observed in the $\log I$ vs. $\log Q$ plot

(Porod region)¹⁶. When the spheres have a rough surface with fractal properties, the slope in the corresponding region will be between -3 and -4. The cross-over between the regions where respectively $P(Q)$ and $S(Q)$ dominate the behaviour of the scattering intensity, gives the size of the individual particles.

In practical situations one always has to evaluate the influence of the imperfectness of the experimental set-up on the signal measured. In small-angle scattering, three characteristics of the experimental design can give rise to distortion of the scattering curves^{27,28}: the collimating system, the detector system, and wavelength effects. The general influence of all three types of distortions on the signal measured is a smearing effect, in which the maxima and minima become less pronounced and the slope of the curve is changed. This problem was already known in the 1950's as well as the solution for the case of an infinite slit (Guinier, p111-120). Many papers have been published on proposed correction methods (overviews given by Schmidt²⁹ and Lambard *et al.*³⁰). Early methods used the differentiation of the measured signal, introducing relatively large errors. In this work, an iterative method which does not need differentiation³¹ is used.

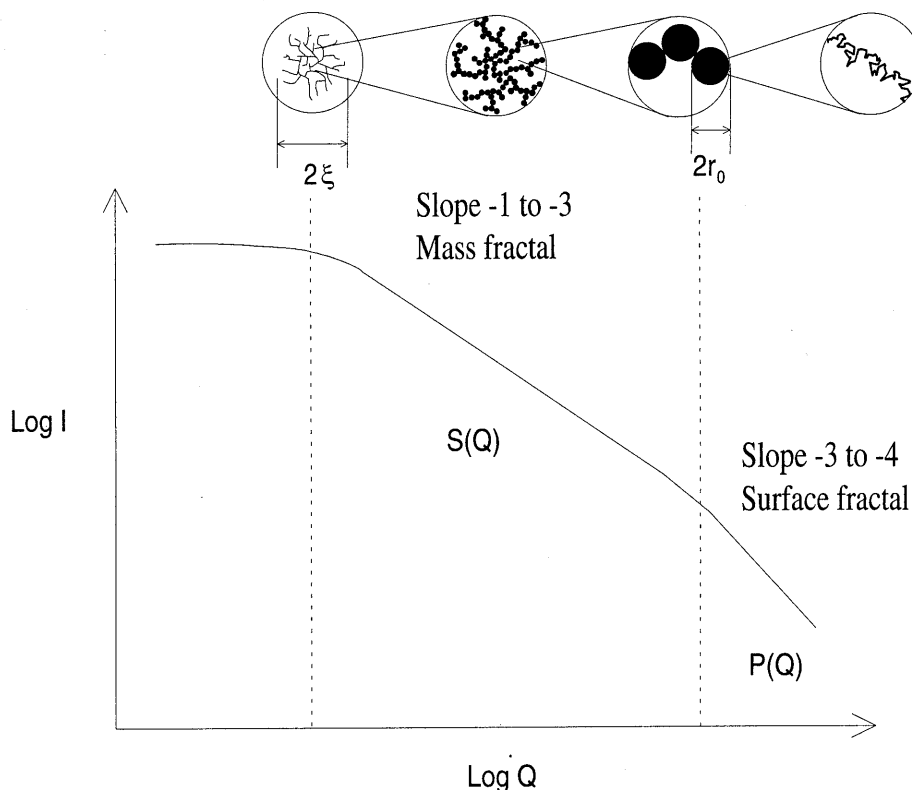


Figure 2: Schematic representation of an aggregate of size ξ with mass fractal properties which is built of primary particles of size r_0 with surface fractal properties. Also schematically the matching small-angle X-ray scattering pattern is shown.

2.3 Experimental

Si-TPA-MFI synthesis

The recipe used is based on a patent of Exxon Chemical³². Synthesis mixtures with a chemical composition $x \text{ Na}_2\text{O} / 1.22 (\text{TPA})_2\text{O} / 10 \text{ SiO}_2 / 117 \text{ H}_2\text{O}$, where $x=0.434$ ($\text{Si}/\text{OH}=3.02$) or $x=0.848$ ($\text{Si}/\text{OH}=2.42$) have been prepared as follows.

1.40 g (for $\text{Si}/\text{OH}=3.02$) or 2.74 g (for $\text{Si}/\text{OH}=2.42$) NaOH (Merck, p.a.) was dissolved in 100g tetra-propylammonium hydroxide (Merck, 20 wt% TPAOH in H_2O) with gentle mixing at room temperature, followed by spoonwise addition of 27.0 g silicic acid powder (Baker, 10.2 wt% H_2O). Thereafter the homogeneous dispersion was boiled under stirring for approximately 10 minutes to obtain a clear solution. The solution was cooled down to room temperature in a water bath, corrected for loss of water during boiling, and filtered through a paper filter (Schleicher and Schüll, Schwarzband). The reaction mixtures were completely clear and aged for less than 1 hour at room temperature before heating to a reaction temperature of 125°C.

Sample cell

To perform *in situ* experiments, an electrically heated brass holder containing a rotating round sample cell (Figure 3) was designed. Rotation was necessary to keep the synthesis mixture homogeneous since only a small spot near the centre of the cell is exposed to the X-ray beam. A rate of approximately 2 revolutions per minute appeared to be fast enough to prevent silicalite crystals from precipitating prematurely.

Two clear mica sheets (Attwater and Sons) were used as windows, with spacing provided by a teflon ring (thickness 0.5 mm). The liquid sample could be heated hydrothermally up to 175°C and contact between the sample and the brass cell was avoided at any moment during the sample preparation or the synthesis. Heating of the sample holder from room temperature to a reaction temperature of 125°C took only 2 minutes. This rotating cell was used for both the combined SAXS/WAXS and the USAXS investigation.

SAXS/WAXS

The time-resolved simultaneous SAXS and WAXS experiments were performed at station 8.2 of the Synchrotron Radiation Source (Daresbury Laboratory, Warrington, U.K.). A schematic representation of the set-up used is given in figure 4. The length of the vacuum chamber between the sample and the SAXS detector was 3.3 m and the resulting ranges covered with the detectors are reported in table 1. The SAXS data were recorded using a position sensitive multi-wire gas filled quadrant detector. The WAXS patterns were collected using a position sensitive pressurised gas detector (INEL). The wavelength of the

X-rays was 1.54 \AA and $\Delta\lambda/\lambda < 4 \cdot 10^{-3}$. More details concerning the camera geometry, data collection, and detectors are given by Bras *et al.*³³ and Lewis *et al.*³⁴.

The intensity of the scattered X-rays was sufficient to collect a small-angle and wide-angle X-ray scattering pattern with a good signal-to-noise ratio every two minutes. The WAXS patterns were used to determine the crystallization behaviour and to check for other crystalline phases than MFI. The integrated intensity in the range between $2\theta = 22.0^\circ$ and 25.1° , where several strong Bragg-reflections of MFI are located is used as a measure for the crystallinity of the sample under investigation. This way we also take into account possible line broadening due to the formation of relatively small crystallites.

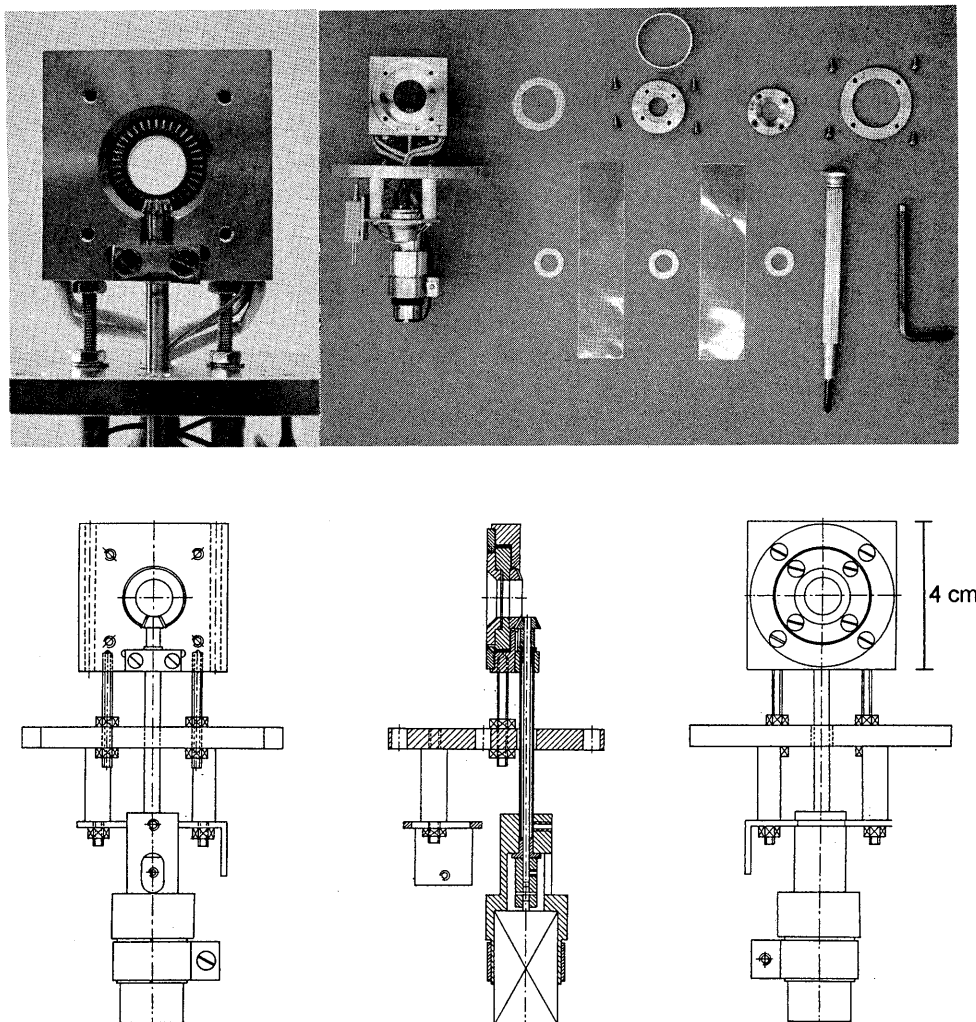


Figure 3: Rotating, electrically heated sample cell used for all scattering experiments. Top left: Close-up on the rotation gear. Top right: All parts of the sample cell. Bottom: Schematic drawing.

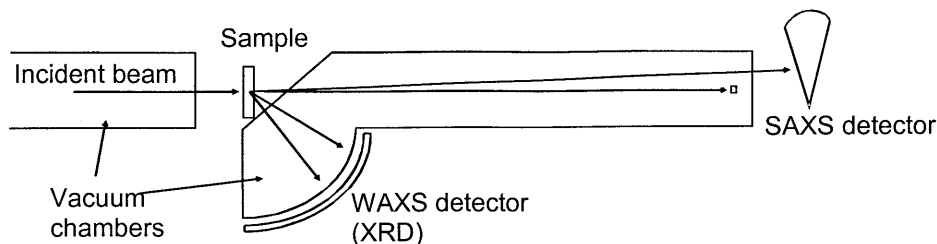


Figure 4: Schematic representation of the combined SAXS and WAXS set-up at station 8.2 of the Synchrotron Radiation Source at Daresbury Laboratory. The distance between the sample and the SAXS detector can be varied between 0.8 and 3.3 m.

To calibrate the SAXS and WAXS detector, the scattering patterns of respectively an oriented specimen of wet rat tail collagen and a sample of fully crystallized zeolite NaA (Procter and Gamble) have been used. The SAXS data were corrected for the detector sensitivity and X-ray beam intensity prior to background subtraction. The scattering signal of water between two mica windows at 125°C was used as background. The WAXS patterns were corrected for the incident beam decay.

USAXS

A Bonse-Hart type of X-ray camera^{12,13} at the high-brilliance small-angle scattering station ID2/BL4 at the European Synchrotron Radiation Facility (ESRF)^{14,15} has been used to record the ultra-small-angle X-ray scattering data (see figure 5). The data reported here have been recorded during two beamtime allocations using different set-ups. The reproducibility of each set-up at different runs is expected to be better than for different set-ups as reported here.

During our first session, only one analyzer crystal (Si (220)) with 3 reflections in the horizontal plane was used. A second analyzer crystal has been omitted to obtain sufficient intensity. Therefore the data of this session had to be corrected for collimation effects (no point-like X-ray beam). For the deconvolution procedure, a program based on the method of Lake³¹ and written by Lesieur³⁰ was used, which iteratively calculates the deconvoluted scattering pattern using a weighting function accounting for the collimation effects. The intensity distribution of the X-ray beam at the sample position is described by a trapezium, of which the large base and small top were determined to be respectively 0.5 and 0.2 mm. The height of the analyzer slit was 1.0 mm and the sample to detector distance was 300 mm.

The set-up for our second session also had an additional second analyzer crystal (Si (111)) with 2 reflections in the vertical direction in order to get a final high resolution detection in the horizontal plane, and resulting in a point-like X-ray beam. Therefore no desmearing of the measured patterns was needed, although lower scattering intensities resulted in a lower Q limit with an acceptable signal to noise ratio. Therefore the upper Q limit was lower compared to the first session (see table 1). As a detector a NaI scintillator or a photo diode were used,

which both showed a linear response over an intensity range of 4 decades. Several scans (4 to 5) over different 2Θ -ranges with sufficient overlap were recorded using different degrees of attenuation of the incident X-ray beam, in order to have intensities on the detector in the linear range. The wavelength of the X-rays used was 0.99 \AA with $\Delta\lambda/\lambda=3\cdot 10^{-4}$.

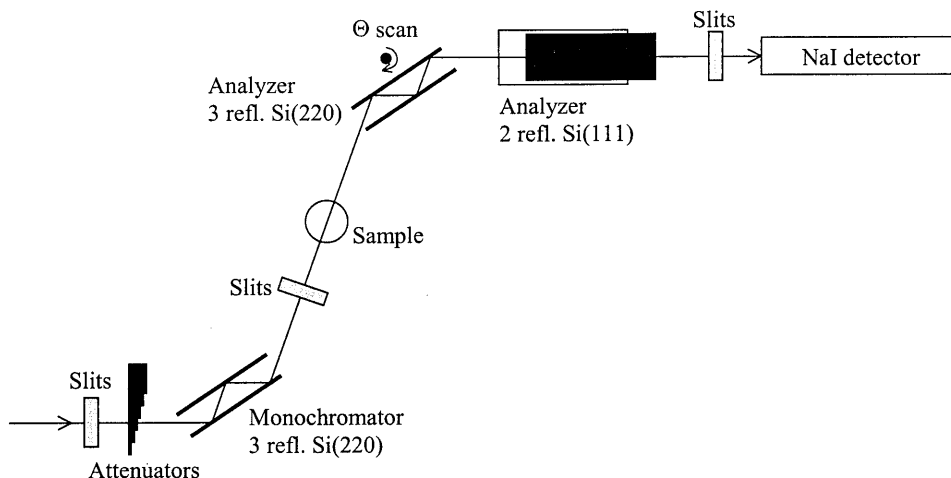


Figure 5: Bonse-Hart set-up at the high-brilliance beamline ID2/BL4 at the European Synchrotron Radiation Facility in Grenoble.

Table 1: Ranges covered in the experiments. The number of crystals for the Bonse-Hart set-up refers to the number of analyzer crystals.

Set-up, detector	2Θ ($^{\circ}$)	Q (nm^{-1})	d (nm)
SAXS, quadrant	0.18 - 3.51	0.13 - 2.5	48 - 2.5
WAXS, curved-INEL	12 - 54	8.5 - 37	0.74 - 0.17
Bonse-Hart, 1 crystals., NaI scint.	$1.4\cdot 10^{-3}$ - 0.45	0.001 - 0.32	6300 - 20
Bonse-Hart, 2 crystals., photo diode	$1.4\cdot 10^{-3}$ - 0.20	0.001 - 0.14	6300 - 45

Data processing and analysis

The basic data correction, the analysis of the time-resolved data, and the interactively fitting of a calculated scattering pattern to measured data have been performed using an in-house developed Graphical User Interface (GUI) based program called *Analyze*, written in the IDL[®] programming language. The program *Analyze* consists of three parts. First a pre-processor is run to read the raw data, to do basic data corrections, and to write the data in *Analyze* format. Second, the analysis of the time resolved data is performed. In the third part, the data can be visualized as a post-process for cases where the output options of analyze do not meet specific wishes.

The pre-processor *pr_otoko* is used to perform basic data corrections for SAXS and WAXS patterns. This includes the correction of the patterns for the detector sensitivity, the intensity of the incident X-ray beam, and the removal of dead channels (optional). The channels of the position sensitive detectors are

correlated to the scattering vector, and the different patterns (frames) are correlated to a physical meaningful parameter, in this case the reaction time. The output of *pr_otoko* is a set of files represented by a header file, containing information about the set.

The main program *Analyze* is written with the objective to have a fast overview of the time resolved data and derive time dependent information. The data can be plotted in various modes (for abscissa: Q , d , 2Θ etc., for ordinate: I , IQ^2 , IQ^4 etc., optional log-scale, 3-dimensional plot, movie showing time frames). From the data, time dependent results like the scattering intensity at a fixed angle, and the evolution of the area of a Bragg reflection can be obtained. All plots can be printed directly to a (network) printer, or to file (several formats are supported, like postscript and computer graphics metafile). Also, the data can be saved to file for post-processing. These output files are in ASCII format, which allows them to be read in almost any program. Extra tools which are part of *Analyze* are *Merge*, and *FitPSD*. *Merge* is a program to join (many) time resolved patterns having overlap in the abscissa. The program *FitPSD* is used to fit the calculated scattering pattern of a polydisperse system of particles to the experimental curve. *FitPSD* includes different types of particles (form factors), and different models for the particle interactions (structure factors). The parameters used in the models can be changed interactively, and the calculated intensity is displayed with the measured pattern. It is written such that it can easily be extended with new models and with multi-modal size-distributions.

The visualization of data often has to meet special specifications for publication. A program is written which reads data sets to the memory straight from the IDL[®] prompt. The data can easily be manipulated and plotted to the screen or to file, using a large variety of standard commands and small programs.

A more detailed description of the program is available from the author of this thesis, and on the internet³⁵.

Electron microscopy

The samples for the electron microscopy (TEM) experiments were also prepared in the synthesis cell used for the SAXS/WAXS and USAXS experiments under the same conditions. After rapid cooling of the cell to room temperature after a certain reaction time, the sample was filtered and washed extensively with de-ionised water over a $0.02\mu\text{m}$ filter (Whatman, Anodisk).

Transmission electron microscopy (TEM) was performed at Delft university using a Philips CM 30 T electron microscope with a LaB_6 filament as the source of electrons operated at 300kV. Samples were mounted on a carbon polymer supported on a copper grid by rubbing the grid against the filter containing the sample, followed by sputtering with carbon to decrease charging in the microscope.

2.4 Results

USAXS data treatment

The scans with the Bonse-Hart set-up, over different intervals of scattering angles, taken with different degrees of attenuation of the incident beam, have been merged to form one pattern. Figure 6 shows the background pattern together with examples of scattering patterns at a short reaction time and at a reaction time when crystals are formed. Before the formation of crystals, or when the concentration of crystals is very low, the signal is just above the background signal, resulting in low signal to noise ratios. When the crystals have been formed, the intensity is a factor 10 or more higher than the background over a large Q range. The scattering patterns obtained with the Bonse-Hart set-up using one analyzer crystal have been desmeared to correct for the slit-like X-ray beam shape and the height of the analyzer slit after background subtraction. It is well known that the desmearing process has a pronounced influence on the slope of the $\log I$ vs. $\log Q$ plot of the scattering patterns (see figure 7). The decrease in the slope ($-3.2 \rightarrow -4$) corresponds with the decrease observed for the slope in the Porod region of a sphere before and after correction if the X-ray source is an infinite slit ($-3 \rightarrow -4$). It also revealed an intensification of the oscillating pattern which corresponds to the form factor of the scattering crystals and there was a slight decrease in the signal to noise ratio.

During our second USAXS session, two analyzer crystals were applied and therefore desmearing of the scattering patterns was not necessary. Figure 8 shows a comparison of the desmeared result of a pattern measured with a set-up with one analyzer crystal, with a corresponding one obtained with two analyzer crystals.

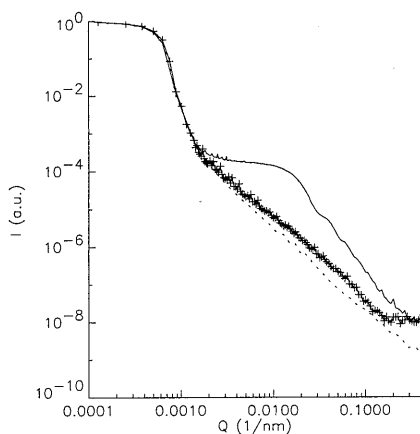


Figure 6: USAXS patterns of the background signal (dotted line), a synthesis mixture before the formation of crystals (plus signs), and after crystallization (solid line). The high intensity at Q -values lower than 0.001 nm^{-1} correspond to the direct beam.

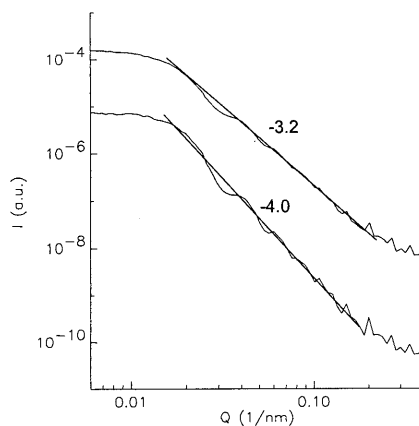


Figure 7: USAXS scattering pattern after crystallization, before (upper curve) and after desmearing (lower curve).

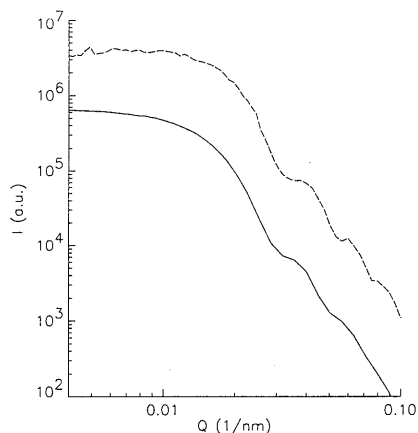


Figure 8: The USAXS pattern obtained with a Bonse-Hart set-up with one analyzer crystal (broken line, time=286 min.), and with a set-up having two analyzer crystals (solid line, time=263 min.) for the synthesis of Si-TPA-MFI with Si/OH=2.42.

SAXS/WAXS

The USAXS-data of our first session had a good overlap in Q -range with our SAXS-data (table 1). Figure 9 shows the merged USAXS and SAXS patterns for synthesis mixtures with Si/OH=3.02 and Si/OH=2.42 after several reaction times, giving information on a very broad Q -range. At relatively short reaction times the signal to noise ratio at low Q values was too low to be plotted.

Figure 10 shows the WAXS patterns for the synthesis with Si/OH=2.42 as a function of time and provides information on the presence of crystalline phases. Bragg reflections appeared when the reaction time exceeds 100 minutes. The detected patterns showed that MFI was formed in all syntheses and that no other crystalline phase was present at any time during the reaction, however, the onset of crystallization depended on the Si/OH-ratio.

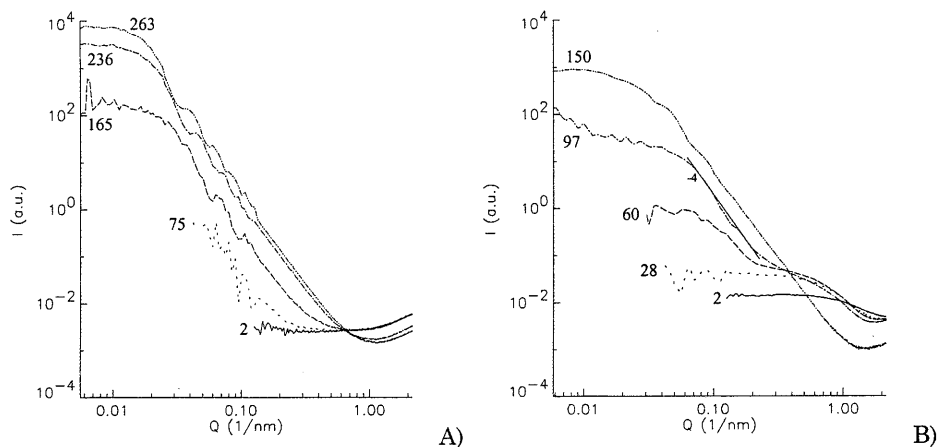


Figure 9: Combined SAXS and USAXS patterns for several reaction times (denoted at the curves in minutes): A) Si/OH=2.42 and B) Si/OH=3.02. The slope of the linear fit is -4.

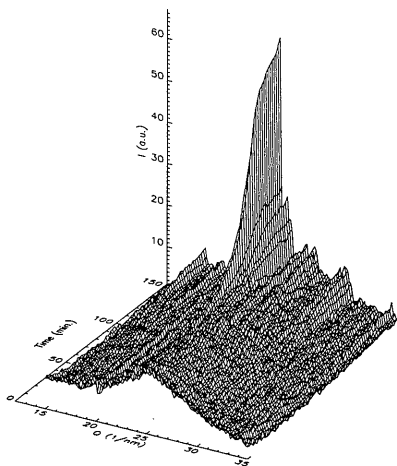


Figure 10: WAXS patterns as a function of time for the crystallization of Si-TPA-MFI from a synthesis mixture having Si/OH=2.42.

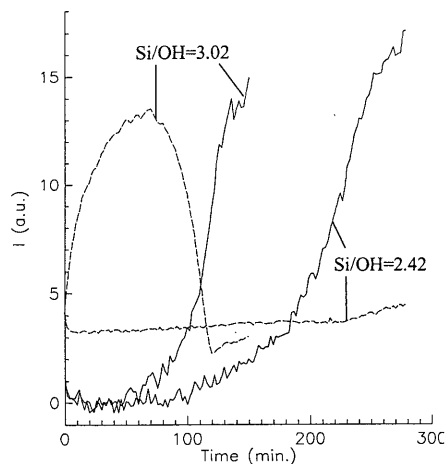


Figure 11: Crystallinity (solid lines) as determined from the WAXS-data as a function of time for both systems, together with the intensity in the SAXS due to scattering at the amorphous colloidal aggregates at $Q=0.6 \text{ nm}^{-1}$ (broken lines).

After ≈ 30 of minutes of heating to reaction temperature, a distinct difference between the scattering curves for the two synthesis mixtures was observed: the scattering of the system with Si/OH=3.02 shows the formation of an increased intensity in the Q range between 0.5 and 1.5 nm^{-1} (see figure 9B), compared to the scattering of the system with Si/OH=2.42 in this range which did not change between 2 and 50 minutes of reaction. The intensity at $Q=0.6 \text{ nm}^{-1}$ as a function of time can be used as a measure for the intensity of this hump, and is compared with the crystallization behaviour in figure 11.

Fitting USAXS patterns

Because the USAXS patterns extend to low Q values, the size of the growing crystals can be determined by fitting calculated patterns corresponding to particles of a certain diameter or particle size distribution to the measured curve (typically for $Q < 0.2 \text{ nm}^{-1}$). Figure 12 compares the results of fitting an observed USAXS pattern with both a population of non-interacting particles with a single diameter and with a population with a particle size distribution. It is clear that the fit to a size distribution is better than the fit with a single diameter. There are still some systematic differences between the calculated and measured profiles for populations with a size distribution. In all cases the intensity of the observed scattering pattern is lower than the calculated one for Q values below the first maximum in the $\log I \cdot Q^4$ vs. $\log Q$ plot.

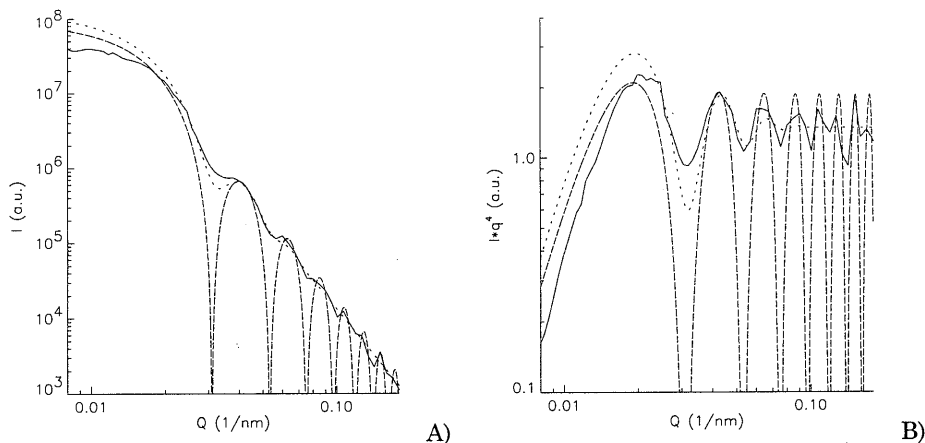


Figure 12: Fitting of the scattering pattern of the system with $\text{Si}/\text{OH}=2.42$ after 263 minutes of reaction (solid line) with the calculated scattering pattern a population of homogeneous spheres with a normal number particle size distribution with an average of 270 nm and a standard deviation of 35 nm (dotted line), and with the pattern corresponding to a single diameter of 290 nm (broken line). Fitting of the $\log I$ vs. $\log Q$ plot (A), and the $\log I \cdot Q^4$ vs. $\log Q$ representation of the same data (B).

The structure factor effects can only be ignored in very diluted systems^{21,36,37}, where the influence of particle interactions on the scattering is negligible. In case of interactions with no tendency to aggregate, a decrease of the observed scattering intensity at angles lower than those corresponding with the size of the scattering entities has to be expected. Due to this influence of the particle interactions on the scattering pattern, it is not correct to determine the average size of the scattering particles from the crossover to the Porod region, nor by the locus of the first maximum in the $\log I \cdot Q^4$ vs. $\log Q$ plot (see figure 12). Therefore, during the fitting procedure the focus was on agreement between the location of the minima and maxima at higher Q values than the first maximum in the $\log I \cdot Q^4$ vs. $\log Q$ plot (e.g. concentrated at $Q > 0.025 \text{ nm}^{-1}$ in figure 12), where the contribution of the structure factor is negligible. Doing so, in almost all fitted patterns it was found that the first two maxima in the $\log I \cdot Q^4$ vs. $\log Q$ plot and the minimum between them are more pronounced in the calculated pattern compared to the observed one, suggesting a lower degree of monodispersity than the one used for the calculation. Contrary, at higher Q values, the form factor oscillations decay faster in the calculated pattern than in the experiment, pointing to a higher degree of monodispersity of the experimental system compared to the one used for the calculation.

Possible explanations for this contradiction are the influence of the structure factor, the imperfection of the desmearing method¹³, and the imperfect spherical shape of the crystals. TEM-images show that the shape of the crystals do not show the typical MFI shape with 90° twinning^{38,39,40}, but the faces are rounded as often seen under conditions favouring fast growth of crystals and in stages that the growth of the crystals is not yet complete. However, we applied the form factor of perfectly spherical particles (equation 3). The use of a model for particles

having a lower degree of symmetry will always lead to less pronounced first maxima and minima in the form factor¹⁹, but for small deviations from spherical particles, the location of the maxima and minima will not be affected much.

The results of the fitted USAXS data are shown in figure 13. The arithmetic mean diameter of the particles determined by the fit is quite accurate since it is deduced from the sharp positions of minima and maxima in the $\log I \cdot Q^4$ vs. $\log Q$ plot, and correspond very well to the average diameter of the crystals as determined from electron microscopy images (figure 13). For both syntheses and both USAXS-sessions, a linear growth of the average crystal size with the reaction time was found: 1.12 and 1.33 nm/min for $\text{Si}/\text{OH}=2.42$, 1.18 and 1.27 nm/min for $\text{Si}/\text{OH}=3.02$. The data concerning the degree of polydispersity of the particle size distribution has to be treated with care, since these results are much more sensitive to the possible distortions of the observed pattern than the average diameter. The ratio of the standard deviation and the average of the particle size distribution, being a measure for the polydispersity, is decreasing continuously during crystal growth (figure 13).

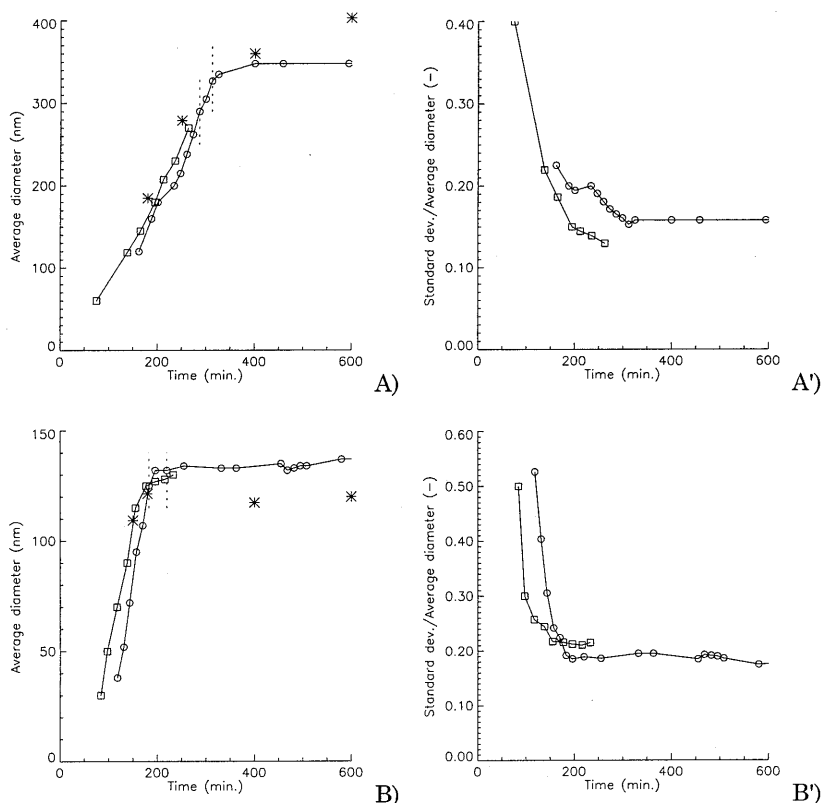


Figure 13: Average diameter and (standard deviation / average diameter) of the particle size distribution of the crystals for syntheses with $\text{Si}/\text{OH}=2.42$ (A) and $\text{Si}/\text{OH}=3.02$ (B). The dotted lines indicate the time ranges in which crystal aggregation was observed. \square : one analyzer crystal, \circ : two analyzer crystals. The asterisks denote the average diameter as determined from electron micrographs.

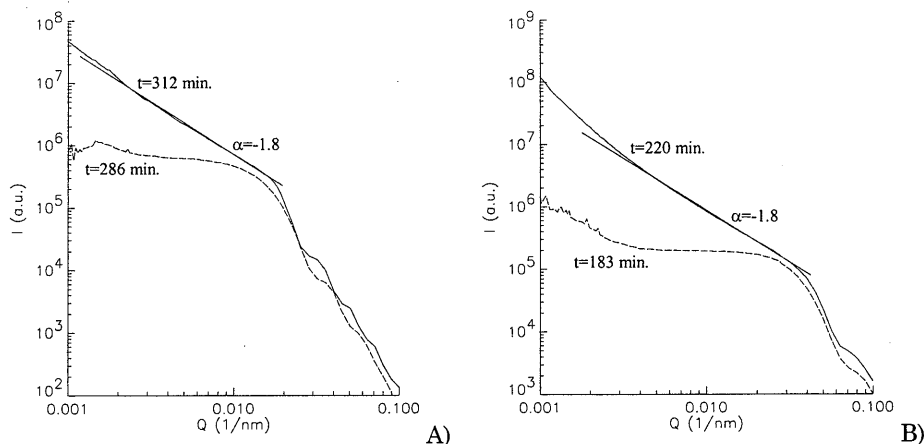


Figure 14: USAXS patterns showing the increase in scattering intensity at very low Q -values due to the aggregation of the crystals for A) $\text{Si}/\text{OH}=2.42$ and B) $\text{Si}/\text{OH}=3.02$. The slopes α correspond to the linear fit with $I(Q) \sim Q^{-\alpha}$.

Crystal aggregation

Using USAXS the crystallization process for long reaction times was studied. After 183 ($\text{Si}/\text{OH}=3.02$) and 286 minutes ($\text{Si}/\text{OH}=2.42$), respectively, a sudden increase in intensity in the low Q region was observed (see figure 14). Again this effect is due to particle interactions, but now resulting in an increase in intensity. This agrees with a model in which the individual scattering entities are aggregated to larger structures. The slope of the linear fit in the low Q region of the log I vs. log Q plot is approximately -1.8 and remains constant in time. For the synthesis with $\text{Si}/\text{OH}=2.42$ using one analyzer crystal, this effect was not observed since no data is available at longer reaction times than 265 minutes.

2.5 Discussion

SAXS/WAXS and USAXS results

The small-angle scattering curves observed after 2 minutes of heating of the synthesis mixtures showed an almost homogeneous scattering over the whole available Q -range. Therefore it is believed that the silicic-acid was completely dissolved to silica-monomers, oligomers, and polymers with a size too small to be observed in the available Q -range.

After several tens of minutes of reaction time, a broad feature in the SAXS pattern appeared at $Q=0.5\text{-}1.5 \text{ nm}^{-1}$ during the synthesis with $\text{Si}/\text{OH}=3.02$, while this hump is absent for the system with $\text{Si}/\text{OH}=2.42$. In an earlier study⁸, this feature was interpreted as being due to scattering from amorphous colloidal aggregates with a size of around 7 nm. Here we find the formation of these colloidal aggregates to be dependent on the alkalinity of the synthesis mixture: at

low alkalinity ($\text{Si}/\text{OH}=3.02$) colloidal aggregates are formed, while they are not observed at high alkalinity ($\text{Si}/\text{OH}=2.42$). The size of the aggregates was estimated to be around 10 nm. At longer reaction times (≥ 60 minutes), the intensity increases at lower angles due to the scattering of colloidal aggregates (Figure 9B, $Q < 0.3 \text{ nm}^{-1}$). Due to the restricted Q -range available, this was first interpreted⁸ as a second aggregation step with the colloidal aggregates present in the solution being the primary particles. Based on the more extended Q -range available using USAXS, we find (figure 9B) that the increasing scattered intensity at Q values lower than 0.3 nm^{-1} is due to the scattering from crystals, showing a Porod slope of -4 in the $\log I$ vs. $\log Q$ plot. Some oscillations are also observed which are due to the form factor of the crystals. We therefore believe now that no second aggregation step of the colloidal aggregates occurs.

For the synthesis with $\text{Si}/\text{OH}=3.02$ there appears to be a correlation between the intensity due to the scattering from the colloidal aggregates and the degree of crystallinity as determined from the WAXS-data (see figure 11). At higher alkalinity ($\text{Si}/\text{OH}=2.42$) we do not observe the presence of colloidal aggregates at any stage during the reaction. This suggests that the size of the particles consumed in the crystallization process is smaller than the minimum size probed by the SAXS, and that the colloidal aggregates are just a kind of storage of amorphous silica in this over-saturated system. In chapter 4 this topic will be discussed again.

Crystal growth

Comparison of the observed growth rate of Si-TPA-MFI ($\sim 1.2 \text{ nm}/\text{min}$) with those reported by Sano *et al.*⁴¹ by *in situ* observation of growing crystals, shows that our results are between the length and width growth rates as determined by extrapolation of their data. From our USAXS data it is not possible to discern between the length and width growth rates, and the electron microscopy images demonstrate that with the shape of our crystals it is hard to define a length and width (see figure 15). When comparing growth rates, one has to keep in mind that these are strongly dependent on factors like the chemical composition of the synthesis mixture, the temperature, aging histories, and agitation or stirring. Therefore, even when taking into account the differences in reaction temperature by an Arrhenius relationship with an activation energy for crystal growth of 50 kJ/mol (approximate average of values reported in literature^{41,10}), faster⁴² as well as slower¹¹ growth rates can be found. In agreement with light scattering results of Persson *et al.*¹¹ we found the growth rate to be about the same for synthesis mixtures of varying alkalinity. Contrary to their results (for $\text{Si}/\text{OH} \geq 2.72$), we found the final size of the crystals to increase with increasing alkalinity (see figures 13 A,B). Fegan and Lowe⁴³ found a decreasing final crystal size for increasing alkalinity, but at very high alkalinities ($\text{Si}/\text{OH} \leq 2$) the final crystal size increased again. This is probably due to a lower amount of viable nuclei forming at very high alkalinities and also due to the absence of a heterogeneous gel phase or colloidal amorphous aggregates which could promote nucleation, as for synthesis mixtures with $\text{Si}/\text{OH}=2.42$.

The USAXS results show that the average size of the growing crystals is approximately the same for reaction times up to 150 minutes. The degree of crystallinity as determined from the WAXS results, being a measure for the volume of crystals in the sample, shows on the same time scale lower crystallinities for the sample with $\text{Si}/\text{OH}=2.42$ compared to $\text{Si}/\text{OH}=3.02$ (see figure 11). These results agree with the presence of a lower number density of crystals in the case of the synthesis with the highest alkalinity.

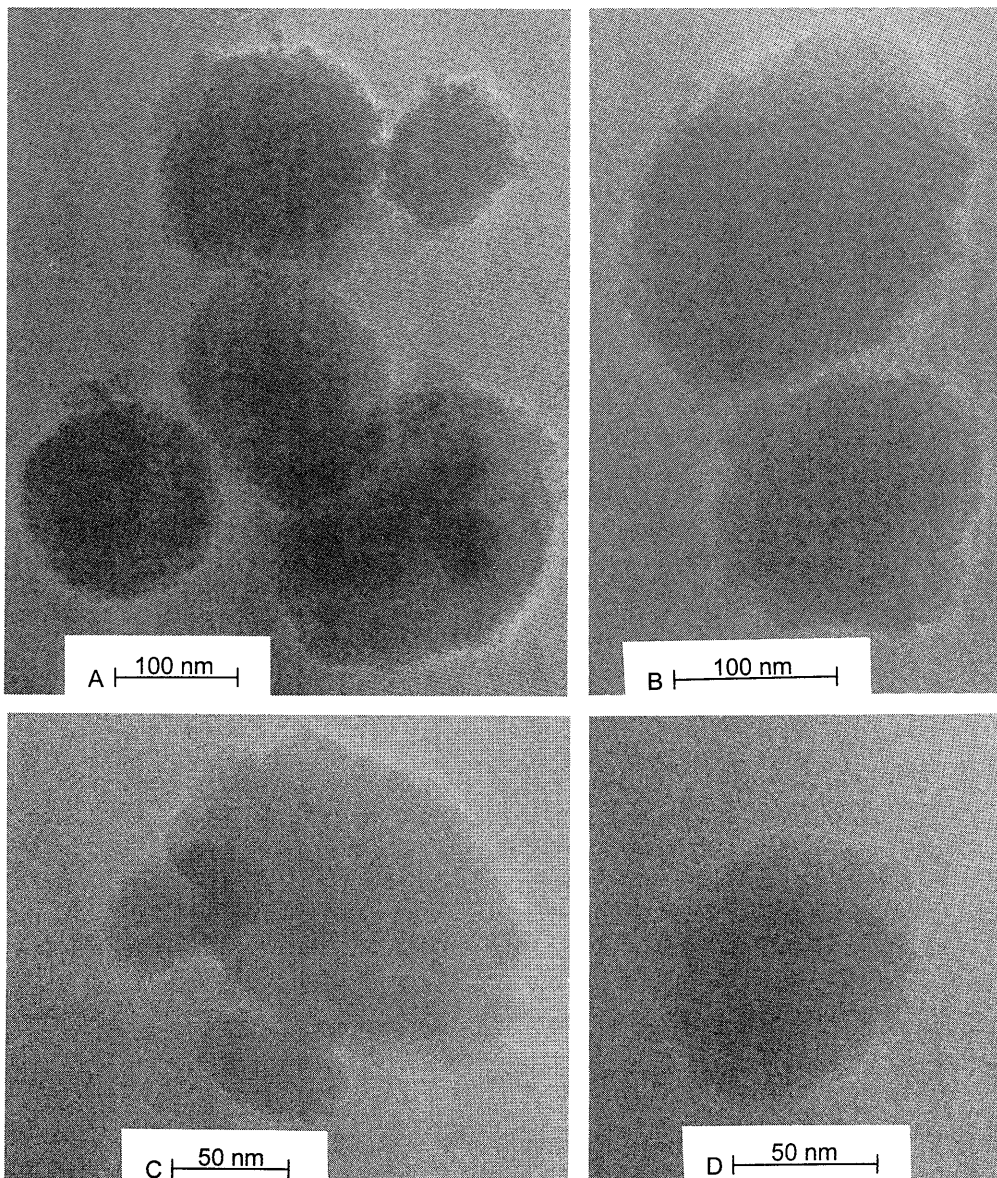


Figure 15: TEM images of crystals: A) and B): $\text{Si}/\text{OH}=2.42$, $t=180$ min., C) and D): $\text{Si}/\text{OH}=3.02$, $t=180$ min.

The electron microscopy pictures confirmed the trend in the average particle size at various crystallization times, and also showed that the population of crystals during and after the growth process is not monodisperse. Schoeman⁴⁴ recently found similar results using cryogenic-TEM and his pictures also showed crystals which are irregularly shaped during the crystallization process.

Crystal aggregation

At reaction times when the linear growth of the crystals has more or less finished (see figure 13 A,B), a sudden increase in scattering intensity is found in the low Q range of the USAXS pattern (see figure 14) for both synthesis mixture compositions. The slope of the straight fit in the $\log I$ vs. $\log Q$ plot agrees with the scattering from mass fractal aggregates which are formed according to a diffusion limited cluster aggregation process (DLCA)^{17,23}. The size of the aggregates can be determined by the transition where the linear fit levels off with decreasing angle. However, the lowest Q angle probed by the USAXS is still too large to be able to determine the size of the aggregates, so they must be larger than 6 μm . This points to a sudden aggregation of the crystals, for $\text{Si}/\text{OH}=2.42$ to occur between a reaction time of 286 and 312 minutes, and for $\text{Si}/\text{OH}=3.02$ between 183 and 220 minutes (no patterns are available between these times). Figure 13 shows that this aggregation step occurs when the linear growth of the crystals had finished. This sudden aggregation process could be related to a change in the composition of the solution. Fegan and Lowe⁴³ pointed out that there can be a sudden change in silicate ion concentration in the solution when the crystallization is in such an advanced stage that all polymeric amorphous silica is consumed. The crystalline phase then controls the silicate ion concentration, and since the solubility of the crystalline phase is far lower than that of the amorphous phase, the silicate ion concentration markedly decreases. For Si/OH -values higher than or equal to 2.0, this effect is accompanied by an increase in the pH. These changes in solution composition might effect the repulsive forces between the individual crystals such that upon a collision of the crystals a high probability of coagulation exists. In this case the aggregation of the crystals will show a crossover from the (slow) reaction-limited type to the (fast) diffusion-limited type, and may result in aggregates having mass fractal properties with a fractal dimension of about -1.8. In the electron microscopy pictures these aggregates were not found (figure 15), which is not surprising taking into account the invasive nature of the sample treatment for electron microscopy and the vulnerability of the aggregates formed according to a diffusion limited cluster aggregation process.

2.6 Conclusions

Our simultaneous SAXS and WAXS results showed that crystal growth of Si-TPA-MFI is possible directly from a clear solution without the presence of an amorphous gel phase during any stage of the crystallization process for a synthesis mixture with $\text{Si}/\text{OH}=2.42$. Colloidal amorphous aggregates were formed in the solution prior to the onset of crystallization for a solution with $\text{Si}/\text{OH}=3.02$.

The USAXS results pointed out that these particles did not show a secondary aggregation step⁸, but are most likely a source of nutrients which will dissolve to subcolloidal particles and/or silicate ions which are consumed in the crystallization process.

Our *in situ* USAXS experiments also showed that the MFI crystals grow linearly with time and that the growth rate is the same for both alkalinities studied. The final crystal size, however, was larger for the higher alkalinity which can be explained in terms of less viable nuclei being formed, resulting in a lower concentration of crystals. Fitting of the USAXS patterns showed that the crystal population was rather polydisperse during the growth stage, which was confirmed by electron micrographs. These micrographs also showed that the growing crystals do not exhibit regular crystal faces, but are more or less spherical with a relatively rough surface.

With the extended Q-range available with the USAXS method we were able to monitor *in situ* the aggregation process of the discrete crystals when the crystal growth approaches completion, which is probably related with the sudden changes in the composition of the liquid phase in this stage.

References

- ¹ Burkett, S.L.; Davis, M.E. *Chem. Mater.* 1995, **7**, 920-928
- ² Burkett, S.L.; Davis, M.E. *Chem. Mater.* 1995, **7**, 1453-1463
- ³ Lobo, R.F.; Zones, S.I.; Davis, M.E. *Journal of Inclusion Phenomena and Molecular Recognition in Chemistry* 1995, **21**, 47-78
- ⁴ Burkett, S.L.; Davis, M.E. *J. Phys. Chem.* 1994, **98**, 4647-4653
- ⁵ Heuvelsland, W.J.M., *Hydrophobic hydration in aqueous solvent mixtures*, thesis, Free University of Amsterdam, 1980
- ⁶ Helmkamp, M.M.; Davis, M.E. *Annu. Rev. Mater. Sci.* 1995, **25**, 161-192
- ⁷ Kubota, Y.; Helmkamp, M.M.; Zones, S.I.; Davis, M.E. *Microporous Mater.* 1996, **6**, 213-229
- ⁸ Dokter, W.H.; Van Garderen, H.F.; Beelen, T.P.M.; Van Santen, R.A.; Bras, W. *Angew. Chem. Int. Ed. Engl.* 1995, **34**, 73-75
- ⁹ Jullien, R.; Botet, R. *Aggregation and fractal aggregates*, World Scientific, 1987
- ¹⁰ Schoeman, B.J.; Sterte, J.; Otterstedt, J.E. *Zeolites* 1994, **14**, 568-575
- ¹¹ Persson, A.E.; Schoeman, B.J.; Sterte, J.; Otterstedt, J.E. *Zeolites* 1994, **14**, 557-567
- ¹² Diat, O.; Bösecke, P.; Ferrero, C.; Freund, A.K.; Lambard, J.; Heintzmann, R. *Nucl. Instrum. Methods Phys. Res. Sect. A* 1995, **356**, 566-572.
- ¹³ Diat, O.; Bösecke, P.; Lambard, J.; de Moor, P.-P.E.A. *J. Appl. Cryst.* 1997, **30**, 862-866
- ¹⁴ Bösecke, P. *Rev. Sci. Instrumen.* 1992, **63**, 438-441
- ¹⁵ Bösecke, P.; Diat, O.; Rasmussen, B. *Rev. Sci. Instrum.* 1995, **66**, 1636-1638
- ¹⁶ Glatter, O.; Kratky, O. *Small Angle X-Ray Scattering*, Academic Press, 1982
- ¹⁷ Teixeira, J. in: Stanley, H.E.; Ostrowsky, N. *On Growth and Form: Fractal and non-fractal Patterns in Physics*, NATO-ASI Series E, **100**, Martinus Nijhoff Publishers, Dordrecht, 1986, 145-162

- ¹⁸ Guinier, A.; Fournet, G. *Small Angle Scattering of X-Rays*, Wiley, New York, Chapman Hall, London, 1955
- ¹⁹ Pedersen, J.S. *Adv. Coll. Interf. Sci.*, 1997, **70**, 171-210
- ²⁰ Mulato, M.; Chambouleyron, I. *J. Appl. Cryst.* 1996, **29**, 29-36
- ²¹ Porod, G. *Monatshefte für Chemie*, 1972, **103**, 395-405
- ²² Schmidt, P.W. In: '*The fractal approach to heterogeneous chemistry*', ed: Avnir, D., John Wiley and Sons Ltd., 1989, 67-79
- ²³ Meakin, P. in: *On growth and form*, NATO ASI ser. E100, Martinus Nijhof, Dordrecht, 1986, pp. 111-135
- ²⁴ Olivi-Tran, N.; Thouy, R.; Jullien, R. *J. Phys. I France* 1996, **6**, 557-574
- ²⁵ Bale, H.D.; Schmidt, P.W. *Physical Review Letters* 1984, **53**, 596-599
- ²⁶ Schmidt, P.W. *J. Appl. Cryst.* 1991, **24**, 414-435
- ²⁷ Ref. 16, pp. 119-125
- ²⁸ Ref. 18, pp. 111-120
- ²⁹ Schmidt, P.W. *J. Appl. Cryst.* 1988, **21**, 602-612
- ³⁰ Lambard, J.; Lesieur, P.; Zemb, T. *J. Phys. I France* 1992, **2**, 1191-1213
- ³¹ Lake, J.A. *Acta Cryst.* 1967, **23**, 191-194
- ³² Verduijn, J.P. *Exxon patent*, , PCT/EP92/02386
- ³³ Bras, W.; Derbyshire, G.E.; Ryan, A.J.; Mant, G.R.; Felton, A.; Lewis, R.A.; Hall, C.J.; Greaves, G.N. *Nucl. Instrum. Methods Phys. Res. Sect. A* 1993, **326**, 587-591.
- ³⁴ Lewis, R.A.; Fore, N.S.; Helsby, W.; Hall, C.; Jones, A.; Parker, B.; Sumner, I.; Worgan, J.S.; Budtz-Jorgensen, C. *Rev. Sci. Instrum.* 1992, **63**, 642-647
- ³⁵ De Moor, P.P.E.A., <http://www.tak.chem.tue.nl/zeolites/peter-paul/research.html>
- ³⁶ Höhr, A.; Neumann, H.B.; Schmidt, P.W.; Pfeifer, P.; Avnir, D. *Phys. Rev. B* 1988, **38**, 1462-1467
- ³⁷ Ref. 16, pp. 38-41 and pp. 189-191
- ³⁸ Cundy, C.S.; Henty, M.S.; Plaisted, R.J. *Zeolites* 1995, **15**, 342-352
- ³⁹ Hay D.G.; Jaeger, H.; Wishier, K.G. *Zeolites* 1990, **10**, 571-576
- ⁴⁰ Jansen, J.C. in: *Introduction to zeolite science and practice*, Ed. Van Bekkum, H.; Flanigen, E.M.; Jansen, J.C. Studies in surface science and catalysis, Elsevier, 1991, **58**, pp. 77-130
- ⁴¹ Sano, T.; Sugawara, S.; Kawakami, Y.; Iwasaki, A.; Hirata, M.; Kudo, I.; Ito, M.; Watanabe, M. In: *Zeolites and Related Microporous Materials: State of the Art 1994*, Studies in Surface Science and Catalysis, Elsevier Science, 1994, **84**, pp. 187-194
- ⁴² Cundy, C.S.; Lowe, B.M.; Sinclair, D.M. *Journal of Crystal Growth* 1990, **100**, 189-202
- ⁴³ Fegan, S.G.; Lowe, B.M. *J. Chem. Soc., Faraday Trans. 1* 1986, **82**, 785-799
- ⁴⁴ Schoeman, B.J. *Zeolites* 1997, **18**, 97-105

Influence of aging and dilution on the crystallization of silicalite-1*

It is well known that parameters as aging of the synthesis mixtures at room temperature prior to heating, and the concentration of the reactants, have an important influence on the crystallization behaviour of zeolites and even on the crystal topology formed. However, knowledge concerning the influence of these parameters on the (trans)formations in the precursors in the synthesis mixtures is very limited. In this chapter we report on the influence of aging and dilution of synthesis mixtures on the formation of colloidal scale precursors and the course of the crystallization.

* Published as: P.-P.E.A. de Moor, T.P.M. Beelen, R.A. van Santen, Influence of aging and dilution on the crystallization of silicalite-1, *J. Appl. Cryst.*, **30** (1997) 675-679

3.1 Introduction

Although a considerable amount of information is available describing numerous synthesis routes of zeolites^{1,2}, mechanisms directing to a given crystalline structure are still poorly understood. Especially the events in the early stages of the synthesis are of critical importance in determining the course of the crystallization³. Even relatively slow processes taking place at room temperature prior to heating to the appropriate crystallization temperature are known to have major influence on the induction period, the crystallization rate, and even the zeolite formed⁴.

A question of considerable debate is the nature of the gel phase and its role in the nucleation and growth mechanisms. Assuming a liquid-phase ion transportation mechanism⁵ nucleation and crystal growth occur only in the liquid phase. The gel phase acts as a source of nutrients for the crystallization process⁶. On the other hand, in the solid hydrogel reconstruction mechanism^{7,8,9} nucleation and crystal growth occur in the heterogeneous gel or at the gel surface by a reconstruction or aging mechanism and can be classified as a solid-solid transformation.

To study (trans)-formation processes in synthesis gels on a colloidal scale, spectroscopic methods like nuclear magnetic resonance and infrared (IR) spectroscopy are not informative. Also, colloidal aggregates and gels are extremely vulnerable, so only *in situ* techniques can provide reliable information. In a previous paper¹⁰ we reported on the crystallization of silicalite-1 from a clear solution, and described a provisional mechanism in which the (trans)-formations on a colloidal scale were correlated with the onset of crystallization. This mechanism includes two aggregation and two densification steps at a colloidal scale. In chapter 2 of this thesis, a more complete set of data and a wider Q-range probed with SAXS persuaded us to a different interpretation of the scattering patterns, involving only one aggregation step. So, although the synthesis mixture keeps its initial, low viscosity and no percolating gel phase is formed at any stage during the reaction, amorphous colloidal aggregates with a size of 10 nm are formed in the clear solution prior to the onset of crystallization.

It is well known that parameters as aging of the synthesis mixtures at room temperature, and the concentration of the reactants have an important influence on the crystallization behaviour of zeolites. Therefore, it is expected that such parameters affect the precursors present in the solution. Here we report on the influence of aging and dilution of synthesis mixtures on the formation of colloidal scale precursors and the course of the crystallization.

3.2 Experimental

The recipe used is based on a patent of Exxon Chemical¹¹. The procedure described and the composition (0.434 Na₂O / 1.22 (TPA)₂O / 10 SiO₂ / 116 H₂O) is the same as used by Dokter *et al.*¹⁰ and we refer to this system as the 'standard system'.

1.40 g NaOH (Merck, p.a.) was dissolved in 100 g tetrapropylammonium hydroxide solution (Merck, 20 w% solution in H₂O) with gentle mixing at room temperature, followed by spoonwise addition of 27.0 g silicic acid powder (Baker, 10.2 w% H₂O). Thereafter the homogeneous dispersion was boiled under stirring for approximately 10 minutes to obtain a clear solution. The solution was cooled down to room temperature in a water bath, corrected for loss of water during boiling, and filtered through a paper filter (Schleicher and Schüll, Schwarzband). At the reaction temperature of 125°C the reaction was completed in 1 to 3 hours. *In situ* SAXS/WAXS experiments were performed on samples with aging times of 0.25, 72, 312, and 624 hours between filtration and heating to reaction temperature. The samples with a SiO₂/H₂O-ratio of 10/292, 10/646, and 10/999 (respectively a 2, 4, and 6 fold dilution) were prepared by adding the appropriate amount of distilled water to a reaction mixture having the standard composition after the filtration.

The sample cell used for all experiments and the X-ray scattering equipment are described in chapter 2.

3.3 Results

SAXS/WAXS and USAXS on the 'standard system'

The SAXS patterns recorded after several reaction stages during the synthesis of silicalite-1 from a reaction mixture having the standard concentration as given in the experimental section, are shown in figure 1A. For a fresh sample and short reaction times (<15 minutes) the scattering intensity is almost constant over the complete Q region measured. After reaction times larger than 20 minutes, an increased intensity at $(-1.15) < \log Q < (-0.8)$ is observed, which is due to the presence of a population of scattering particles with a size of up to 10 nm. A schematic representation of the observed features during the complete course of the synthesis and their interpretation is given in figure 2. The slope of a linear fit in the center of this region is approximately -2.1. These particles are believed to be amorphous aggregates of silica particles, since no indication of any bands is present in the WAXS pattern. At reaction times longer than 40 minutes the intensity in the low Q region starts to increase and after about 64 minutes a small linear region in the log I vs. log Q plot appears. At the same time, the scattered intensity at $2\Theta=23.2^\circ$ in the WAXS pattern starts to increase, pointing to the formation of silicalite-1 crystals (see figure 1B). At longer reaction times the increased intensity at small angles in the SAXS pattern forms a linear region with a slope of approximately -3.6, which agrees with scattering at a crystal with surface fractal properties^{12,13} (surface fractal dimension 2.4). This interpretation was confirmed by USAXS experiments (Chapter 2).

At reaction times larger than 64 minutes, two effects can be observed. Both the scattered intensity in the low Q region and the (501)-reflection at $2\Theta=23.2^\circ$ (figure 1B) increase, corresponding with an increase in the amount of crystalline product. At high Q values the scattered intensity from the colloidal aggregates

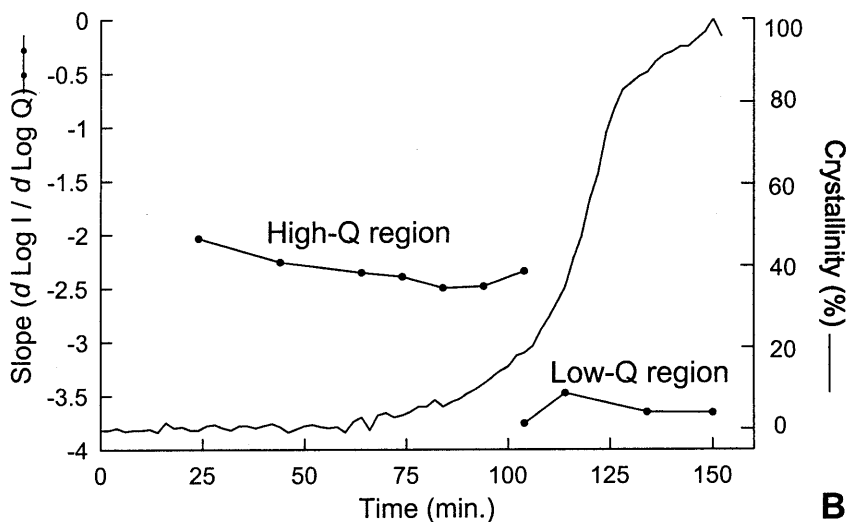
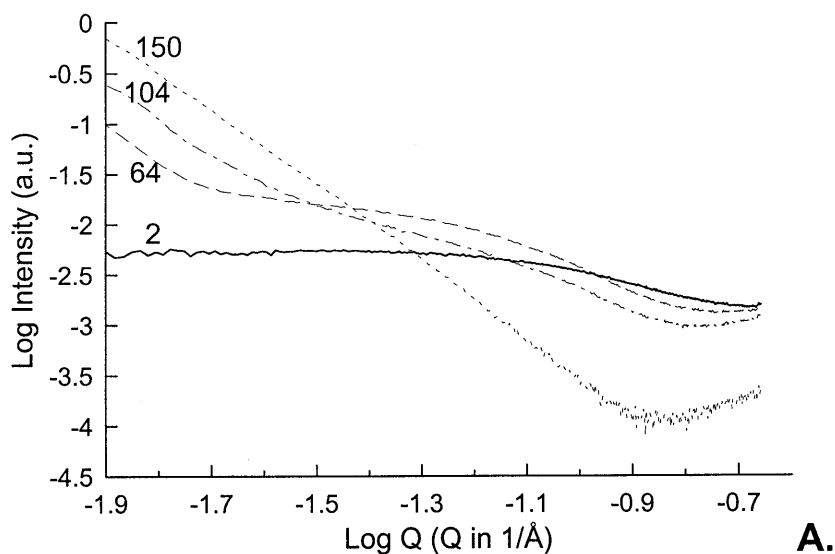


Figure 1: A. Overview of the SAXS patterns recorded during the synthesis of silicalite-1 from a clear solution (standard composition), aged at room temperature for only 15 minutes prior to heating to reaction temperature. The labels at the curves correspond to the reaction time in minutes. B. The slope in two regions of the log I vs. log Q plot of the SAXS pattern and the crystallinity. The maximum height of the (501)-reflection has arbitrarily set to correspond with 100% crystallinity.

lowers, indicating a decrease in their concentration. The slope of the log I vs. log Q curve in the appropriate region shows a decrease from -2.0 to -2.5 when the reaction time increases from 20 to 90 minutes (see curve denoted 'high Q region' in figure 1B).

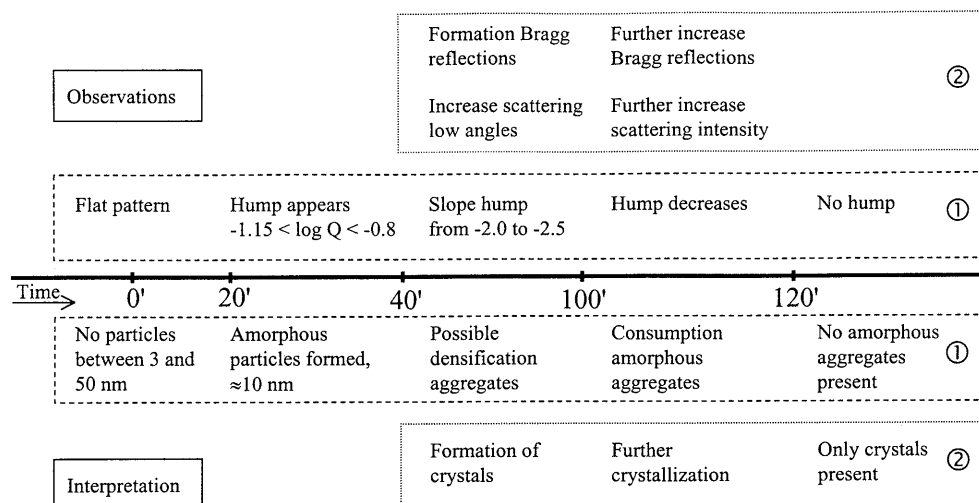


Figure 2: Schematic representation of the features observed in the scattering patterns of the 'standard' system (above the time line), and the interpretation in terms of particle populations (below the time line). Observations and interpretations have been categorized in being related with the amorphous aggregates (①) and crystals (②).

This could be in accord with a densification of aggregates by a reconstruction or aging process, but the range of the linear fit is too small to draw any definite conclusions in terms of mass fractal dimensions of these aggregates¹⁴. However, in contrast with the results by Dokter *et al.*¹⁰, on a system with the same composition, but aged for 7 days at room temperature prior to the SAXS/WAXS experiment¹⁵, the densification of these aggregates into smooth particles (characterised with to a slope of -4 in the $\log I$ vs. $\log Q$ plot) is not found.

At reaction times larger than 120 minutes no scattering intensity from the colloidal aggregates could be observed, corresponding with a complete consumption in the crystallization process. Now the scattering pattern shows a smooth bend at $\log Q \approx -1.3$. For $\log Q$ values smaller than -1.3 a slope of approximately -3.6 (surface fractal dimension -2.4) is found while for larger $\log Q$ values a slope -4 is found. This suggests that the growing crystals show surface fractal properties on a length scale larger than 12 nm, while they are smooth on smaller length scales.

Effect of aging time at room temperature

The WAXS patterns showed that silicalite-1 was formed in all syntheses, and that it was the only detectable crystalline material. The intensity of the (501)-reflection of silicalite-1 in the WAXS pattern for samples with different aging times prior to heating to reaction temperature, is shown in figure 3. In all syntheses a sigmoidal crystallization curve is found. At increasing aging time at room temperature, both the maximum intensity of the (501)-band and the induction period (see table 1) decrease. The SAXS patterns for the different syntheses all showed strong similarity with those shown in figure 1A. Since the

same aggregate size and slope in the $\log I$ vs. $\log Q$ plot were found on the same time scale, no influence of the aging on the scattering of the aggregates was observed. Even for aging longer than 7 days, no indication has been found for the densification of the aggregates to smooth particles, characterised by a slope -4 in the scattering curve, as described by Dokter *et al.*¹⁰. The only influence of the aging was found on the time scale at which the features described in previous section related to the onset of crystallization took place.

Variation of $\text{SiO}_2/\text{H}_2\text{O}$

Figure 4 shows the WAXS-patterns of the synthesis mixtures with various degrees of dilution after 150 minutes of heating at 125°C . As expected the intensity of the Bragg reflections in the diluted systems is lower than in the standard system corresponding with the silica concentration in the system. Therefore, in figure 5 the height of the (501)-reflection is normalised for the silica concentration in the sample, showing that the crystallization behaviour is independent of the silica concentration for $\text{SiO}_2/\text{H}_2\text{O}$ -ratios between 10/116 and 10/999.

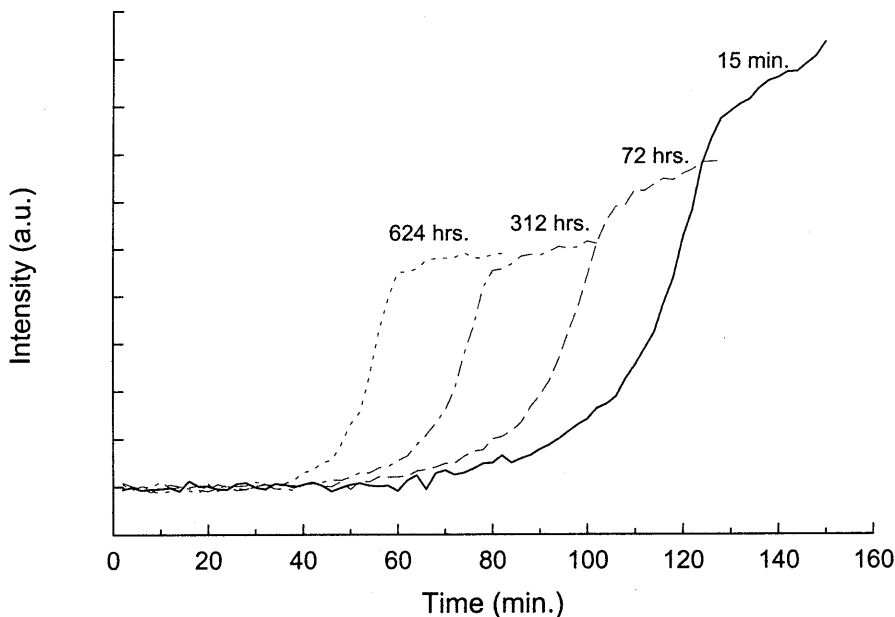


Figure 3: The crystallinity as a function of time (standard composition) for different aging times at room temperature prior to heating to the reaction temperature.

Table 1: Approximation of the induction times ($t_{\text{ind.}}$) at various aging times (t_{aging}) at room temperature prior to heating to the reaction temperature.

T_{aging} (h.)	0.25	72	312	624
$t_{\text{ind.}}$ (min.)	60	48	38	32

Generally the SAXS patterns for the diluted systems showed the same features as described for the 'standard system' as shown in figure 1. However, there were two differences concerning the formation of the amorphous colloidal aggregates, which become clear when one compares the lines for the different $\text{SiO}_2/\text{H}_2\text{O}$ -ratios denoted 'high Q region' in figure 6. In this figure only the crystallization curve of the 'standard system' is shown for clarity. First, the aggregates are formed in an earlier stage in the diluted synthesis mixtures compared to the standard one. Second, the slope in the appropriate region of the $\log I$ vs. $\log Q$ plot decreases to the lower values upon an increase of the dilution. The size of the aggregates is found constant at approximately 10 nm for all syntheses. At $\text{SiO}_2/\text{H}_2\text{O}$ -ratios smaller than 10/116 an increasing intensity is found in the low Q region for reaction times longer than 100 minutes, which eventually results in a linear range over almost the complete Q-range when the scattering from the aggregates has completely disappeared. Again the slope in this range is approximately -3.6, suggesting that crystals are formed with surface fractal properties independent of the initial concentration of the reactants in the synthesis mixture.

3.4 Discussion

In general, the SAXS patterns for the crystallization of silicalite-1 from a clear solution show the same features irrespective of the degree of dilution and the aging time prior to heating (see figure 2 for a schematic representation of the observed features and the interpretation). For fresh synthesis mixtures the scattered intensity is almost constant over the whole Q-range measured. Therefore, it is believed that the silicic-acid powder is dissolved completely during the 10 minutes boiling of the synthesis mixture, and that only silica-monomers, -oligomers, or -polymers with a size smaller than 3 nm are present in the solution (primary particles). After heating to 125°C, colloidal aggregates with sizes up to 10 nm are formed within several tens of minutes. These are believed to be amorphous, since no indication of any band is found in the WAXS pattern at this stage. At the onset of crystallization as determined by the intensity of the (501)-reflection, the intensity in the low Q region of the SAXS spectrum increases, pointing to the formation of relatively large crystals (>50 nm). This interpretation is confirmed by the USAXS patterns in the previous chapter. At this stage, three types of siliceous component are present in the synthesis mixture: primary particles (smaller than 3 nm), amorphous colloidal aggregates (up to 10 nm), and crystals (larger than 50 nm). Cundy *et al.*¹⁶ quantitatively determined each type of siliceous component with *ex situ* chemical methods. Our *in situ* combined SAXS/WAXS results agree with their results. At long reaction times the scattering from the aggregates completely disappears, and crystallization continues. This suggests a solution-mediated growth mechanism, in which the primary particles are smaller than 3 nm. This is in accord with the mechanism proposed by Burkett and Davis^{17,18}. In this mechanism the structure-directing role of organic templates is explained in terms of interactions between the organic molecules, water and the silicate species. The water, organised in a hydrophobic hydration sphere in the vicinity of the organic molecules, is replaced by silicate species¹⁹. Thus, the geometry of the organic species is translated into the inorganic component through multi-positional

molecular-level interactions. These organic-inorganic composite species then combine to form materials containing longer-range order.

In this study, no influence of the aging upon the formation of aggregates has been observed. However, upon increasing aging at room temperature, both the nucleation and the crystallization rate increase. This increased crystallization rate probably is due to a higher concentration of growing crystals (higher rate of nucleation), since the growth rate of the individual crystals is not expected to be affected. Since there is no effect of the aging period on the formation of the colloidal precursors, the higher rate of nucleation probably is related with reorganisations on smaller length scales than probed in these experiments (< 3 nm). Since the scattering intensity at the aggregates vanishes during the crystallization process, they are believed to dissolve to smaller entities which are consumed in the crystal growth process (further discussed in chapter 4).

For systems with varying $\text{SiO}_2/\text{H}_2\text{O}$ -ratios, the nucleation and crystal growth rate are found to be constant. This means that the diffusion of nutrients to the crystal surface is not rate-determining in the growth process, and agrees with a surface reaction controlled crystallization mechanism as suggested by Schoeman *et al.*²⁰. In such a case, the crystal surface will be covered with a layer of amorphous or semi-crystalline material which is still subject to reorganisation processes. This may be the explanation why no smooth crystals (characterized by a slope of -4 in the $\log I$ vs. $\log Q$ plot) are found.

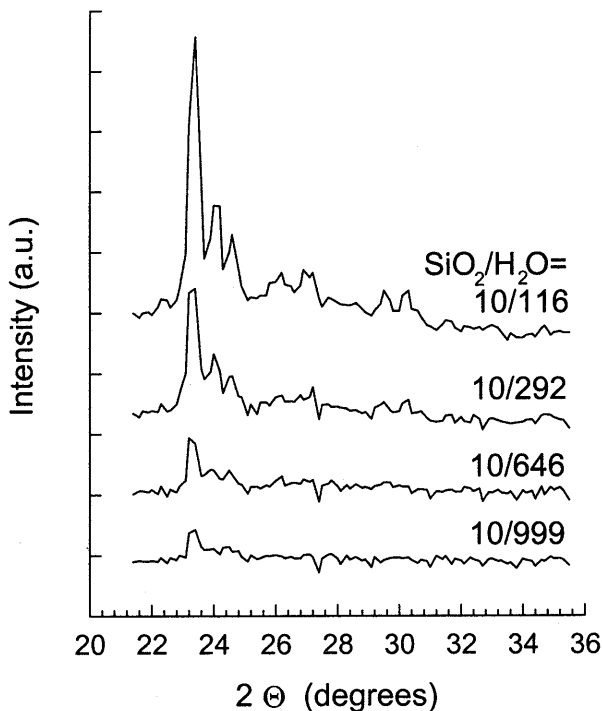


Figure 4: Comparison of the WAXS patterns for the synthesis mixtures with various $\text{SiO}_2/\text{H}_2\text{O}$ -ratios kept at 125°C for 150 minutes.

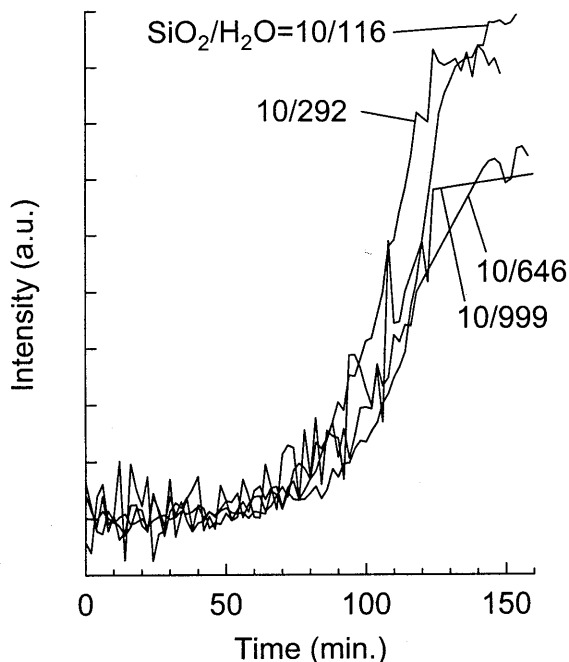


Figure 5: Crystallinity for synthesis of silicalite-1 at various $\text{SiO}_2/\text{H}_2\text{O}$ -ratios as a function of time. The intensity of the (501)-reflection has been normalised for the silica concentration in the synthesis mixture.

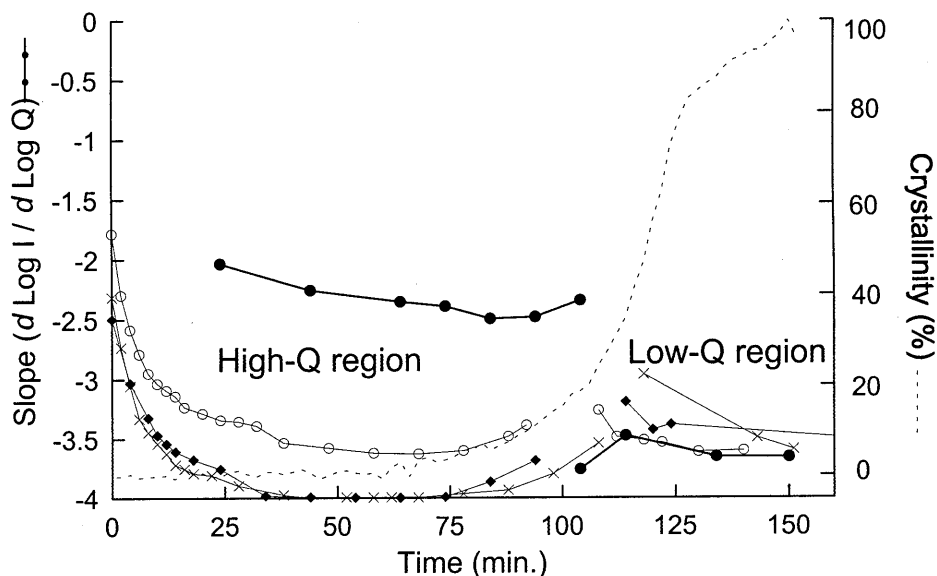


Figure 6: The slope in two regions of the $\log I$ vs. $\log Q$ plot of the SAXS pattern for systems with different $\text{SiO}_2/\text{H}_2\text{O}$ -ratios: 10/116 (\bullet), 10/292 (\circ), 10/646 (\blacklozenge), and 10/999 (\times). Only the crystallization curve of the 'standard system' with $\text{SiO}_2/\text{H}_2\text{O}=10/116$ is shown.

In this study for all syntheses the SiO_2/OH^- ratio was 3.02, and the formation of aggregates was observed. Here we found a decrease in the slope of the $\log I$ vs. $\log Q$ plot for the scattering from the aggregates with decreasing concentration of the reactants at constant SiO_2/OH^- . For $\text{SiO}_2/\text{H}_2\text{O}=10/116$ a slope of -2.5 is found, corresponding with a mass fractal dimension of 2.5, while for $\text{SiO}_2/\text{H}_2\text{O}=10/292$ a slope of approximately -3.6 is observed, pointing to the formation of aggregates with surface fractal properties. For more dilute systems ($\text{SiO}_2/\text{H}_2\text{O}=10/646$ and $10/999$) the formation of smooth particles with a Euclidean surface dimension of 2 (slope -4) is found. However, since the range of the linear region is small, it is not possible to draw any definite conclusions in terms of mass-fractal dimensions, but these results strongly suggest that the $\text{OH}^-/\text{H}_2\text{O}$ -ratio influences the structure of the colloidal aggregates.

3.5 Conclusions

Room temperature aging of the synthesis mixtures prior to the heating to reaction temperature increased both the nucleation and the crystal growth rate without having any effect on the formation of amorphous colloidal aggregates.

Dilution of the reaction mixtures prior to heating to the reaction temperature was found not to affect the nucleation and crystal growth rate, but affected the formation of colloidal aggregates. The change in slope in the scattering curves probably is related with a change of the structure of the aggregates formed due to an variation of the $\text{OH}^-/\text{H}_2\text{O}$ -ratio in the reaction mixture. The independence of the rate of crystallization on the concentration of the reactants agrees with a reaction controlled crystal growth mechanism. The growth units are expected to be smaller than 3 nm.

References

- ¹ Barrer, R.M. *Hydrothermal Chemistry of Zeolites*, London: Academic Press., 1982
- ² Jacobs, P.A.; Martens, J.A. *Synthesis of high-Silica Aluminosilicate Zeolites*, Studies in surface science and catalysis, **33**, Amsterdam, The Netherlands: Elsevier science publishers BV., 1987
- ³ Twomey, T.A.M.; Mackay, M.; Kuipers, H.P.C.E.; Thompson, R.W. *Zeolites* 1994, **14**, 162-168
- ⁴ Katovic, A.; Subotic, B.; Smit, I.; Depotovic, L.A.; Curic, M. *Zeolite Synthesis*. ACS Symp. Ser. 398, edited by M.L. Occelli and H.E. Robson, 1989, pp. 124-139
- ⁵ Gabelica, Z.; Nagy, J.B.; Debras, G.; Derouane, E.G. *Proceedings of the Sixth International Zeolite Conference*, edited by Olson, D.; Bisio, A., 1984, pp. 914-924
- ⁶ Iton, L.E.; Trouw, F.; Brun, T.O.; Epperson, J.E. *Langmuir*, 1992, **8**, 1045-1048
- ⁷ Chang, C.D.; Bell, A.T. *Catalysis Letters*, 1991, **8**, 305-316
- ⁸ Wenyang, X.; Jianquan, L.; Wenyuan, L.; Huiming, Z.; Bingchang, L. *Zeolites*, 1989, **9**, 468-473
- ⁹ Serrano, D.P.; Uguina, M.A.; Ovejero, G.; Van Grieken, R.; Camacho, M. *Chem. Commun.*, 1996, 1097-1098

- ¹⁰ Dokter, W.H.; Van Garderen, H.F.; Beelen, T.P.M.; Van Santen, R.A.; Bras, W. *Angew. Chem. Int. Ed. Engl.*, 1995, **34**, 73-75
- ¹¹ Verduijn, J.P. *Exxon patent*, PCT/EP92/02386, 1992
- ¹² Bale, H.D.; Schmidt, P.W. *Phys. Rev. Lett.*, 1984, **53**, 596-599
- ¹³ Schmidt, P.W. *The fractal approach to heterogeneous chemistry*, Ed. Avnir, D., John Wiley and Sons, 1989, pp.67-79
- ¹⁴ Teixeira, J. *On Growth and Form: Fractal and non-fractal Patterns in Physics*, NATO-ASI Series E, **100**, Ed.: Stanley, H.E.; Ostrowsky, N. Martinus Nijhoff Publishers, Dordrecht, 1986, pp. 145-162
- ¹⁵ Dokter, W.H. *personal communication*, 1995
- ¹⁶ Cundy, C.S.; Henty, M.S.; Plaisted, R.J. *Zeolites*, 1995, **15**, 342-352
- ¹⁷ Burkett, S.L.; Davis, M.E. *J. Phys. Chem.*, 1994, **98**, 4647-4653
- ¹⁸ Burkett, S.L.; Davis, M.E. *Chem. Mater.*, 1995, **7**, 1453-1463
- ¹⁹ Flanigen, E.M.; Bennett, J.M.; Grose, R.W.; Cohen, J.P.; Patton, R.L.; Kirchner, R.M.; Smith, J.V. *Nature*, 1978, **271**, 512-516
- ²⁰ Schoeman, B.J.; Sterte, J.; Otterstedt, J.E. *Zeolites*, 1994, **14**, 568-575

Nucleation and crystal growth in Si-TPA-MFI synthesis*

Using a combination of X-ray scattering set-ups, we were able to cover a continuous range of length scales spanning over four orders of magnitude (0.17 - 6000 nm). This allowed us to probe all nanometer-scale precursors present in the synthesis mixtures. In this chapter we apply these combined techniques to the crystallization of Si-TPA-MFI from a clear solution, and show that two types of precursor particles are present: 2.8 nm sized primary units and aggregates (≈ 10 nm). The role of each of these precursors has been clarified by investigating the influence of the synthesis conditions on the formation and consumption of these particles during the complete crystallization process.

* Submitted for publication as: P.-P.E.A. de Moor, T.P.M. Beelen, R.A. van Santen, *in situ* observation of precursors in Si-TPA-MFI nucleation and crystal growth with small-angle X-ray scattering, *J. Phys. Chem.*

4.1 Introduction

Zeolites are crystalline, microporous, aluminosilicates which are used in a broad variety of applications as molecular sieves (e.g. separation processes), as catalysts (e.g. as cracking catalysts in petrol refining), and as ion exchange agent¹. Improvement of known applications and the prospect of new ones are a continuing driving force to investigate the possibility to synthesize zeolites with new (combinations) of properties². Therefore there is significant research aimed at understanding the mechanism of the assembly of small entities to zeolites. The ultimate goal is the ability to create zeolites by rational design³.

The vast majority of zeolites are synthesized under hydrothermal conditions from alkaline aqueous solutions. Traditionally, investigations of zeolite synthesis were mainly based on observations of end products in relation with changes of the reactants and the process conditions. Recently, using NMR spectroscopy, information was obtained on the structure of the silicate species in the synthesis mixture (for example see ref. 4), and on the interactions between silicate species and the organic structure-directing agents^{5,6}. In general, these spectroscopic methods showed the importance of effective interaction of the organic molecules with the silicate species, but did not give information on the nanometer structure of the entities in solution. Therefore, there is an information gap between the molecular scale entities present in solution and the crystal structures formed. The main reason for this gap is the fundamental problem that most spectroscopic methods do not allow to probe structures which are much larger than a few bond lengths (typically larger than 1 nm). Furthermore, one prefers to perform *in situ* experiments since the intermediates in solution are expected to be built by relatively weak bonds and to be strongly dependent on the surrounding solution. Therefore drying will most likely be destructive.

The above problems can be circumvented using scattering of X-rays at (very) small angles. With high-brilliance synchrotron radiation, we are also able to perform time-resolved experiments. By simultaneously measuring the scattering at small and wide angles (SAXS and WAXS, respectively), correlations could be found between the (trans)formations of nanometer-scale structures and the presence of crystalline structures. Using ultra-small-angle scattering (USAXS), we are able to probe the scattering at the surface of the crystals⁷. From these data we can follow *in situ* the evolution of the particle size distribution of the product crystals.

Using these techniques we investigated the crystallization of Si-TPA-MFI during the complete course of the reaction over an extended range of length scales compared to previous chapters. The presence of two types of nanometer-scale precursors could now be demonstrated: 2.8 nm primary units and aggregates (≈ 10 nm) composed of these units. The alkalinity of the synthesis mixture has been varied, and appears to have an influence on both the formation of the aggregates and the crystallization behaviour. Combined with crystallizations with seed crystals added, these results show the importance of aggregation of the

primary units in the nucleation process. The temperature dependence of the growth of the crystals revealed that this is a reaction controlled process, which probably involves the integration of primary units at the growing crystal.

4.2 Experimental

Syntheses

Si-TPA-MFI synthesis mixtures with composition $10.0 \text{ SiO}_2 : 2.44 \text{ TPAOH} : x \text{ NaOH} : 114 \text{ H}_2\text{O}$ were prepared according to a recipe based on an Exxon Chemical patent⁸. The alkalinity, expressed as the ratio Si/OH in the synthesis mixture, has been varied by changing the amount of NaOH. Si/OH-ratios of 2.12, 2.42, 2.57, 2.72, and 3.02 correspond with $x=2.28, 1.70, 1.45, 1.24,$ and 0.87 respectively. The preparation method will be outlined here for a synthesis mixture having Si/OH=3.02.

1.40 g NaOH (Merck, p.a.) was dissolved in 100g tetra-propylammonium hydroxide (Merck, 20 wt% TPAOH in H₂O) with gentle mixing at room temperature, followed by spoonwise addition of 27.0 g silicic acid powder (Baker, 10.2 wt% H₂O). Thereafter the homogeneous dispersion was boiled under stirring for approximately 10 minutes to obtain a clear solution. The solution was cooled down to room temperature in a water bath, corrected for loss of water during boiling, and filtered through a paper filter (Schleicher and Schüll, Schwarzband), and successively through a 0.45 µm filter (Schleicher and Schüll, Spartan 30/B). The reaction mixtures were completely clear and aged for less than 1 hour at room temperature before heating to a reaction temperature of 125°C. All scattering measurements have been performed *in situ* in a special rotating (2 r.p.m.), electrically heated sample cell. The sample thickness was 0.5 mm and mica windows (thickness 0.25µm) were used.

Seeds

The Si-TPA-MFI seed crystals have been prepared from a synthesis mixture having Si/OH=3.02 which was heated for 18 h. at 95°C. The seeds have been separated from the mother liquor by centrifugation and decantation, after which they were redispersed in deionised water using an ultrasonic bath. This washing treatment was repeated three times and resulted in a stable colloidal crystal dispersion. The seeds were added to the synthesis mixture just before heating to reaction temperature. The amount of SiO₂ added by the crystals was calculated on basis of the amount of SiO₂ in the fresh synthesis mixture.

The number of crystals in the product compared to the number of seeds added to the fresh synthesis mixture can be expressed as the fraction f_s :

$$f_s = \frac{N_{\text{crystal}}}{N_{\text{seed}}} = \frac{\bar{V}_{\text{seed}}}{\bar{V}_{\text{crystal}}} \left(1 + \frac{x}{p}\right) \quad (1)$$

Here N_{part} refers to the number of particles, x =the fraction SiO_2 converted to MFI, p =weight fraction of seeds added. \bar{V}_{part} is the average volume of the particle population. The subscript seed refers to the seed crystals, whereas the subscript crystal refers to the crystals in the final product.

SAXS and Bonse-Hart set-up

The combined SAXS and WAXS experiments have been performed at station 8.2 of the Synchrotron Radiation Source at Daresbury Laboratory (United Kingdom)⁹, using a camera length of 0.8 ($0.4 < Q < 7 \text{ nm}^{-1}$) and 3.4 m ($0.1 < Q < 2.5 \text{ nm}^{-1}$). Using the high intensity synchrotron radiation and position sensitive detectors, we were able to collect SAXS and WAXS patterns simultaneously with a good signal to noise ratio every two minutes. The data were normalised for the intensity of the X-ray beam, and corrected for detector sensitivity prior to background correction. The scattering from water at reaction temperature has been used as background pattern. For the calibration of the SAXS and WAXS patterns, respectively the scattering of an oriented specimen of wet rat tail collagen and the diffraction of a fully crystallized sample of zeolite NaA have been used. The wavelength for station 8.2 is fixed at 1.54 Å.

The USAXS experiments have been performed at the high-brilliance beamline ID2/BL4 of the European Synchrotron Radiation Facility in Grenoble (FR) using a Bonse-Hart type of camera¹⁰ ($0.001 < Q < 0.3 \text{ nm}^{-1}$). A configuration with two analyser crystals has been used, so no desmearing was necessary. The first analyzer crystals (Si(220)) was used to scan the angle, and there were three reflections in the horizontal plane. A second analyzer crystal (Si(111), two reflections) is used as a collimator in the vertical direction in order to obtain a comparable angular resolution in both vertical and horizontal directions. The wavelength of the X-rays was 1.0 Å. A NaI scintillator was used as detector, which shows a linear response over 4 decades of intensity. Several scans (4-5) over different 2θ -ranges with sufficient overlap were recorded using different degrees of attenuation of the incident X-ray beam, in order to have intensities on the detector in the linear range. Because of the high-brilliance of the undulator beamline ID2, a complete pattern could be recorded in only 15 minutes despite the inherent low efficiency of the Bonse-Hart set-up and the scanning mode of recording.

The Q -ranges obtained with the USAXS, SAXS and WAXS showed sufficient overlap to allow an accurate merging of the patterns.

SAXS data analysis

SAXS data provide information about the presence of different particle populations and some of the particle properties like particle size distribution, their shape and the type of their interactions. The size distribution of the (growing) crystals in the synthesis mixtures has been determined by fitting the calculated scattering pattern of a population of interacting spheres to the measured curve. In the calculation of the form factor, the crystals have been

assumed to have a normal size distribution and a spherical shape^{7,11}. For calculating the structure factor, the Percus-Yevick approximation for hard-sphere interactions has been applied. The influence of the polydispersity on the structure factor has been taken into account using the 'local monodisperse approximation' of Pedersen¹², which proves to give good results up to volume fractions of 0.4. In our experiments, the volume fraction of crystals in the mother liquor will be typically 0.05 at full crystallization. The small contribution of the structure factor to the calculated intensity has been included for completeness sake.

Electron microscopy

The samples for the transmission electron microscopy (TEM) experiments were prepared in the synthesis cell used for the SAXS/WAXS and USAXS experiments under the same conditions. After rapid cooling of the cell to room temperature at a chosen reaction time, the sample was filtered and washed extensively with de-ionised water over a 0.02 μ m filter (Whatman, Anodisk).

Transmission electron microscopy was performed at Delft university using a Philips CM 30 T electron microscope with an LaB₆ filament as the source of electrons operated at 300kV. Samples were mounted on a carbon polymer supported on a copper grid by rubbing the grid against the filter containing the sample, followed by sputtering with carbon to decrease charging in the microscope.

4.3 Results

SAXS and WAXS patterns of Si-TPA-MFI syntheses at different alkalinities

The crystallization of Si-TPA-MFI at 125°C from completely water-clear synthesis mixtures with varying alkalinity (expressed in the ratio Si/OH) was studied *in situ* with simultaneous SAXS and WAXS. The time-resolved scattering patterns are depicted in figure 1. The upper limit of the plotted Q-range (d-spacing \approx 0.9 nm) is chosen to reveal the formation of the first Bragg reflections. The lower Q-limit (d-spacing \approx 50 nm) is determined by smallest angle which can be probed at station 8.2 at Daresbury Laboratory. Independent of the alkalinity, a broad hump is observed around $Q \approx 2.2 \text{ nm}^{-1}$. The intensity decreases during the crystallization (as observed by the growth of the Bragg reflections in the high Q region). This hump is due to scattering at a particle population which we will refer to as the primary units, with an estimated average size of 2.8 nm ($d_{\text{part}} = 2 \cdot \pi / Q_{\text{max}}$). At very low Q-values (large d-spacings), an increasing scattering intensity is observed for every alkalinity, corresponding with scattering at large structures. This increasing intensity is due to the scattering at the surface of the growing crystals (confirmed by USAXS, see chapter 2). Between the hump at $Q \approx 2.2 \text{ nm}^{-1}$ and the scattering at the crystals at very low Q-values, an alkalinity dependent shoulder is observed, which is most apparent for the synthesis mixture with Si/OH=3.02 (figure 1D). The size of

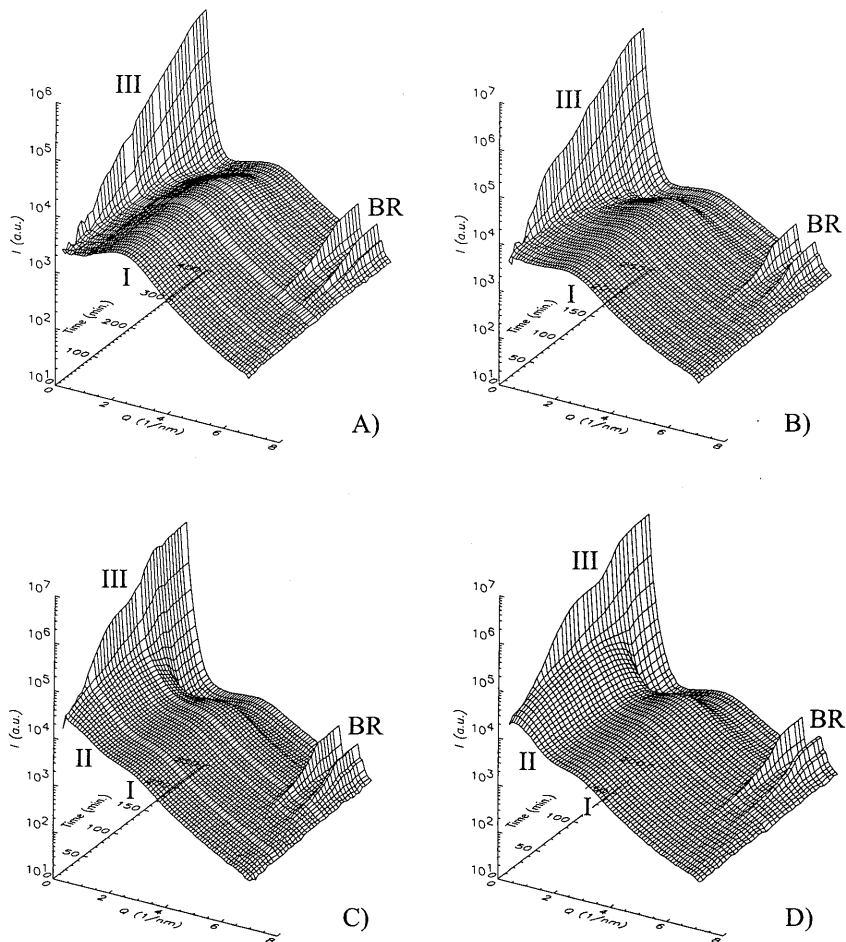


Figure 1: Time-resolved SAXS patterns for Si-TPA-MFI synthesis for different Si/OH-ratios: A) 2.24 B) 2.57 C) 2.72 D) 3.02. Scattering particle types: I=primary units, II=aggregates, III=crystals, BR=Bragg reflections.

particles giving rise to the increased intensity is approximately 10 nm, and they are believed to be aggregates of the 2.8 nm sized primary units. The formation of these aggregates is more pronounced when the alkalinity decreases (in the order A, B, C, D in figure 1). As the crystallization starts, the scattered intensity at the aggregates decreases.

Details of the scattering curves and the changes therein are more clear in figure 2, showing snapshots at various reaction times. For each alkalinity, the following curves have been plotted (note the increasing reaction times at increasing alkalinity):

1st: After 10 minutes of heating.

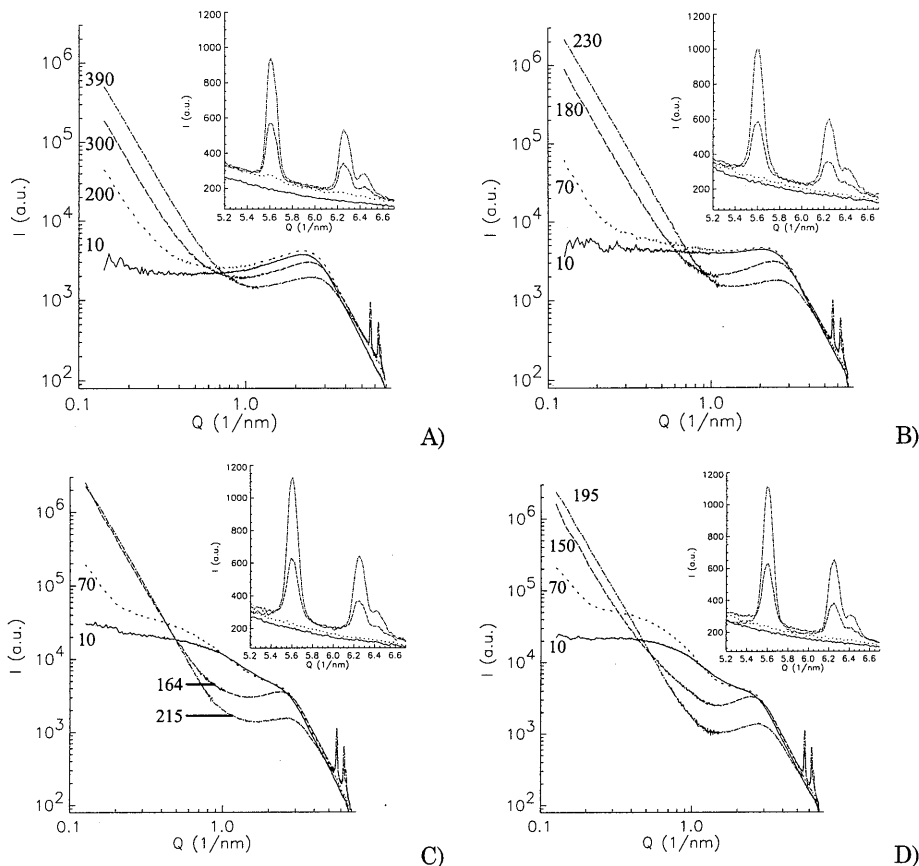


Figure 2: SAXS patterns after various reaction times for Si-TPA-MFI synthesis mixtures with different Si/OH-ratios: A) 2.24 B) 2.57 C) 2.72 D) 3.02. The curves correspond to the following stages in the crystallization process (reaction times annotated at curves in min.): 1st: Shortly after heating, 2nd: Onset of crystallization, 3rd: $\approx 50\%$ crystallization, 4th: full crystallization. The inset of each plot shows a close-up of the Bragg reflections in the high Q region.

2nd: At the onset of crystallization as determined by the appearance of the first sign of Bragg reflections.

3rd: When the area of the Bragg reflections is approximately 50% of their final value.

4th: When the area of the Bragg reflections reached its final value.

These curves show the presence of the hump around $Q \approx 2.2 \text{ nm}^{-1}$ due to the scattering at the primary particles as well as the increasing intensity at very low Q-values from the scattering at the crystals formed. Now the effect of the alkalinity on the formation of aggregates of primary units is clearly seen at $Q \approx 1 \text{ nm}^{-1}$. For relatively high alkalinity (Si/OH=2.42, figure 2A), the formation of aggregates is not clearly observed. If the alkalinity increases, the presence of a shoulder around $Q \approx 1 \text{ nm}^{-1}$ is more pronounced. The scattering patterns from the

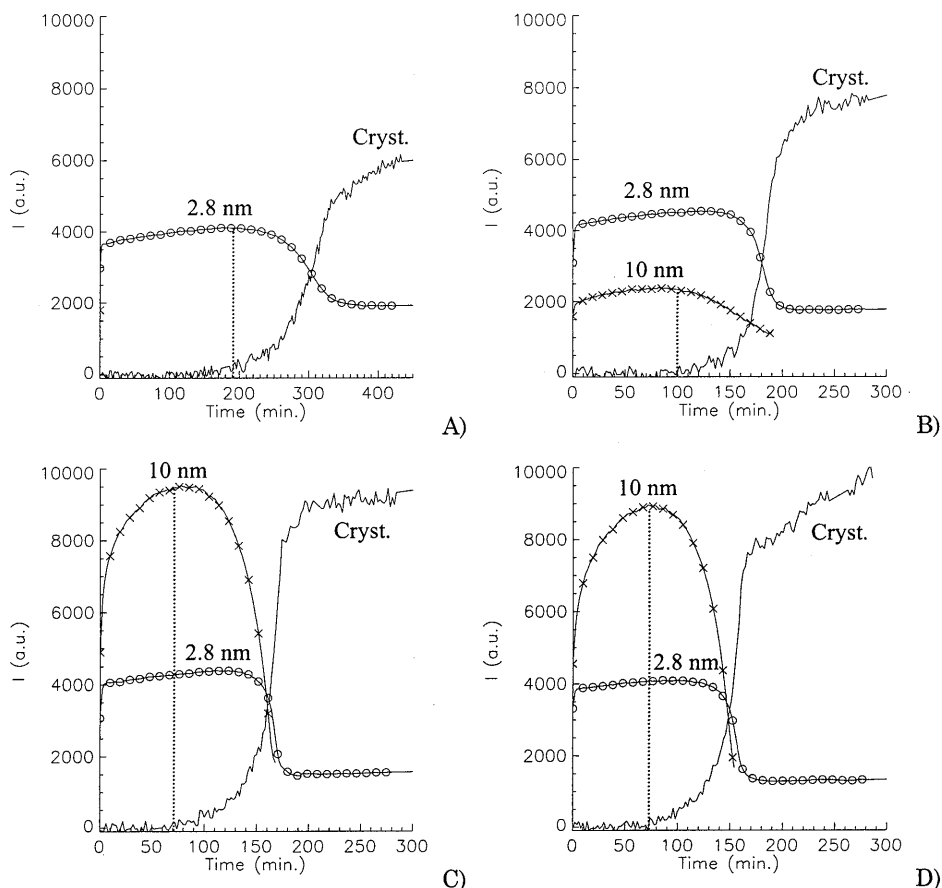


Figure 3: Time dependent scattering intensity at fixed angles, corresponding with a d -spacing of 2.8 nm (primary units) and 10 nm (aggregates), together with the area of the Bragg reflections of the product Si-TPA-MFI crystals, for Si-TPA-MFI synthesis mixtures with different Si/OH-ratios: A) 2.24 B) 2.57 C) 2.72 D) 3.02. The scattered intensity at the aggregates (\times) has only been plotted when their presence could be demonstrated clearly from the scattering curve, and was divided by 2 for clarity.

synthesis mixtures with Si/OH=2.72 and 3.02 show the size of the aggregates to increase between 10 and 70 minutes of heating. For all alkalinities we observe a decrease in scattering intensity at the primary units and their aggregates (if present) between the onset of crystallization (2nd curve in figure 2A to D) and full crystallization (4th curve). However, the consumption of both precursor particle types appears not to start at the same time: for the synthesis mixtures with the lowest alkalinities, a decrease in scattering intensity from the ≈ 10 nm aggregates (Figure 2C and D, going from 2nd to 3rd curve) is clearly observed before the decrease in intensity due to the 2.8 nm primary units (going from 3rd to 4th curve).

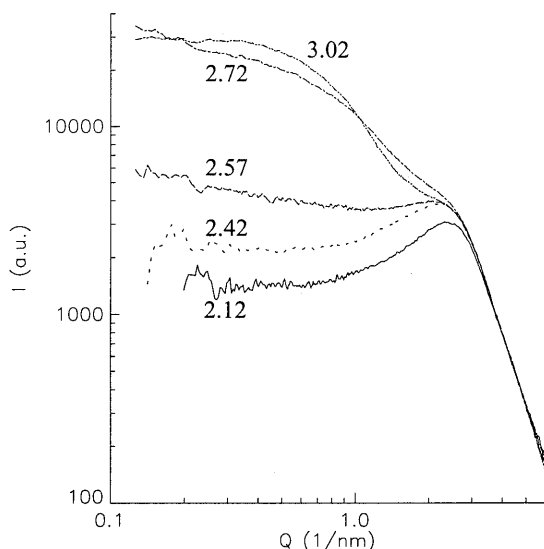


Figure 4: SAXS patterns of Si-TPA-MFI synthesis mixtures after 20 minutes of heating at 125°C. Si/OH-ratios are denoted at the curves.

In order to obtain more information about how the different particle populations are correlated, the evolution of the scattering intensity at certain, fixed angles has been plotted together with the area of the Bragg reflections as a measure of the conversion of the silica to the product Si-TPA-MFI crystals (figure 3). For synthesis mixtures where the formation of ≈ 10 nm sized aggregates is observed (Si/OH=2.57, 2.72, and 3.02, figure 3B, C, and D), the time of the onset of crystallization as determined from the appearance of the Bragg reflections in the WAXS (vertical dotted lines) coincides with the maximum in scattered intensity from the aggregates. The decrease in intensity at a d-spacing of 2.8 nm (primary units) starts significantly later. Only for the high alkalinity synthesis mixture (Si/OH=2.42) the onset of crystallization coincides with the start of the decrease of scattering intensity at the 2.8 nm particles.

To show the influence of the alkalinity on the formation of precursors, the scattering patterns are compared after 20 minutes of heating (figure 4). This plot shows that the formation of the 2.8 nm sized primary units is independent of the alkalinity ($Q \approx 2.2 \text{ nm}^{-1}$). A maximum in the SAXS pattern is attributed to independent particles with preferred interparticle distances, due to a high concentration and/or due to repulsive interactions. The formation of aggregates (attractive force dominates), results in an increase in intensity at larger d-spacings compared to the composing particles (smaller Q-values). For synthesis mixtures having Si/OH-ratios of 2.72 and 3.02 we clearly observe the formation of an increased intensity at Q-values lower than 2.2 nm^{-1} , which corresponds to the formation of aggregates of primary units. At decreasing Si/OH, the scattering at the aggregates decreases, while even no indication is observed for a synthesis mixture with Si/OH=2.12.

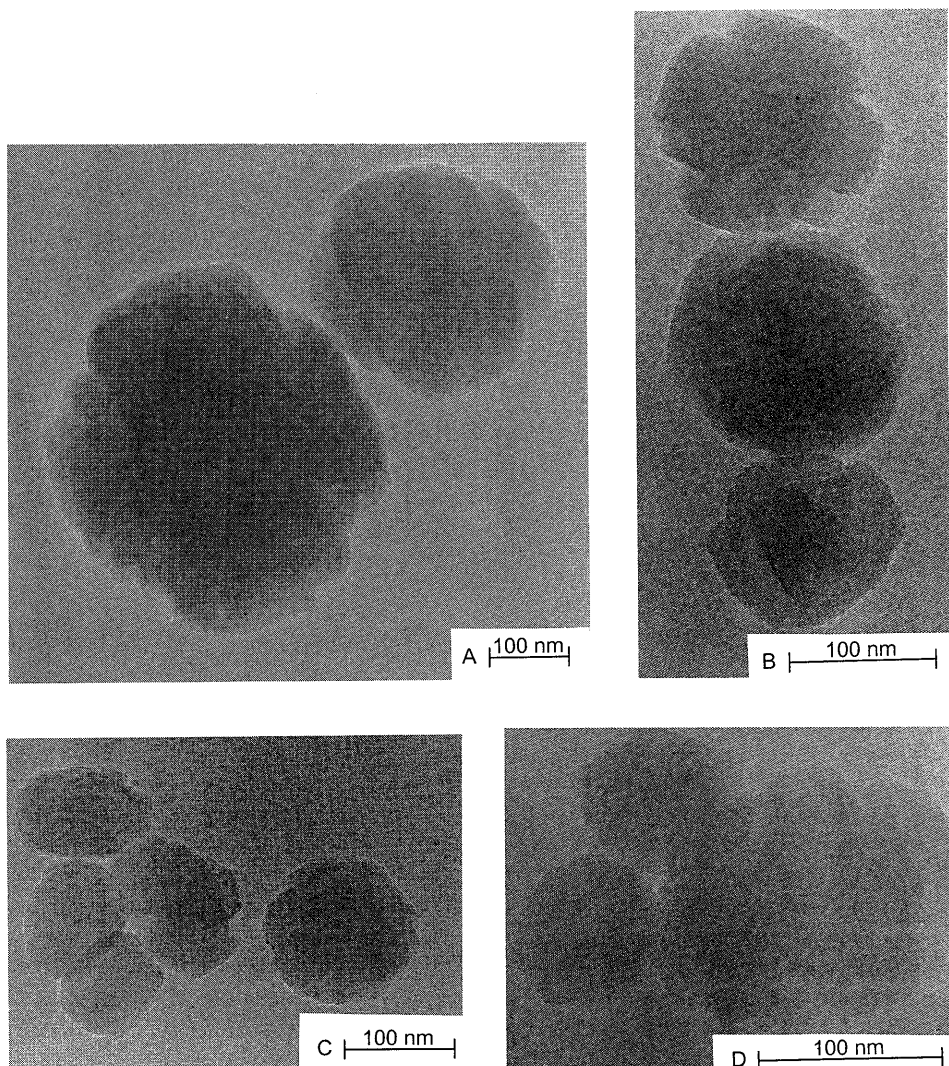


Figure 5: TEM micrographs for Si-TPA-MFI crystals obtained after 10 h. of heating to 125°C for Si/OH-ratios of the synthesis mixture of A) 2.24 B) 2.57 C) 2.72 D) 3.02. Please note that the scale bars are not the same for the four images.

The shape of the crystalline product has been investigated using transmission electron microscopy. The micrographs of product obtained after 10 h. of heating to 125°C for Si-TPA-MFI synthesis mixtures having various alkalinities show that the product can be classified in two categories depending on the Si/OH-ratio of the synthesis mixture (Figure 5). For Si/OH-values of 2.72 and 3.02 the crystals are spherical or elliptical, and show a cauliflower like appearance at the surface. For higher alkalinities (Si/OH=2.42 and 2.57), approximately 2/3rd of the crystals show multiple intergrowths. The remaining 1/3rd of the crystals shows a morphology as found for Si/OH=2.72 and 3.02. The size of the crystals from the

synthesis mixture with $\text{Si}/\text{OH}=2.42$ is larger than the product from solutions with higher Si/OH -ratios. TEM micrographs (not shown) from synthesis mixtures with $\text{Si}/\text{OH}=2.42$ which were heated for various times, showed that for relatively short reaction times (180 and 250 min.) no intergrowths were observed and the crystals had a cauliflower like appearance. For longer reaction times (400 and 600 min.), multiple intergrowths are observed in approximately $2/3^{\text{rd}}$ of the crystals.

Crystallization behaviour and crystal growth

The rates of conversion of the (amorphous) silica to the crystalline Si-TPA-MFI structure can be determined from the changing areas of the Bragg reflections. In this study, the growth curves of several Bragg reflections have been compared to find whether there was a difference in growth rate in the different crystalline directions, but such a difference has not been found by us for Si-TPA-MFI. The change in the area of the first intense Bragg reflection at $2\theta=7.95^\circ$ was used. Figure 6A shows the SiO_2 conversion for the synthesis at different alkalinities. This plot shows that the conversion rate does not change very much for Si/OH -values of 3.02, 2.72, and 2.57, although a decrease in final peak area can be observed for decreasing Si/OH . There is a significant decrease in conversion rate for lower Si/OH -values, and the formation of crystalline material is extremely slow for $\text{Si}/\text{OH}=2.12$ (first sign of Bragg reflection after 25 h. of heating, after 60 h intensity ≈ 10 in same arbitrary units as used in Figure 6A). The final area of the Bragg reflections is a measure for the conversion of the SiO_2 to zeolite. Figure 6B shows the conversion for synthesis mixtures with different Si/OH -ratios as determined in *ex situ* experiments (in stainless steel autoclaves). In order to have a faster conversion to MFI for the synthesis with $\text{Si}/\text{OH}=2.12$, seeds have been added, while no seeds were added to the other synthesis mixtures. The addition of a small amount of crystalline SiO_2 (<1 wt%) is not

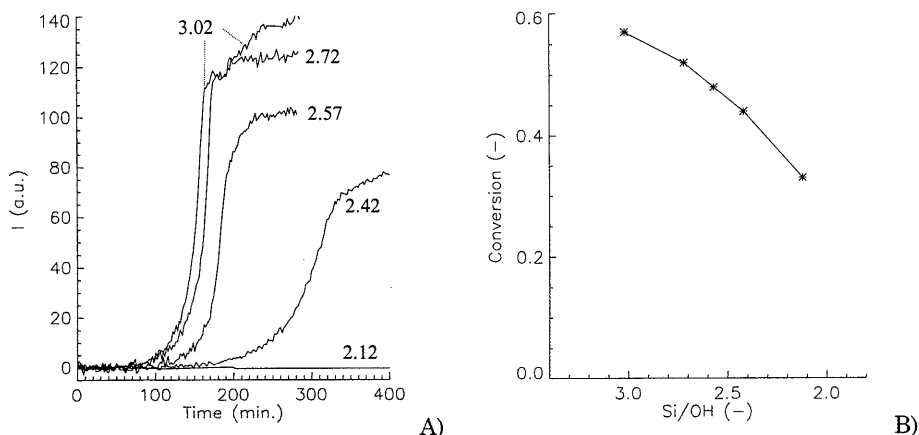


Figure 6: A) Area of the Si-TPA-MFI Bragg reflections as determined from the WAXS for synthesis mixtures with Si/OH -values as denoted at the curves. B) The conversion of amorphous SiO_2 to Si-MFI for different Si/OH -values. Crystallization in stainless steel autoclaves, 24 h. at 125°C . 0.5wt% seeds have been added in the synthesis with $\text{Si}/\text{OH}=2.12$.

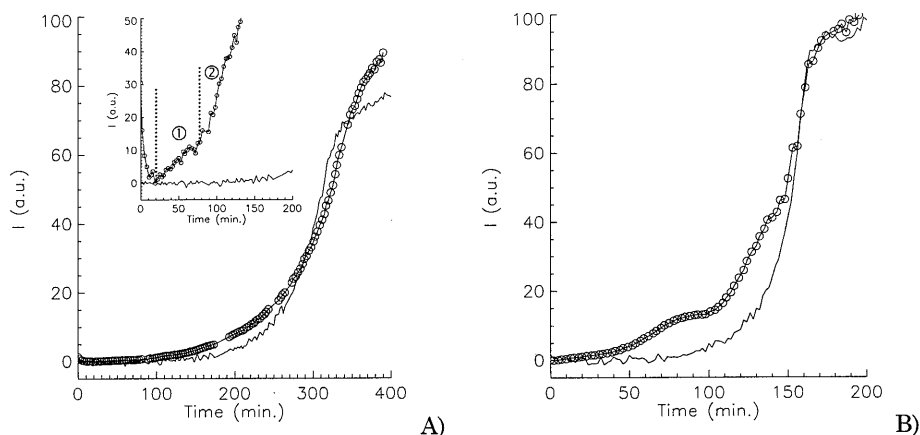


Figure 7: Scattering intensity at the surface of the crystal at $Q=0.15 \text{ nm}^{-1}$ (SAXS, symbol: \circ), and the area of the MFI Bragg reflection (WAXS, solid lines) for Si-TPA-MFI synthesis with Si/OH-ratios of A) 2.42 and B) 3.02. The intensity of the SAXS has been multiplied with an arbitrary constant. The inset of A) shows the same plot for short reaction times (different constant in multiplication of SAXS intensity).

expected to influence the final conversion. The same trend for varying alkalinity is observed both for the final area of the Bragg reflections (figure 6A) and for the SiO_2 conversion as determined in the *ex situ* experiments (figure 6B). Note that these values cannot be compared for Si/OH=2.12 since the area of the Bragg reflection is far from reaching its final value even after 60 hours of heating.

From our scattering data we get two types of information about the growing crystals. The Bragg reflections reveal details of the crystal lattice (WAXS or XRD), and the scattering at the surface from the crystals (SAXS) contains information concerning the size and shape of the crystals. Figure 7 compares the area of the Bragg reflections with the scattering intensity at $Q=0.15 \text{ nm}^{-1}$ ($d=42 \text{ nm}$), where the SAXS intensity has been multiplied with an arbitrary constant to fit the WAXS curve. For Si/OH=2.42 (figure 7A) the same trend is found, but for Si/OH=3.02 (figure 7B) some systematic differences can be observed. As can be seen in figure 2D, the scattered intensity at $Q=0.15 \text{ nm}^{-1}$ has a contribution of the scattering at the crystals, as well as from the $\approx 10 \text{ nm}$ sized aggregates. These results show that one needs to be careful when interpreting the scattering at very low angles as a measure for the crystallinity. For Si/OH=2.42 the formation of aggregates is not apparent from the scattering curves in figure 2A. The inset in figure 7A shows the trends at short reaction times (after 200 minutes the first sign of Bragg reflections appears). Here the scattering at the surface of the crystal shows two regions: in region ① a slow increase in intensity is found, and in region ② faster increase is observed. Probably region ① is mainly due to scattering at aggregates being formed, and in region ② the scattering at the crystals is dominating. Note that this increase in region ② is observed well before the formation of Bragg reflections.

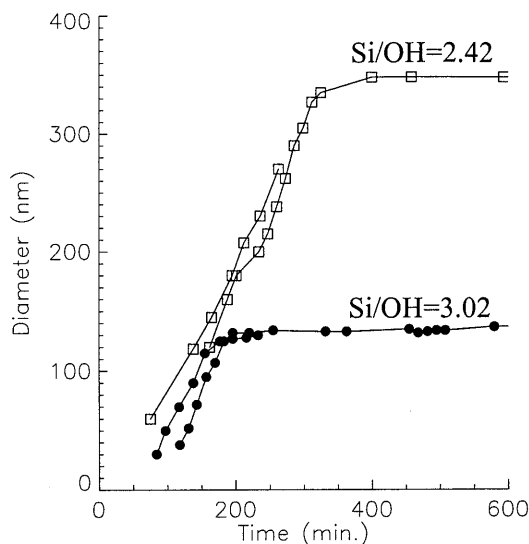


Figure 8: Mean diameter of the crystals as determined by fitting the calculated scattering pattern for a polydisperse system of spheres to the experimental USAXS patterns⁷ for synthesis mixtures with Si/OH values of 2.42 (□) and 3.02 (●).

To confirm that the growing intensity at the very low Q -region is due to scattering at the growing crystals, USAXS experiments have been performed. The Bonse-Hart set-up used together with the high intensity X-rays available at ID2/BL4 of the ESRF, allows probing structures with a size up to 6 microns. These results (chapter 2) showed that the increase in intensity in the low Q region indeed is due to scattering at the growing crystals. Figure 8 shows the mean size of the crystals as determined by fitting the calculated scattering pattern from a polydisperse system of spheres to experimental USAXS data. The linear growth rate of the crystals was found to be the same for both alkalinities (≈ 1.2 nm/min), while the final size of the crystals by far was the largest for the synthesis mixture having the highest alkalinity (Si/OH=2.42).

Influence of seeds

Figure 6 shows that the conversion of silica to MFI is extremely slow for the synthesis mixture having Si/OH=2.12. To be able to discern whether this slow crystallization is due to difficult nucleation or to slow crystal growth (or both), reactions have been performed with adding various amounts of Si-TPA-MFI seeds to the fresh synthesis mixture. To identify the seeds, the stable colloidal seed suspension has been investigated with X-ray scattering and TEM. Figure 9A shows the scattering pattern of a seed suspensions (2.684 wt% SiO₂) compared with the calculated scattering pattern for a polydisperse system of spheres with a normal distribution with a mean diameter of 68 nm and a standard deviation of 14 nm. This particle size distribution shows good agreement with that as determined from TEM images (Figure 9B).

Various amounts of seeds have been added to fresh synthesis mixtures with $\text{Si}/\text{OH}=2.12$ and in all cases a high increase in the crystallization rate was observed compared to the unseeded synthesis mixture. Figure 10 shows the scattering patterns for the synthesis mixture with 0.1 wt% seeds. The scattering pattern after addition of the seed crystals at room temperature (Figure 10, RT), confirms that the scattering at crystals is detected earlier from the scattering at the surface of the crystals in the SAXS-regime than from the diffraction from the internal crystal lattice in the WAXS-regime (as illustrated also in figure 7A). After heating the growth of the crystals can be followed in the USAXS region due to scattering at their surface. When the growth of the crystals has finished, a sudden aggregation of the crystals is observed to aggregates with a size larger than $6\ \mu\text{m}$ (Figure 10, 400 min). The actual size of the aggregates can not be determined since their size exceeds the maximum d-spacing probed in the USAXS experiments. The slope of the linear region in the $\log I$ vs. $\log Q$ plot due to the scattering at these aggregates is -1.8 , which is in agreement with the scattering at aggregates formed by a diffusion limited aggregation process.

The size distribution of the growing seed crystals has been estimated by fitting the calculated scattering pattern of a polydisperse system of spheres to the measured USAXS pattern for synthesis mixtures having $\text{Si}/\text{OH}=2.12$ with 2.5, 0.5, 0.1 and 0.02 wt% seeds added. The evolution of the mean crystal diameter during synthesis for all systems is shown in figure 11. As expected, a synthesis mixture without seeds showed no scattering intensity above the background pattern until the experiment was stopped after 11 h. of heating (because of end of beamtime at the ESRF).

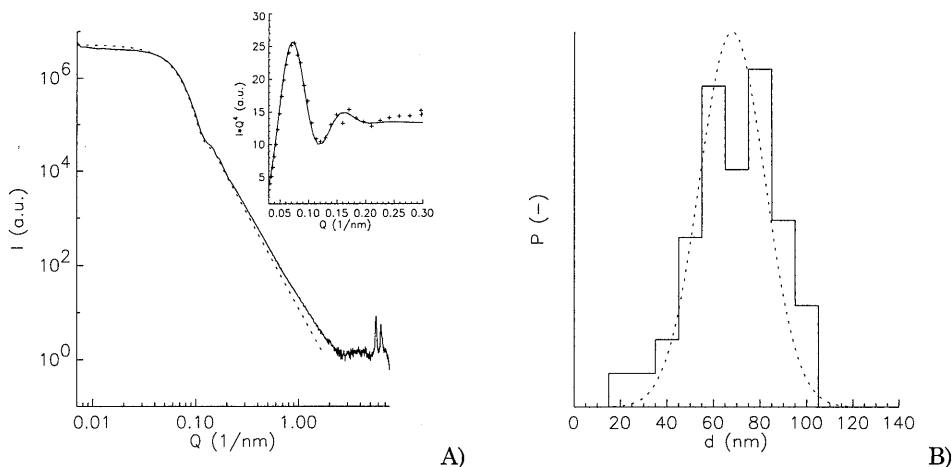


Figure 9: A) (U)SAXS pattern for the seed suspension (solid line) together with the calculated pattern (dotted line) for a polydisperse system of spheres with a normal distribution having a mean diameter of 68 nm and a standard deviation of 14 nm. The IQ^4 vs. Q plot in the inset clearly shows the form factor oscillations in both experimental (+ signs) and calculated data (solid line). B) The particle size distribution used for the calculation (dotted line) and the size distribution of the seed crystals as determined from TEM images (88 crystals measured).

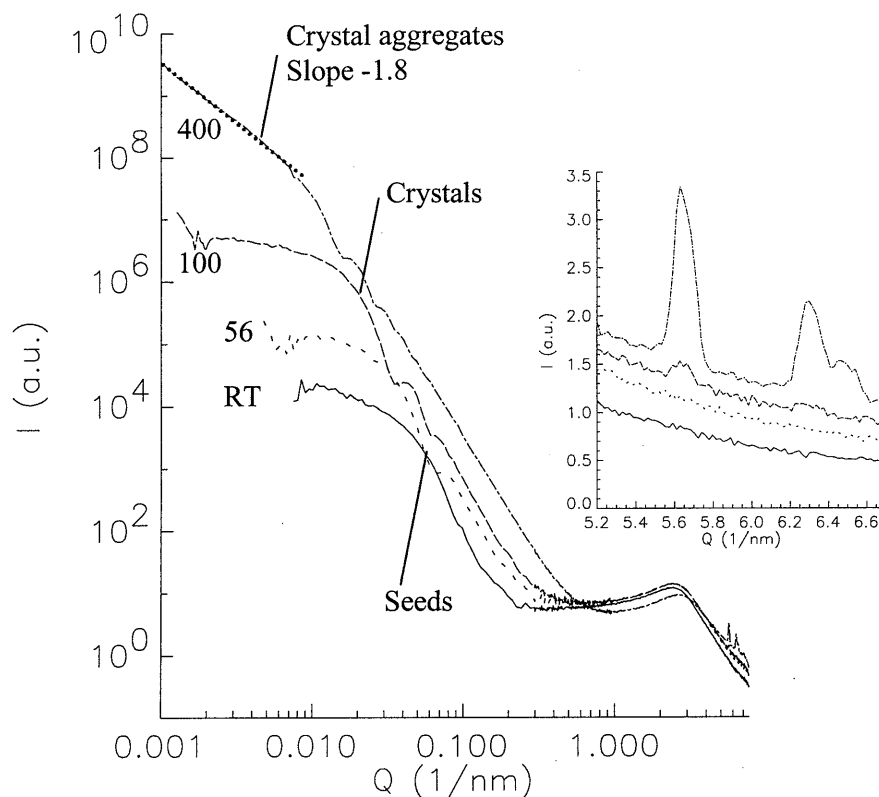


Figure 10: Si-TPA-MFI crystallization from a synthesis mixture with Si/OH=2.12 having 0.1 wt% seeds. The reaction times are denoted at the curves. The inset focuses on the formation of the Bragg reflections in the high-Q region.

For all seed concentrations a linear growth is observed, after which the size of the crystals is constant. The linear growth rate is approximately 1.8 nm/min. independent of the seed concentration (Table 1). Surprisingly, this growth rate is not the same as for unseeded synthesis mixtures having Si/OH=2.42 and 3.02 (Figure 8), but approximately 50% higher. A similar increase in growth rate for seeded versus unseeded synthesis mixtures has been observed before by Twomey *et al.*²⁰. The size of the extrapolation of the linear growth curve to zero reaction time shows an initial mean crystal diameter which is in good agreement with the mean size of the seeds. The final size of the crystals increases with the decreasing amount of seeds, which can be explained by an increasing amount of nutrients available per growing crystal. The SiO₂ conversion after 12 h. of heating was determined from *ex situ* experiments in stainless steel autoclaves. The fraction of amorphous SiO₂ converted into MFI was fairly constant at 0.32 for all amounts of seeds added (see Table 1). For the case with 0.020 wt% seeds, the end of the linear growth region and the final crystal size cannot be determined accurately since the growth curve just levels off near the end of the experiment (Figure 11, around 650 minutes). However, according to the SiO₂ conversion the reaction is

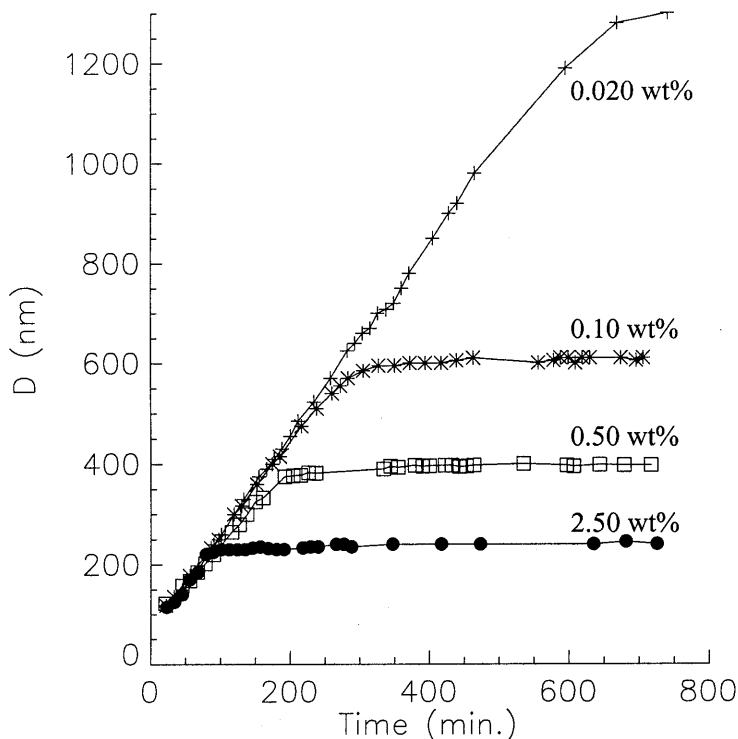


Figure 11: Mean crystal diameter as determined from fitting the calculated scattering pattern of a polydisperse system of spheres to the experimental USAXS patterns for a synthesis mixture with $\text{Si}/\text{OH}=2.12$ with seeds added. The weight percentage seeds (g SiO_2 seeds / g SiO_2 in synthesis mixture) is denoted at the curves.

Table 1: Crystallization Si-TPA-MFI from synthesis mixture with $\text{Si}/\text{OH}=2.12$ with various amounts of seeds. The offset and growth rate are calculated from the linear fit to the data in the linear growth region. The offset is the extrapolation to zero reaction time.

wt% seeds	End linear growth (min.)	Final size (nm)	Conversion (SiO_2 basis)	Offset (nm)	Growth rate (nm/min.)	Fraction growing seeds (-)
2.50	90	240	0.34	64	1.8	0.34
0.50	190	397	0.32	68	1.6	0.36
0.10	295	610	0.32	68	1.8	0.49
0.02	≈650	≈1300	0.31	65	1.9	0.25

expected to be finished after 12 h. of heating, since then the SiO_2 conversion was found to be independent of the amount of seeds (Table 1).

The comparison of the particle size distributions as determined by the fitting procedure with USAXS patterns and from electron microscopy images (Figure 12) reveals some small systematic differences between the results of the two

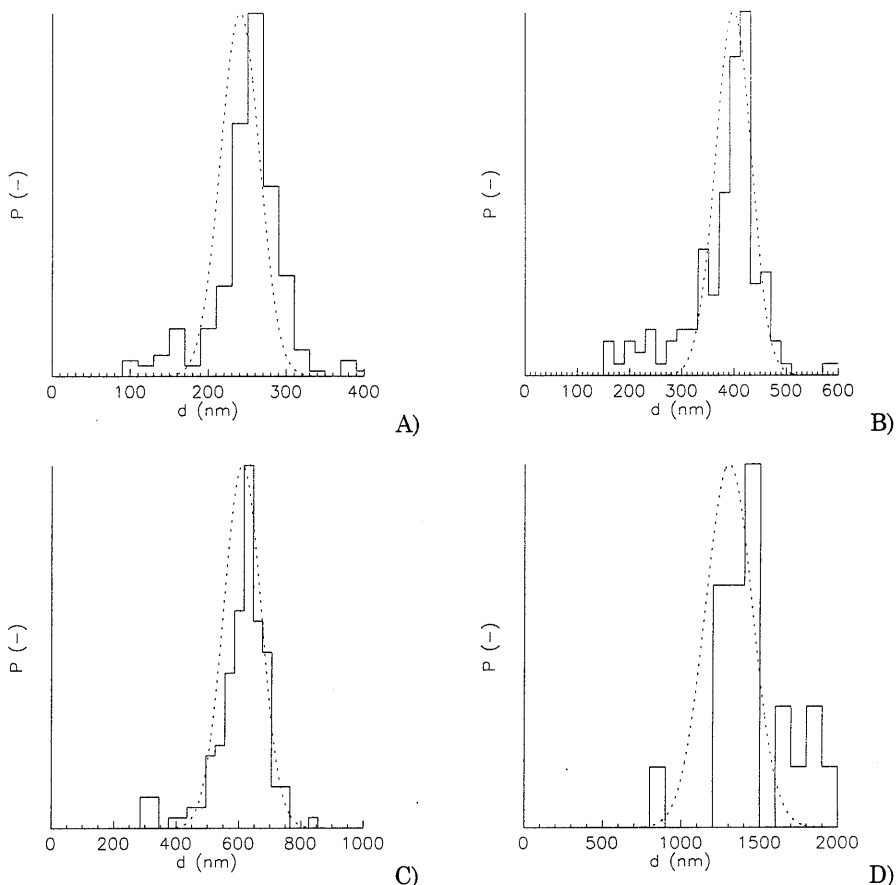


Figure 12: Crystal size distribution for Si-TPA-MFI synthesis mixtures with $Si/OH=2.12$ and various amounts of seed crystals after 12 h. of heating at $125^{\circ}C$. The dotted line gives the size distribution as resulted from the fitting procedure of the USAXS data. The histogram is the result of measured particle sizes from TEM images. A), B), C) and D) represent respectively 2.50, 0.50, 0.10, 0.020 wt% seeds, and the number of crystals measured from TEM images is respectively 228, 142, 144, and 21.

methods. The maximum in the particle size distribution is at slightly larger diameters for the TEM results compared to the fitting results. Also, the particle size distribution from the TEM results appears not to be symmetric, having a longer tail on the small diameter side of the maximum (except for 0.020 wt% seeds, but the histogram from the TEM results is based on a small number of crystals and therefore not very reliable). Altogether there is satisfying agreement between the results of the two methods.

The number of crystals in the product relative to the number of seeds added can be calculated using the particle size distribution of both seeds and product, the weight fraction seeds added, and the SiO_2 conversion (equation 1, p. 43). Here the particle size distribution as resulted from the fitting procedure has been used to

calculate the average volume of the seeds and the crystals in the final product. This ratio does not show a clear trend with the weight fraction of seeds, but the results show that the number of crystals in the final product is about $1/3^{\text{rd}}$ of the number of seeds added. The electron microscopy images of the product did not show the presence of unreacted seed crystals (Figure 12).

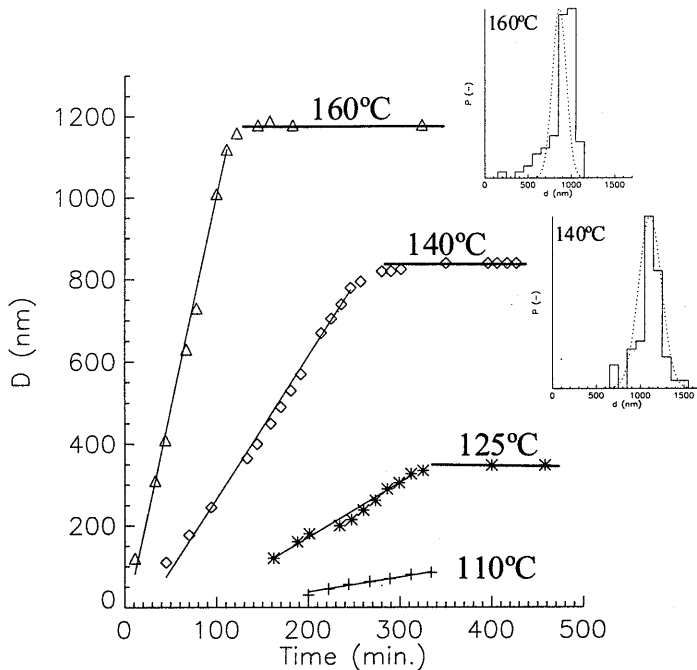
Synthesis temperature

To determine the activation energy for crystal growth, the crystallization from synthesis mixtures with $\text{Si}/\text{OH}=2.42$ has been performed at various temperatures, and was studied *in situ* with USAXS. The mean diameter of the growing crystals has been determined by fitting the calculated scattering pattern of a polydisperse population of spherical crystals to the measured USAXS curve. Figure 13A shows the size evolution of the crystals as a function of reaction time. From this plot it is clear that the crystals grow linearly in time, and that the expected lower linear growth rate is found for lower reaction temperatures. For reaction temperatures of respectively 110, 125, 140, and 160°C, the linear growth rate was respectively 0.36, 1.35, 3.49, and 10.4 nm/min.. The particle size distributions of the final product for the syntheses at 140 and 160°C as determined from the USAXS fitting procedure and from TEM images show good agreement (Figure 13A, inset). The apparent activation energy for Si-TPA-MFI crystal growth was determined to be 83 kJ/mol from the Arrhenius type of plot in Figure 13B. In literature there is quite some scattering in the value for the apparent activation for crystal growth (Table 2).

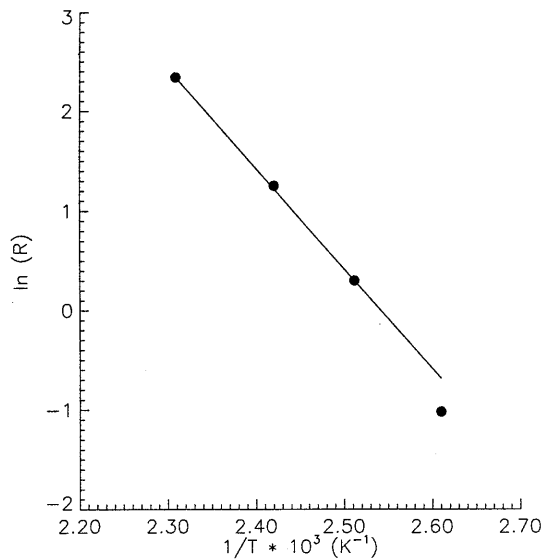
4.4 Discussion

Precursor and product particles

The small-angle scattering patterns (figures 1 and 2) provide information on the formation and consumption of nanometer-scale precursor particles and the crystalline product. Irrespective of the alkalinity, the presence of 2.8 nm sized primary units was observed from the onset of the reaction. The primary units are therefore expected to be formed during the dissolution of the silicic acid in the TPAOH solution. The estimated size of these particles is the same as reported for visible light scattering experiments by Schoeman^{13,14}. From NMR experiments, it is known that silicate species interact with TPA cations prior to the onset of crystallization⁵. TPA is clearly identified as being present in the precursor particles from contrast variation SANS experiments on synthesis mixtures¹⁵ and Raman experiments on particles extracted from the aqueous solution¹³. Ordering in the silica (observation of 560 cm^{-1} IR band) in structures typical for the MFI crystal topology was observed before the onset of the crystallization⁶. Combining this evidence from varying experiments, we believe the observed particles to be composite organic-inorganic particles which do contain some ordering of the silica related with the MFI structure, but not fully organized yet in a crystalline lattice.



A)



B)

Figure 13: A) Crystal growth for synthesis mixtures with Si/OH=2.42 at various temperatures as denoted at the curves. The insets show the particle size distribution of the final product as determined from the fitting procedure and from TEM images for reaction temperatures of 140 and 160°C. B) Arrhenius plot from the linear growth rates of the diameter of the crystals as determined from the growth curves.

Table 2: Apparent activation energy for Si-TPA-MFI crystal growth in the length and the width (respectively E_{length} and E_{width}), and for crystals (E_{crystal}) when no distinction was made. The values between parentheses for crystal growth have been calculated here from the reported values for length and width growth by averaging, for comparison of the activation energies for crystal growth.

Source	E_{length} (kJ/mol)	E_{width} (kJ/mol)	E_{crystal} (kJ/mol)
Schoeman <i>et al.</i> ¹⁶			42
Sano <i>et al.</i> ¹⁷	61	36	(48)
Feoktistova <i>et al.</i> ¹⁸	64.5	46.5	(55)
Cundy <i>et al.</i> ¹⁹	79	62	(70)
Watson <i>et al.</i> ¹⁵			70
This study			83
Twomey <i>et al.</i> ²⁰			96

The formation of a second population of precursor particles is strongly dependent on the alkalinity of the synthesis mixture (Figure 4). These particles are believed to be aggregates of the primary units, and the scattering curves (Figure 2C and D) show that their size increases with reaction time to approximately 10 nm until they are consumed in the crystallization process.

From our X-ray scattering data on crystallizations from clear solutions, there are two methods to track the formation of crystals (third particle population): from the scattering at the crystal surface, which is observed at relatively large length scales (small angles), and from the diffraction at the internal crystalline lattice of the crystals (Bragg reflections). Figure 7A illustrates that the scattered intensity at the surface of the crystal is observed much earlier than the diffraction at the crystalline lattice (also clear in Figure 1,2, and 10,RT). However, one has to be careful in the interpretation of the scattering intensity at very low angles, since also the scattering at large, non-crystalline structures as the aggregates of primary units is observed in this region (Figure 7B). Therefore, the area of the Bragg reflections as observed in the high Q region is taken as a measure for the conversion of SiO₂ to crystalline material.

Role nanometer-scale precursors

To elucidate the role of the precursor particles, their formation and consumption has to be related to the crystallization behaviour. Figure 6B shows that the final SiO₂ conversion decreases with increasing alkalinity. This can be explained by a higher dissolution rate of the crystals at higher alkalinity. For Si/OH ratios of 3.02, 2.72, and 2.57 the rate of SiO₂ conversion to MFI is similar, as is shown in figure 6A. For lower Si/OH-values (higher alkalinities) however, a clear decrease in conversion rate is observed, whereas the rate is extremely low for Si/OH=2.12. Also, the fitting of the USAXS patterns shows that the growth rate of the crystals is the same for Si/OH=2.42 and 3.02. This means that the slower conversion of SiO₂ to Si-MFI for increasing alkalinity cannot be attributed to a lower growth

rate (higher dissolution rate) of the crystals, but results from a lower number of crystals due to a reduced rate of nucleation.

This is confirmed by the experiments with $\text{Si}/\text{OH}=2.12$, which show a very slow crystallization (Figure 6A). This would mean that growth does not occur since the crystallization is blocked due to the absence of nucleation. As a control experiment to check whether a synthesis mixture is able to grow Si-TPA-MFI crystals, seeds have been added to by-pass the nucleation step. The scattering experiments (Figure 10) show that normal crystal growth is observed when seeds have been added to a fresh synthesis mixture having a Si/OH -ratio of 2.12. This proves that in a synthesis mixture having $\text{Si}/\text{OH}=2.12$ without seeds, nucleation is (almost) impossible, while growth is possible once crystals are present.

By simultaneously measuring small- and wide-angle scattering, we are able to correlate the crystallization behaviour to the presence and consumption of nanometer-scaled precursor particles. Figure 4 illustrates that the 2.8 nm sized primary units (peak at 2.2 nm^{-1}) are invariant for Si-TPA-MFI synthesis mixtures with varying alkalinity. In contrast, the formation of aggregates of these primary units is dependent on the alkalinity, and shows a strong correlation with the number of crystals, i.e. the rate of nucleation: a high nucleation rate is observed when a high concentration of aggregates is observed (high Si/OH -ratios), while the nucleation rate (almost) vanishes when no formation of aggregates is observed. The formation of aggregates of primary units is therefore believed to be an essential step in the nucleation.

The role of the primary units and their aggregates is confirmed by the evolution of their concentrations in relation to the conversion of amorphous SiO_2 to Si-MFI. The role of the aggregates in the nucleation process is strengthened by the onset of their consumption at the beginning of the crystallization (Figure 3B, C and D). The strong decrease of the scattered intensity from the aggregates also shows that only a small fraction of them transforms into viable nuclei, and that the vast majority dissolves to smaller precursor particles. The scattering at the primary units is almost constant until most of the aggregates have disappeared as shown in figure 3 and figure 2B,C,D (3rd curve). Probably the dissolution of the aggregates compensates the consumption of the primary units in the crystallization process. After the aggregates have disappeared, a fast consumption of the primary units is observed. Therefore, the omnipresent 2.8 nm sized primary units probably play a key role in the crystal growth process.

Seeding

The influence of seeding on the crystal growth behaviour has been investigated for Si-TPA-MFI synthesis mixtures with $\text{Si}/\text{OH}=2.12$, showing very slow nucleation when no seeds are added. The crystal growth history has been followed by fitting the scattering pattern of a polydisperse system of interacting spheres with the experimental scattering patterns. Also, the size distributions from the fitting procedure at the scattering curves of the seed crystals (Figure 9) and final product of the reactions (Figure 12) show good agreement with those as

determined from the TEM images. Therefore we believe that the fitting procedure of the scattering data yields reliable information on the size history of the crystals. An advantage of using small-angle X-ray scattering for this purpose is that this allows to determine *in situ* the crystal growth over the entire length range on one and the same sample, even when the system becomes turbid during the synthesis.

Figure 10 illustrates that the scattering patterns for a synthesis mixture having $\text{Si}/\text{OH}=2.12$ with 0.10 wt% seeds added, show strong agreement with the patterns for a synthesis mixture having $\text{Si}/\text{OH}=2.42$ without seeds (Figure 2A). When the growth of the crystals has finished, aggregation of the discrete crystals is observed to aggregates with a mass fractal dimension of 1.8 (Figure 10, 400 min.). This feature was previously observed for unseeded synthesis mixtures having $\text{Si}/\text{OH}=2.42$ and 3.02 (chapter 2). The size of the aggregates could not be determined, since it exceeds the maximum probed length-scale of 6 microns. This sudden aggregation of the discrete crystals is believed to be due to a change in the composition of the solution, resulting in a decrease of the repulsive forces between the crystals.

The number of crystals in the product relative to the number of seeds added can be calculated from the silica conversion, the weight fraction of seeds added, and the particle size distributions of the seed crystals and the final product (equation 1, p. 43). This fraction shows that the number of crystals in the final product is in the order of one third of the number of seeds (Table 1). A possible effect is that the added seeds do not grow, but that they only induce nucleation in synthesis mixtures that show no nucleation in the unseeded situation. But, the offset of the growing crystals for the synthesis mixtures having various degrees of seeding in all cases is close to the size of the seed crystals. Therefore it is believed that the seeds actually grow to the final product crystals. Another possible explanation of the fact that just one third of the seeds grows to crystals is that a fraction of them is inert. This explanation is not favoured since no crystals in the size range of the seeds are observed in the electron microscopy images of the product. Therefore we believe that approximately one third of the seeds added to the synthesis mixture grows, while the rest (predominantly the smaller fraction) dissolves, similar to Ostwald ripening in silica particles²¹.

By varying the amount of seed crystals, we are able to control the number of growing crystals in the synthesis mixture. Figure 11 shows that the linear growth rate is independent of the weight fraction of seeds (ranging from 0.020 to 2.5 wt%). Therefore, the formation of structures which are consumed in the crystal growth process is not the rate limiting step. This is in agreement with the observation that the 2.8 nm sized primary units are present from the start of the reaction. The growth rate dependence on the reaction temperature shows an apparent activation energy for crystal growth of 83 kJ/mol (Figure 13). Although there is significant scattering in this value in literature, all values are well above the activation energy of 12-17 kJ/mol which is to be expected for a diffusion controlled growth mechanism²². In a previous study²³ (Chapter 3), we found the conversion of SiO_2 to MFI to be independent on the concentration of the synthesis

mixture, which also means that the crystal growth is not diffusion controlled. This is in accord with the abundant presence of the primary units and with a growth mechanism where the integration of the primary units at the crystal surface is the rate limiting step.

4.5 Conclusions

The results presented here show that a combination of USAXS and SAXS/WAXS experiments is a powerful tool to probe *in situ* a broad range of length scales covering all precursor and product particle populations during the whole course of the zeolite crystallization. The crystal particle size distribution as determined from the fitting of a calculated scattering pattern of a polydisperse system of spheres to the measured patterns shows good agreement with the distribution as determined from electron microscopy images. Comparing these results with the results in chapters 2 and 3 shows the importance of performing experiments covering the complete range of length scales relevant for the assembly process.

For the crystallization of Si-TPA-MFI from a clear synthesis mixture, three particle populations are observed: primary units, their aggregates, and the crystals. Both the primary units and their aggregates are precursors and are consumed during the formation of the crystalline product. By varying the alkalinity of the fresh synthesis mixtures and the use of seed crystals we were able to show that the aggregation of the 2.8 nm sized primary units is an essential step in the nucleation process. The crystal growth probably is the reaction controlled integration of primary units at the crystal surface.

References

- 1 Van Bekkum, H.; Flanigen, E.M.; Jansen, J.C. (Ed.), *Introduction to zeolite science and practice*, Studies in surface science and catalysis, Elsevier, 1991, **58**
- 2 Davis, M.E.; Katz, A.; Ahmad, W.R. *Chem. Mater.*, 1996, **8**, 1820-1839
- 3 Davis, M.E.; Lobo, R.F. *Chem. Mater.*, 1992, **4**, 756-768
- 4 Bell, A.T. in: Occelli, M.L.; Robson, H.E. (Eds.) *Zeolite synthesis*, ACS Symp. Ser. 398, American Chemical Society, Washington DC, 1989, pp. 66-82
- 5 Burkett, S.L.; Davis, M.E. *J. Phys. Chem.* 1994, **98**, 4647-4653
- 6 Burkett, S.L.; Davis, M.E. *Chem. Mater.* 1995, **7**, 920-928
- 7 De Moor, P.-P.E.A.; Beelen, T.P.M.; Komanschek, B.U.; Diat, O.; Van Santen, R.A. *J. Phys. Chem. B*, 1997, **101**, 11077-11086
- 8 Verduijn, J.P. *Exxon patent*, PCT/EP92/02386, 1992
- 9 Bras, W.; Derbyshire, G.E.; Ryan, A.J.; Mant, G.R.; Felton, A.; Lewis, R.A.; Hall, C.J.; Greaves, G.N. *Nucl. Instrum. Methods Phys. Res. Sect. A*, 1993, **326**, 587
- 10 Diat, O.; Bösecke, P.; Lambard, J.; De Moor, P.-P.E.A. *J. Appl. Cryst.* 1997, **30**, 862
- 11 Mulato, M.; Chambouleyron, I. *J. Appl. Cryst.* 1996, **29**, 29-36
- 12 Pedersen, J.S. *J. Appl. Cryst.*, 1994, **27**, 595-608
- 13 Schoeman, B.J., in: Chon, H.; Ihm, S.-K.; Uh, Y.S. (Eds.) *Progress in zeolite and microporous materials*, Studies in surface science and catalysis, Elsevier Science B.V., 1997, **105**, pp. 647-654

- ¹⁴ Schoeman, B.J. *Zeolites* 1997, **18**, 97-105
- ¹⁵ Watson, J.N.; Iton, L.E.; Keir, R.I.; Thomas, J.C.; Dowling, T.L.; White, J.W. *J. Phys. Chem. B*, 1997, **101**, 10094-10104
- ¹⁶ Schoeman, B.J.; Sterte, J.; Otterstedt, J.E. *Zeolites* 1994, **14**, 568-575
- ¹⁷ Sano, T.; Sugawara, S.; Kawakami, Y.; Iwasaki, A.; Hirata, M.; Kudo, I.; Ito, M.; Watanabe, M. In: *Zeolites and Related Microporous Materials: State of the Art 1994*, Studies in Surface Science and Catalysis, Elsevier Science, 1994, **84**, pp. 187-194
- ¹⁸ Feoktistova, N.N.; Zhdanov, S.P.; Lutz, W.; Bülow, M. *Zeolites*, 1989, **9**, 136-139
- ¹⁹ Cundy, C.S.; Lowe, B.M.; Sinclair, D.M. *Faraday discuss.*, 1993, **95**, 235-252
- ²⁰ Twomey, T.A.M.; Mackay, M.; Kuipers, H.P.C.E.; Thompson, R.W. *Zeolites*, 1994, **14**, 162-168
- ²¹ Iler, R.K. *The chemistry of silica*, John Wiley and Sons, 1979
- ²² R.M. Barrer, *Hydrothermal Chemistry of Zeolites*, Academic Press, London, 1982, chapter 5
- ²³ De Moor, P.-P.E.A.; Beelen, T.P.M.; Van Santen, R.A. *J. Appl. Cryst.*, 1997, **30**, 675-679

Gelating systems*

In the synthesis of zeolites, in general a heterogeneous gel phase is formed upon mixing of the reagents or when the synthesis mixture is brought to reaction temperature. During the crystallization process, changes in the physical appearance of the gel can be observed, often accompanied by shrinkage and subsequent expelling of liquid. Therefore a different mechanism compared to crystallization from clear solutions might be expected. In this chapter we discuss the crystallization of Si-MFI, Si-BEA, and Si-MTW from gelating systems, taking full advantage of the possibility using USAXS to probe large structures in a concentrated, turbid system, together with small, nanometer-scale entities. The comparison of the gelating Si-MFI with the clear solution synthesis discussed in chapter 4, and the extension to other zeolite morphologies, provides strong support on the generality of the observed features for the mechanism of organic-mediated zeolite crystallization.

* Submitted for publication: P.-P.E.A. de Moor, T.P.M. Beelen, R.A. van Santen, K. Tsuji, M.E. Davis, SAXS and USAXS investigation on nanometer scaled precursors in organic-mediated zeolite crystallization from gelating systems, *Chem. Mater.*

5.1 Introduction

Microporous crystalline solids are industrially important materials applied in catalysis, ion exchange, and gas separation processes. Because of their well-defined (crystalline) morphology, there is a close relationship between their microscopic structure and macroscopic properties. This relationship has been a large incentive for the synthesis of new materials with novel pore architectures and crystal compositions¹. Many investigations have been carried out to understand the mechanisms in the conversion of amorphous reactants to microporous crystalline frameworks.

Traditionally, investigations on mechanisms in the crystallization of zeolites are often based upon observations of the products formed. Knowledge concerning the intermediates and their transformations is limited, mainly due to two experimental problems. Firstly, the intermediates are often built from particles connected by relatively weak bonds, which makes them very fragile, and so only *in situ* experiments can give reliable results. Secondly, the dimensions of the intermediates are such (>1 nm) that most spectroscopic techniques are not informative. Some problems can be circumvented using light scattering techniques^{2,3,4} and crystallizations from water-clear solutions. Unfortunately, visible light scattering does not allow to observe all precursor particles during the whole course of the crystallization process. Also, in most zeolite crystallizations a turbid gel phase is formed, for which visible light scattering cannot be informative.

Because thin layers of reaction mixtures are transparent to X-rays, we use X-ray scattering to probe samples irrespective of their consistency and appearance. The diffraction of nano-sized entities by X-rays is observed at (very) small angles (<1°). For the crystallization of Si-TPA-MFI from a clear solution, we were able to probe the formation and transformations of precursor particles during the whole course of the crystallization process^{5,6} (see chapter 4). We observed the formation of 2.8 nm sized primary units, as also reported by Schoeman for fresh synthesis mixtures^{3,4}. Additionally, we found a second population of amorphous precursor particles to be present (size ≈10 nm), depending on the alkalinity of the synthesis mixture. Using simultaneous small- and wide-angle X-ray scattering (SAXS/WAXS) we probed *in situ* on one sample the formation of the different precursor particles and their subsequent consumption in the nucleation and crystal growth process.

In this chapter a small-angle X-ray scattering study is presented on the organic-mediated crystallization of Si-MFI, Si-BEA, and Si-MTW from gelating systems, taking full advantage of the possibility to probe precursor particles in a heterogeneous gel phase. Using a combination of ultra-small-angle X-ray scattering (USAXS) and simultaneous SAXS/WAXS, we probed an extremely broad range of length scales (4 decades), allowing us to identify both the structure of the gel phase and the formation of nanometer-scaled primary units. The observed precursors in the crystallization of Si-MFI from a gel phase using

trimethylene-bis(N-hexyl, N-methyl-piperidinium) as structure-directing agent are compared with those formed in the synthesis of Si-TPA-MFI from a clear solution as discussed in chapter 4. Si-BEA and Si-MTW are synthesised using the same structure-directing agent at different concentrations, with the identification of correlations between the precursors present in the synthesis mixture and the crystalline structure formed as the main objective.

5.2 Experimental

The structure-directing agents used for the synthesis of Si-MFI, Si-BEA, and Si-MTW, as well as the recipes for the zeolite crystallizations, were kindly provided by Katsuyuki Tsuji in the group of Mark Davis, department of Chemical Engineering, California Institute of Technology.

The crystallization of Si-MFI using trimethylene-bis(N-hexyl, N-methyl-piperidinium) as structure-directing agent⁷, from a synthesis mixture with molar composition $10 \text{ SiO}_2 : 3.0 \text{ R(OH)}_2 : 0.5 \text{ NaOH} : 350 \text{ H}_2\text{O}$, was performed at 160°C . In both the synthesis of Si-BEA at 150°C and of Si-MTW at 160°C , we used trimethylene-bis(N-benzyl, N-methyl-piperidinium) as structure-directing agent. For Si-BEA the molar composition of the synthesis mixture was $10 \text{ SiO}_2 : 1.50 \text{ R(OH)}_2 : 0.5 \text{ NaOH} : 350 \text{ H}_2\text{O}$, and for Si-MTW it was $10 \text{ SiO}_2 : 0.70 \text{ R(OH)}_2 : 1.3 \text{ NaOH} : 350 \text{ H}_2\text{O}$. The preparation method of the synthesis mixtures was identical for all syntheses using bis-piperidinium compounds, and will be outlined here for the case of Si-MFI.

In a recovery flask 0.40 mmol NaOH ($=0.32 \text{ g}$ of $5 \text{ wt}\%$ solution in H_2O) was added to 1.20 mmol trimethylene-bis(N-hexyl, N-methyl-piperidinium) dihydroxide solution (1.486 g of 0.8074 mmol/g solution in H_2O) and shaken gently to get a homogeneous solution. 8 mmol tetraethyl-orthosilicate ($=1.70 \text{ g}$, Aldrich, $98 \text{ wt}\%$) was added and the mixture was stirred for 3 hours. The ethanol formed during the hydrolysis was removed using a vacuum evaporator at approximately $40\text{--}45^\circ\text{C}$. Deionised water was added to obtain a molar ratio $\text{H}_2\text{O}/\text{SiO}_2=35$ (total weight synthesis mixture: 6.092 g). For Si-MFI, the fresh synthesis mixture was white cloudy, while it was an almost water-clear solution in case of Si-BEA and Si-MTW. After heating to reaction temperature a heterogeneous gel phase is formed within a few minutes in all cases.

Synthesis of Si-TPA-MFI from a completely water-clear solution with molar composition $10 \text{ SiO}_2 : 2.437 \text{ TPAOH} : 1.695 \text{ NaOH} : 113.9 \text{ H}_2\text{O}$ was performed at 125°C as reported elsewhere⁸ (see also chapter 2). In the preparation of the TPA-free solution (water glass), the molar composition was $10 \text{ SiO}_2 : 4.132 \text{ NaOH} : 113.9 \text{ H}_2\text{O}$.

All measurements have been performed *in situ* in a special rotating (2 r.p.m.), electrically heated sample cell. The sample thickness was 0.5 mm and mica windows (thickness $0.25\mu\text{m}$) were used. The scattering of water between mica windows at reaction temperature has been used as background pattern.

The combined SAXS and WAXS experiments have been performed at station 8.2 of the Synchrotron Radiation Source at Daresbury Laboratory (UK)⁹, using a camera length of 0.8 ($0.4 < Q < 7 \text{ nm}^{-1}$) and 3.4 m ($0.1 < Q < 2.5 \text{ nm}^{-1}$). The USAXS experiments have been performed at the high-brilliance beamline ID2/BL4 of the European Synchrotron Radiation Facility in Grenoble (FR) using a Bonse-Hart type of camera¹⁰ ($0.001 < Q < 0.3 \text{ nm}^{-1}$). A configuration with two analyser crystals has been used, so no desmearing was necessary. The Q -ranges obtained with the USAXS and SAXS showed sufficient overlap to allow an accurate merging of the patterns. Details concerning the combined SAXS and WAXS set-up and the Bonse-Hart type of camera, and some basic principles on the interpretation of SAXS data, can be found in chapter 2.

5.3 Results

The results presented here are from both gelating and clear solution zeolite synthesis mixtures. The distinction is based on the appearance of the synthesis mixture: in a gelating system a heterogeneous, percolating SiO_2 network is formed (i.e. a solid gel phase), while this is absent in the crystallization from a clear solution. In this thesis we use the term gel particles for all amorphous precursors which are very large compared to the monomers they are built of ($\geq 10 \text{ nm}$). This means that the term gel particles can be used for precursor particles in a clear solution, where they do not form a percolating network but rather are present as dissolved particles.

MFI

The fresh liquid synthesis mixture had a white cloudy appearance. The scattering pattern from the fresh sample at room temperature (figure 1A), shows two weak 'shoulders', each of which represents the scattering at one type of particles. The hump at approximately $Q=0.02 \text{ nm}^{-1}$ is due to scattering by gel particles with a size of the order of 300 nm ($d=2\pi/Q$). The shoulder around $Q=2.5 \text{ nm}^{-1}$ is due to scattering from nanometer-scaled precursors, which we denote primary units.

Within a few minutes of heating to a reaction temperature of 160°C , a solid gel phase was formed. The scattering from the primary units now showed a maximum, as illustrated by the scattering pattern after 4 h (Figure 1A, I). This maximum points to the presence of interacting particles, such that preferred distances between the particles exist. This results in a maximum in the structure factor for this particle population, which gives a maximum in the observed scattering intensity^{11,12}. The size of the particles is approximated to be $2.8\text{-}3.0 \text{ nm}$ from the position of the maximum ($d=2\pi/Q$). At smaller scattering angles we now observe the scattering at two populations of gel particles. The smallest population ($\approx 40 \text{ nm}$, Figure 1A, II) gives rise to a linear region with a slope of -3.8 in the $\log I$ vs. $\log Q$ presentation of the scattering pattern, which corresponds with scattering at gel particles with a rather smooth surface^{13,14} (a slope of -4 would correspond to a perfectly smooth surface of spherical particles). The

shoulder at $Q \approx 0.01$ is probably the scattering from the gel particles which were already present at room temperature, but which have grown promptly after heating to the order of 600 nm, resulting in a shift to smaller angles of the crossover to homogeneous scattering.

Two types of scattering patterns were recorded for reaction times longer than 6 hours, depending on the part of the heterogeneous gel phase in the sample which was probed (Figure 1A, 10 h. and 12h.). The first type shows the scattering of two different precursor particles: the nanometer-scale primary units, and gel structures with a size of ≈ 600 nm (Figure 1A, 10 h.). The pattern after 12 hours of heating shows two maxima: at high angles, which corresponds to the presence of the primary units, and at very small angles ($Q \approx 0.01$) a similar pattern. We can interpret this second maximum in the same way as the one due to the primary units: the scattering is due to strongly interacting particles which show preferred interparticle distances. Here the individual particles are have a magnitude of approximately 600 nm. Since no crystallinity has been detected by the *in situ* WAXS at these reaction times (Figure 1B), the scattering entities with a size of 600 nm can be interpreted as being amorphous gel particles.

The onset of crystallization as determined from the appearance of Bragg reflections in the WAXS pattern was observed between 45.5 and 48 h. of heating (Figure 1B). After a significant degree of crystallization took place (Figure 1B, 54 h.), a decrease of the concentration of primary units is observed in the SAXS (Figure 1A, D).

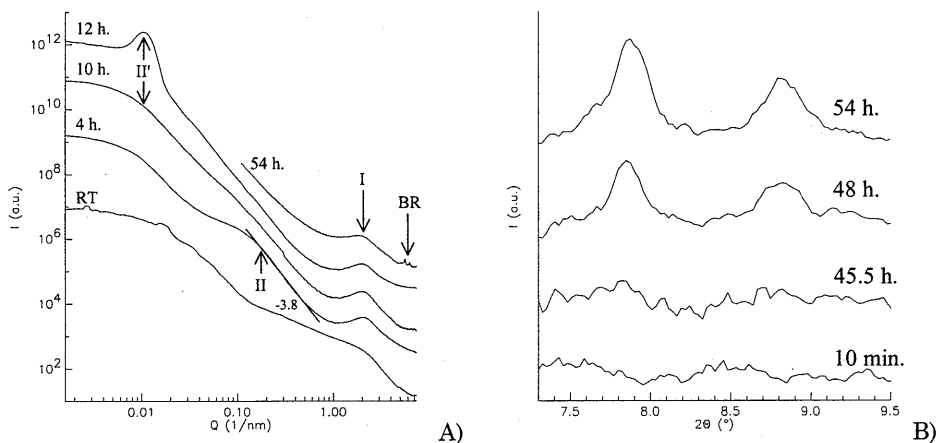


Figure 1: A) Scattering patterns of a Si-MFI synthesis mixture using trimethylenebis(*N*-hexyl, *N*-methyl-piperidinium) as structure-directing agent. The annotations give the reaction time (the annotation RT refers to a fresh synthesis mixture at room temperature, before heating) and the slope of the linear fit. I: 2.8-3.0 nm sized primary units, II: ≈ 40 nm gel particles, II': ≈ 600 nm gel particles, BR: Bragg reflections. For sake of clearness, the patterns have been shifted vertically. B) The first two Bragg reflections as observed by the WAXS-pattern after various reaction times.

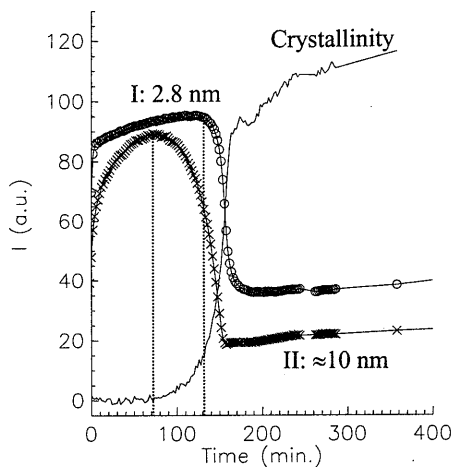


Figure 2: Scattering intensity from the different particle populations and the crystallization behaviour as determined from the area of Bragg reflections for the crystallization of Si-TPA-MFI from a clear solution with Si/OH=3.02 (taken from ref. 6). I: 2.8 nm sized primary units, II: ≈ 10 nm gel particles

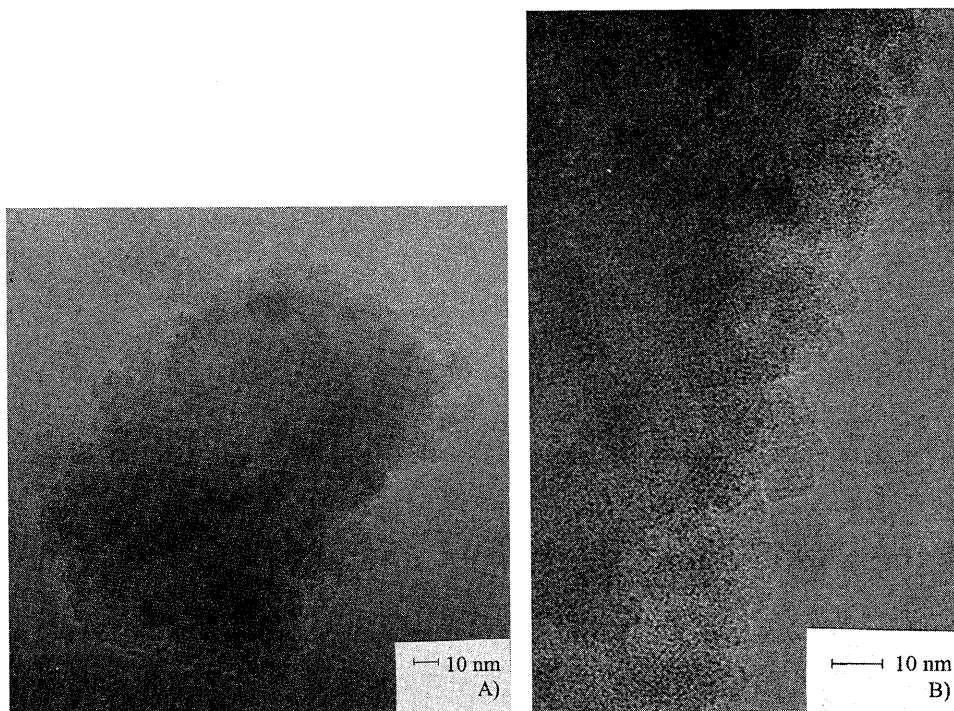


Figure 3: TEM micrographs of Si-MFI prepared using trimethylene-bis(N-hexyl, N-methyl-piperidinium). A) A representative crystal. B) The surface morphology.

For the crystallization of MFI from a water-clear synthesis mixture, using TPA as a structure-directing agent, we found a correlation between the formation and consumption of precursor particles on one side, and the crystallization behaviour as determined from the Bragg reflections⁶ on the other side (see chapter 4). 2.8 nm sized particles were observed from the onset of the reaction and amorphous ≈ 10 nm sized gel particles were formed prior to the onset of crystallization. As the crystallization starts, the consumption of the ≈ 10 nm sized gel particles is observed prior to the effective consumption of the 2.8 nm primary units (Figure 2). A similar behaviour is observed in the gelating system using trimethylene-bis(N-hexyl, N-methyl-piperidinium) as organic molecule: amorphous gel particles with a size of several tens of nanometers are formed after heating, while 2.8 nm sized primary units are present from the onset. The consumption of the gel particles (II in Figure 1A and 2) is observed prior to the consumption of the 2.8 nm sized particles. In the case of the clear solution synthesis, the consumption of the gel particles (≈ 10 nm) corresponds with the onset of crystallization, while their consumption in the heterogeneous gel synthesis is observed well before the onset of crystallization (Figure 1B).

The transmission electron microscopy images show crystals with a broad size range from 80 to 600 nm. The particles do not show clear crystal faces, but were more or less cauliflower-shaped (Figure 3A). The rough surface of the crystals gives the impression that it is composed of 10 to 20 nm sized crystalline particles which mostly have the same orientation as the crystal. However, on close observation fringes can be observed which indicate the existence of several orientations at the surface (Figure 3B).

BEA

The scattering pattern of the fresh synthesis mixture of Si-BEA at room temperature is similar to that for the Si-MFI synthesis described above (Figure 4A). Since no USAXS data is available, the Q-range for the BEA and MTW cases is smaller than for MFI. After heating to reaction temperature (150°C) we again observed the formation of rather smooth (slope -3.9) particles with a size in the order of several tens of nanometers. In this experiment we were able to follow their growth, by approximating their size from the Q-value where the linear fit levels off upon decreasing angle. The growth of the particles appears to be linear against the logarithm of the reaction time (Figure 4B). After 10 hours of heating, the scattering of the gel particle population could not be observed any longer, because the size of the particles was larger than the maximum d-spacing which could be probed. These particles are believed to be amorphous since no sign of crystallinity is observed in the WAXS pattern yet.

As in the synthesis of Si-MFI, again the formation of nanometer-scale primary units was observed. Their size now is estimated to be 2.6 nm (Figure 4A, I). However, no pronounced maximum was observed for this synthesis, possibly because of the lower concentration of the structure-directing agent for the synthesis of Si-BEA compared with the Si-MFI example. The first sign of crystallization of Si-BEA was observed after 32 h. of heating (Figure 4C). Because

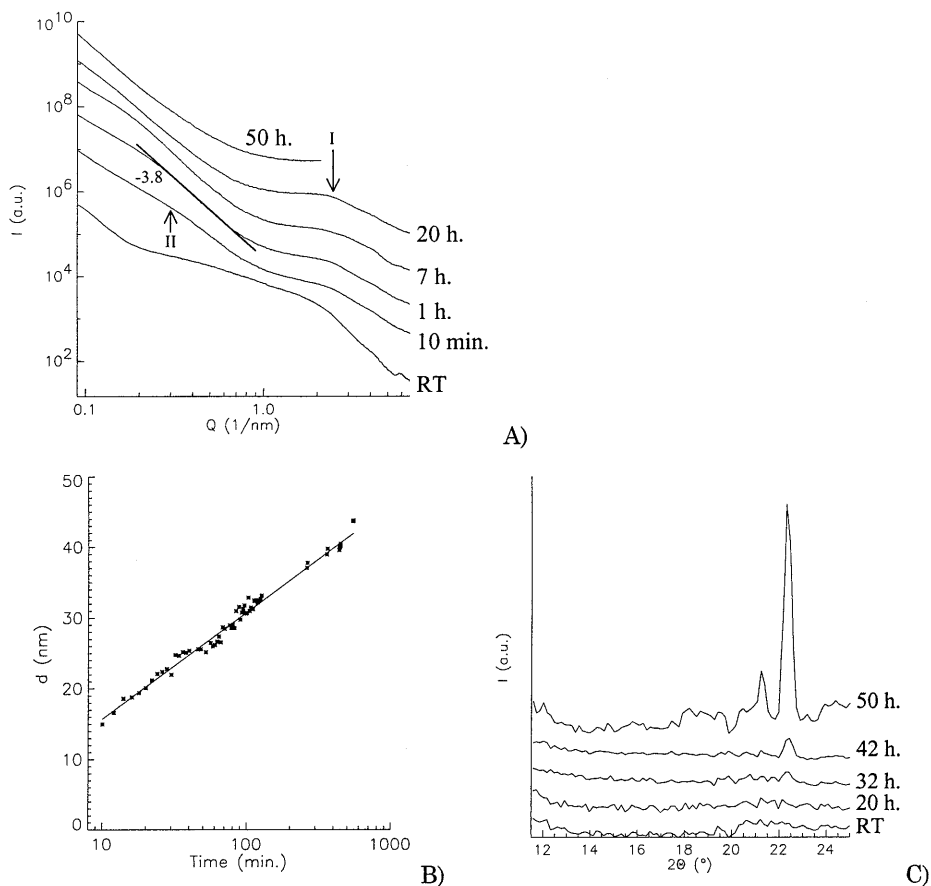


Figure 4: A) Scattering patterns of Si-BEA synthesis mixture with trimethylenebis(*N*-benzyl, *N*-methyl-piperidinium) as structure-directing agent. The annotations denote the reaction time (RT refers to a fresh synthesis mixture before heating) and the slope of the linear fit. I: 2.6 nm sized primary units, II: growing amorphous gel particles. Patterns have been shifted vertically. For a reaction time of 50 h. only a restricted Q -range was available. B) The size of the growing gel particles II as determined from the crossover where the scattering at the rather smooth particles (slope ≈ -4) levels off at decreasing scattering angle. C) The WAXS pattern for the crystallization of Si-BEA after various reaction times.

the Q -range available was restricted for reaction times longer than 20 h., no correlation between the crystallization process and the consumption of precursor particles could be observed.

MTW

The scattering pattern for the synthesis mixture for Si-MTW at room temperature (Figure 5) shows resemblance to the corresponding patterns for the Si-MFI and Si-BEA syntheses. A slight indication of ≈ 15 nm particles is observed ($Q \approx 0.4 \text{ nm}^{-1}$). After heating to a reaction temperature of 160°C , the scattered

intensity from these particles increases, and a slope -4 in the $\log I$ vs. $\log Q$ plots corresponds to the formation of smooth particles. These entities are believed to be amorphous since no sign of Bragg reflections is detected in the time range available. In contrast with the Si-BEA system, we do not find a growth of these particles until 12 hours of heating. Again, we find the scattering at nanometer-scale precursors around $Q \approx 2 \text{ nm}^{-1}$. The scattering at these entities is less pronounced than for Si-BEA but seems to increase with increasing reaction time. The lower intensity is possibly related to a lower structure-directing agent concentration (less than half) for Si-MTW compared to the Si-BEA situation. The size of these particles is estimated to be 2.5-3.0 nm.

Additionally, a clearer shoulder is observed in the scattering pattern from the Si-MTW synthesis mixture at $Q \approx 4.2 \text{ nm}^{-1}$, which can be explained by the presence of scattering entities of approximately 1.5 nm. On close observation, a sign of such a feature can also be observed in the scattering pattern of Si-BEA after 7 hours of heating (Figure 4A). Unfortunately, no observations for the synthesis of Si-MTW for reaction times longer than 12 hours are available (due to restricted beamtime at the synchrotron), so the crystallization process could not be followed.

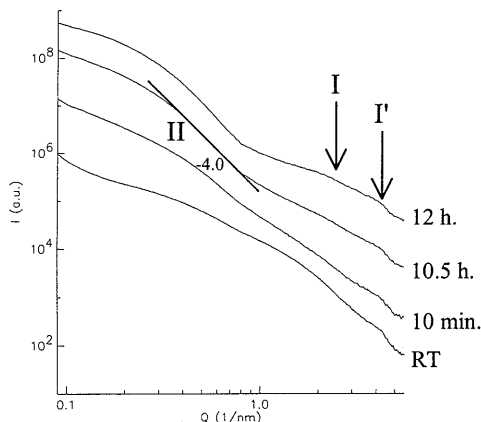


Figure 5: Scattering patterns of Si-MTW synthesis mixture during the initial stage of the reaction (no data available after 12 h. of heating). I: $\approx 2.5\text{-}3.0 \text{ nm}$ sized primary units, I': $\approx 1.5 \text{ nm}$ primary units, II: $\approx 15 \text{ nm}$ gel particles.

5.4 Discussion

When comparing the scattering patterns observed for the syntheses of different zeolite types from a gel phase, common features have been found. For the three synthesis mixtures prior to heating to reaction temperature the scattering patterns were similar, which is to be expected in view of the similar preparation methods. After heating to reaction temperature, formation of two categories of precursor particles has been observed: gel particles (between 10 and 600 nm) and primary units of the order of a few nanometers.

For the Si-MFI synthesis we have shown that two types of gel particles are present, sized 40 and 600 nm, respectively. A population of particles with a size of several tens of nanometers was present in all three gelating systems, and

consist of entities with rather smooth surfaces as illustrated by a slope near -4 in the $\log I$ vs. $\log Q$ plot (Figure 1A, 4A, 5). From the SAXS patterns for the Si-BEA synthesis mixture we could deduce that these particles grow in time (Figure 4B). In the clear solution synthesis of Si-TPA-MFI, we also observed the formation of gel particles (≈ 10 nm), from which the scattering intensity decreased during crystallization process (Figure 2). This decrease in scattering intensity points to the consumption of the gel particles and coincides with the onset of crystallization. This can be explained by their transformation into nuclei, and their dissolution to smaller species which are consumed in the crystal growth process. For Si-MFI from a heterogeneous gel, this gel particle population was not observed for reaction times longer than 10 h. (Figure 1A), which is significantly before the onset of crystallization as determined from the formation of Bragg reflections. Therefore, a different explanation for the disappearance of their scattering is more probable. It is unlikely in this stage of the reaction (well before crystallization) that the gel particles disappear by dissolution. Our data suggests that the particles become indistinguishable from the much larger (600 nm) gel particles. Probably the 40 nm particles are already part of the 600 nm gel structures, and transform in the aging process. After fusing, finally only the larger structure can be recognised. In this situation there is not a consumption of the particles, but the process can be described better by a transformation, the 40 nm particles becoming indistinguishable as separate entities. Therefore, similar processes in both gel phase and clear solution synthesis can be expected, like the transformation of the gel particles to nuclei and dissolution to smaller entities which are consumed in the crystal growth.

The second category of precursor particles, nanometer-scaled primary units, appears to be present in all three systems studied here. For Si-MFI, these primary units have the same size (≈ 2.8 nm) in both the synthesis from a heterogeneous gel and from a clear solution, using resp. trimethylene-bis(N-hexyl, N-methyl-piperidinium) and TPA⁶ as structure-directing agent (Figure 6, see also chapter 4). This suggests that the size of the primary units is determined by the properties of the structure-directing agent other than its tertiary size. Also, in both synthesis mixtures we observe a decrease in scattering intensity from the primary units during the crystallization (Figure 1A, 54h. and Figure 2). This points to the consumption of these nanometer-scale precursors in the crystallization process, irrespective of the consistency of the synthesis mixture.

The scattering from the primary units is less pronounced for Si-BEA and Si-MTW than for Si-MFI, probably due to the concentration of the structure-directing agent in the synthesis mixture: the lower the concentration of the organic molecules, the less pronounced the scattering pattern of the nanometer-scaled primary units (Figure 6). The scattering patterns for Si-MTW suggest that two different populations of primary units are present, with an estimated size of 3 nm and 1.5 nm, where the presence of the smallest population is most pronounced (I and I', respectively, in Figure 5). The scattering at the 1.5 nm sized particles has not been observed in the case of Si-MFI (Figure 1A) and Si-TPA-MFI⁶, and

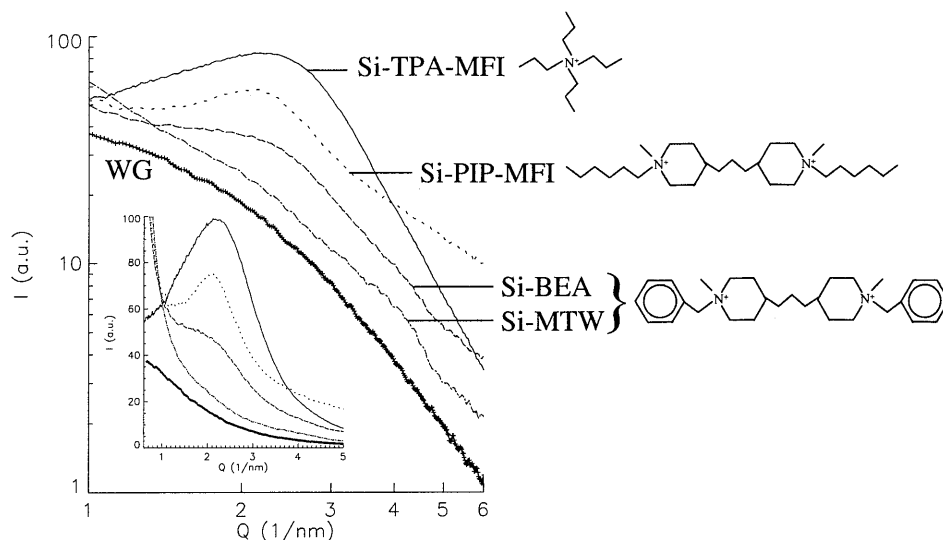


Figure 6: Log I vs. log Q representation of the SAXS patterns for different zeolite synthesis mixtures after heating to reaction temperature, but well before the onset of crystallization. The pattern annotated with WG corresponds to a solution without any organic (water glass). The inset shows the same plot with linear axes.

only a weak indication is observed for the Si-BEA synthesis (Figure 4A, 7h., $Q \approx 4.2 \text{ nm}^{-1}$). This suggests that these 1.5 nm particles are specific for the crystallization of Si-MTW.

A similar change in the crystalline structure formed using one organic structure-directing agent has been observed for the crystallization of Si-MFI and Si-ZSM-48 with 1,6-hexanediamine^{15,16}. From synthesis mixtures with the same composition, the intersecting 10-ring pore structure MFI is formed at relatively low temperatures (120°C), while the linear 10-ring pore structure of Si-ZSM-48 is formed at higher temperatures (150°C). Burkett and Davis¹⁶ used ^1H - ^{29}Si cross polarisation NMR to probe the organic-inorganic interactions at early stages of the zeolite synthesis. They found the intermolecular cross polarisation at an early stage in zeolite synthesis (X-ray amorphous synthesis mixture) to be much more efficient for the synthesis of Si-MFI than for Si-ZSM-48. This suggests the closest contact between organic and inorganic components to be present in the Si-MFI. Based on these results, and on the observation that Si-ZSM-48 can be synthesised using a variety of organic molecules, Burkett and Davis concluded that 1,6-hexanediamine acts as a real structure-directing agent in the Si-MFI synthesis, and as a pore filling agent for Si-ZSM-48. Both in present study and in a previous publication⁷, the crystallization of the intersecting 12-ring pore architecture BEA was found to dominate at relatively low temperatures (135-150°C), while the linear 12-ring pore zeolite MTW more readily crystallises at higher temperatures (150-165°C). Again, we suspect this change to be due to a transition from true structure-directing (BEA) to pore filling (MTW), which might be related with the conformation of the organic⁷ compound. Thus, the observation

of the additional 1.5 nm primary units for MTW compared to BEA could be related with different organic-inorganic interactions, and therefore different types of crystallization mechanisms.

The primary units observed here probably play an important role in the nucleation and crystallization mechanism. For the crystallization of Si-MFI from a completely clear solution, using TPA as a structure-directing agent and silicic acid as the silica source, we clearly identified primary units in the synthesis mixtures (chapter 4). Now, for the first time, we show that in a completely different synthesis mixture (a bis-piperidinium as the structure-directing agent and TEOS as the silica source), also primary units with the same size are present besides large gel structures (compare Si-TPA-MFI and Si-PIP-MFI in Figure 6). As a control experiment we prepared a solution for which TPA was omitted (water glass), and no formation of primary units has been observed.

The size of the primary units scales well with the unit cell dimension of the zeolite being formed (MFI: $2.0 \times 2.0 \times 1.3$ nm), and Schoeman³ reports that they do contain TPA. Burkett and Davis^{17,18} studied the interaction between template molecules (TPA) and silica species prior to the onset of crystallization. They trapped the composite organic/inorganic species by silylation methods and showed they contained an IR band at 560 cm^{-1} , which is indicative of organization of the silicate into rings of the type in the MFI crystals. These results could not be rationalised in light of single TPA molecules surrounded by silicate species. The observation of the 2.8 nm sized primary units enables understanding of previous results since their size allows several template molecules and silica to interact and form organization specific for the zeolite topology. Therefore we believe that the primary units observed contain template molecules and play an important, and most probably essential role in the zeolite nucleation and crystal growth process.

Resemblances have been observed in the formation of precursors in the crystallization of all-silica zeolites from gelating systems as reported in this chapter, and as reported in chapter 4 from a clear synthesis mixture. In all cases nanometer-scaled primary units were found to be present prior to heating. At reaction temperature, the formation of amorphous gel particles in the size range of several tens of nanometers was observed. The agreement between the precursor particles formed in both systems for crystallising Si-MFI and the consumption of the primary units, suggests there is a common assembly process irrespective of the formation of a heterogeneous gel phase.

5.5 Conclusions

Using *in situ* X-ray scattering techniques we were able to probe the precursor particles in gelating synthesis mixtures for the organic-mediated crystallization of zeolites Si-MFI, Si-BEA, and Si-MTW. Two categories of precursors have been observed: gel particles, and nanometer-scaled primary units.

Two types of gel particles were observed: one with a size of several tens of nanometers which was shown to grow with time for the synthesis of Si-BEA. The second type of gel particles was much larger (≈ 600 nm for Si-MFI). A comparison with the results obtained from Si-TPA-MFI crystallizations from a clear solution, in which also gel particles (≈ 10 nm) are formed, shows that the formation of such large gel structures or a heterogeneous gel phase is no requisite for zeolite nucleation and growth.

We showed that nanometer-scaled primary units are present in gelating synthesis mixtures. For Si-MFI these particles have the same size (2.8 nm) as observed in the synthesis from a completely clear solution. This size allows us to understand the observation of a IR band at 560 cm^{-1} prior to the formation of long range order: several template molecules can interact with silicate species in one particle to form order of the type as observed in the final crystal. The size of the primary units is not determined by the size of the organic structure-directing agent used, but probably by its ability to order a silica shell around itself.

Synthesis mixtures containing trimethylene-bis(N-benzyl, N-methyl-piperidinium) can crystallize to Si-BEA and Si-MTW, depending on the synthesis conditions. For the synthesis of Si-BEA, 2.6 nm sized primary units are observed, while for Si-MTW predominantly 1.5 nm sized particles are present. These results, and a comparison with the synthesis of Si-MFI or Si-ZSM-48 (using 1,6-hexanediamine) dependent on the temperature, suggests that the organic molecule acts as a real structure-directing agent in the synthesis of Si-BEA, while it functions as a pore filling agent for Si-MTW.

References

- ¹ Lobo, R.F.; Zones, S.I.; Davis, M.E. *Journal of Inclusion Phenomena and Molecular Recognition in Chemistry* 1995, **21**, 47
- ² Twomey, T.A.M.; Mackay, M.; Kuipers, H.P.C.E.; Thompson, R.W. *Zeolites* 1994, **14**, 162
- ³ Schoeman, B.J. In *Progress in zeolite and microporous materials*; Chon, H.; Ihm, S.-K.; Uh, Y.S., Eds., Studies in surface science and catalysis, **105**, Elsevier Science B.V. 1997; pp. 647
- ⁴ Schoeman, B.J., Regev, O., *Zeolites* 1996, **17**, 447
- ⁵ De Moor, P.-P.E.A.; Beelen, T.P.M.; Komanschek, B.U.; Diat, O.; Van Santen, R.A. *J. Phys. Chem. B* 1997, **101**, 11077
- ⁶ De Moor, P.-P.E.A.; Beelen, T.P.M.; Komanschek, B.U.; Van Santen, R.A. *Microporous and Mesoporous Materials* 1998, in press
- ⁷ Tsuji, K.; Davis, M.E. *Microporous Mater.* 1997, **11**, 53
- ⁸ De Moor, P.-P.E.A.; Beelen, T.P.M.; Van Santen, R.A. *Microporous Mater.*, 1997, **9**, 117
- ⁹ Bras, W.; Derbyshire, G.E.; Ryan, A.J.; Mant, G.R.; Felton, A.; Lewis, R.A.; Hall, C.J.; Greaves, G.N. *Nucl. Instrum. Methods Phys. Res. Sect. A*, 1993, **326**, 587
- ¹⁰ Diat, O.; Bösecke, P.; Lambard, J.; De Moor, P.-P.E.A. *J. Appl. Cryst.* 1997, **30**, 862
- ¹¹ Bertram, W. *J. Appl. Cryst.* 1996, **29**, 682

- ¹² Höhr, A.; Neumann, H.B.; Schmidt, P.W.; Pfeifer, P.; Avnir, D. *Phys. Rev. B* 1988, **38**, 1462
- ¹³ Bale, H.D.; Schmidt, P.W. *Physical Review Letters* 1984, **53**, 596
- ¹⁴ Martin, J.E.; Hurd, A.J. *J. Appl. Cryst.* 1987, **20**, 61
- ¹⁵ Franklin, K.R.; Lowe, B.M. *Zeolites* 1988, **8**, 495
- ¹⁶ Burkett, S.L.; Davis, M.E. *Chem. Mater.* 1995, **7**, 1453
- ¹⁷ Burkett, S.L.; Davis, M.E. *J. Phys. Chem.* 1994, **98**, 4647
- ¹⁸ Burkett, S.L.; Davis, M.E. *Chem. Mater.*, 1995, **7**, 920

The Assembly Process of Organic-Mediated Zeolite Synthesis*

The organic-mediated assembly of zeolites has been studied with a combination of wide-angle, small-angle, and ultra-small-angle X-ray scattering. In this concluding chapter the main results on the synthesis of MFI from clear solutions (Chapter 2-4) and the synthesis of Si-MFI, Si-MTW, and Si-BEA from gelating systems (Chapter 5) will be reviewed. To test the hypothesis concerning the role of intermediates in the crystallization of zeolites described in these chapters, new results will be presented on Si-MFI synthesis mixtures containing a 'dimer' or a 'trimer' of tetrapropylammonium (TPA) as structure-directing agent, as well as a synthesis using tetraethylorthosilicate as silica source. Synthesis mixtures of all silica MEL/MFI intergrowth (using tetrabutylammonium) and aluminum containing SOD (using tetramethylammonium) will also be reported.

Based on the in situ data spanning over four orders of magnitude (0.17 nm - 6000 nm) on zeolites synthesized under a large variety of conditions, we present a mechanistic picture for the organic-mediated crystallization of zeolites. It is shown that nanometer-sized entities comprised of TPA and silica function as primary building units that aggregate to form viable nuclei that initiate the growth of zeolite crystals. The nucleation mechanism of TPA-MFI thus involves ordering on first the nanometer scale, after which order at larger length-scales is obtained from the order derived in the primary building units. The primary building units are specific for the crystalline structure formed. The sequential formation of order from small (primary units), to medium (nuclei), to large length-scales (crystals) is consistent with other assembly processes, e.g. the construction of biological entities.

* Submitted for publication: P.-P.E.A. de Moor, T.P.M. Beelen, B.U. Komanschek, L.W. Beck, P. Wagner, M.E. Davis, R.A. van Santen, Imaging the assembly process of the organic-mediated synthesis of a zeolite, *Chemistry - A European Journal*.

6.1 Introduction

The elucidation of the mechanisms by which complicated macroscale objects are formed by self-assembly remains one of the most difficult challenges. Substantial efforts are currently underway to unravel the protein folding problem, whose solution would provide a direct link between chemistry and biology. Likewise, pathways employed by living organisms to organise inorganic materials, e.g., bone formation and shaping, defy complete description at this time. Thus, there is a continuing need to understand the rules used for the formation of complicated structures. It is crucial to be aware of the fact that the assembly processes need not be the same over all length scales.

The assembly of pure-silica zeolites by the use of organic molecules that assist in the synthesis process and are accommodated in the final structures is an example of an assembling hybrid system. Unlike the inorganic materials that are formed in living systems (simple unit cells or building units - material is 'shaped' over large length scales), zeolites have extremely complicated unit cells. Additionally, there are no strong chemical bonds formed between the organic and inorganic fractions of the composite material; co-operative behaviour of weak interactions, e.g., Van der Waals forces, dictate the assembly process. Thus, isolation of intermediates is most likely destructive and only *in situ* observations are reliable. When synthesising an organic-zeolite composite, organization on length scales from sub-nanometer (organic molecule) to micron (final crystal) is important. Aside from the experimental difficulties in using spectroscopies like NMR, IR, Raman and UV/Visible on zeolite reaction mixtures, these methods probe structures or interactions on a very small length-scale and can only provide information on one portion of the assembly process. Additionally, dynamic light scattering (DLS) can yield information over a larger length-scale region but is subject to limitations when multiple size populations exist or when large particles exist in high concentrations and when a heterogeneous gel phase is present. These difficulties are circumvented using X-ray scattering. Small-angle scattering of X-rays and neutrons can provide information from length scales between microns and Ångströms in a broad variety of systems, e.g. in the structure of complex biological materials like wood and bone¹, the microstructure of emulsions², and the evolution of the morphology and three-dimensional spatial arrangement of the precipitates during decomposition of alloys³. However, many structures show variations on a broad range of length scales, requiring a combination of techniques to be studied effectively. We use a combination of USAXS and simultaneous SAXS and WAXS to continuously probe an extremely broad range of length scales (0.17 nm - 6µm), that is needed to monitor all precursors and products during zeolite crystallization. The brilliant X-ray sources at the Daresbury Laboratory and the European Synchrotron Radiation Facility are employed to allow *in situ*, dynamic observations. Using these techniques, we report on the assembly of Si-MFI from different synthesis mixtures with various structure-directing agents and silica sources. We present evidence that 2.8 nm sized primary units are the key intermediates for the zeolite synthesis.

6.2 Preparation of zeolite synthesis mixtures

Completely clear synthesis mixtures with chemical composition $x \text{ Na}_2\text{O} : 1.22 (\text{TPA})_2\text{O} : 10 \text{ SiO}_2 : 117 \text{ H}_2\text{O}$ were prepared using silicic acid as silica source as described in chapter 2. Here x was varied to obtain the Si/OH-ratios between 2.12 and 3.02. For syntheses using bis-(tripropylammonium) hexamethylene dihydroxide ('dimer' of TPA) and bis-(tripropylammonium-N-N'-hexamethylene) N",N" dipropylammonium trihydroxide ('trimer' of TPA), the ratio R/SiO₂ was respectively kept to 1.22:10 and 0.81:10 and $x=0.848$ (Si/OH=2.42). The synthesis temperature was 125°C. The 'dimer' and 'trimer' of TPA were kindly provided by Larry Beck of the group of Mark Davis, department of Chemical Engineering, California Institute of Technology.

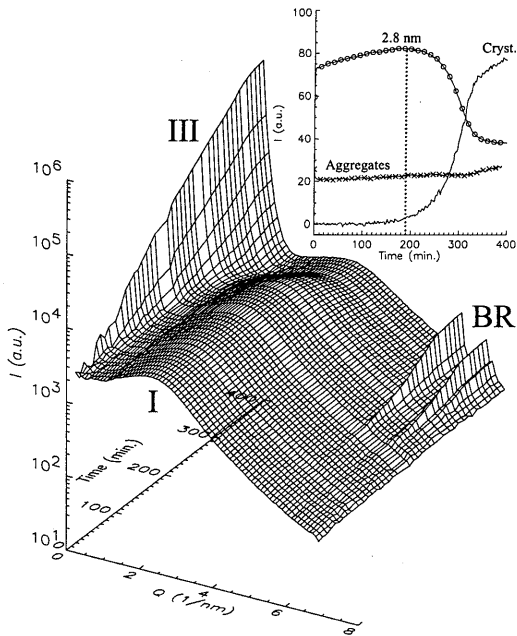
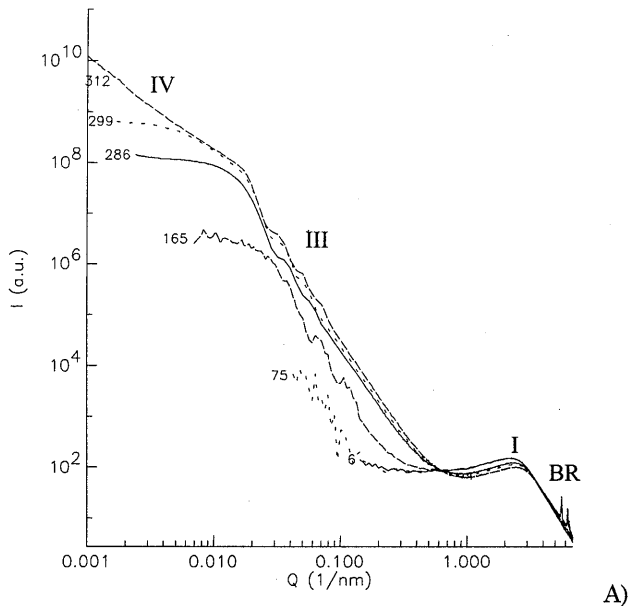
Synthesis mixtures using TEOS as a silica source with chemical composition $9 \text{ TPAOH} : 25 \text{ SiO}_2 : 480 \text{ H}_2\text{O} : 100 \text{ EtOH}$ have been prepared as reported by Schoeman⁵. The aging time between mixing the reagents and heating to the synthesis temperature of 125°C was 24 h.

The synthesis of Si-MFI from a heterogeneous gel phase using trimethylene-bis(N-hexyl, N-methyl-piperidinium) dihydroxide and tetraethylorthosilicate as a silica source with composition $10 \text{ SiO}_2 : 3.0 \text{ R}(\text{OH})_2 : 0.5 \text{ NaOH} : 350 \text{ H}_2\text{O}$ was performed at 160°C as described elsewhere⁴.

MFI/MEL intergrowth crystals were prepared at 125°C from a synthesis mixture having $0.55 \text{ Na}_2\text{O} : 1.26 (\text{TBA})_2\text{O} : 10 \text{ SiO}_2 : 150 \text{ H}_2\text{O}$, where TBA is tetrabutylammonium. SOD was crystallized at 110°C from a solution with $0.55 \text{ Na}_2\text{O} : 2.80 (\text{TMA})_2\text{O} : 0.2 \text{ Al}_2\text{O}_3 : 10 \text{ SiO}_2 : 90 \text{ H}_2\text{O}$, where TMA is tetramethylammonium hydroxide. Silicic acid was used as silica source and the preparation was as for Si-TPA-MFI.

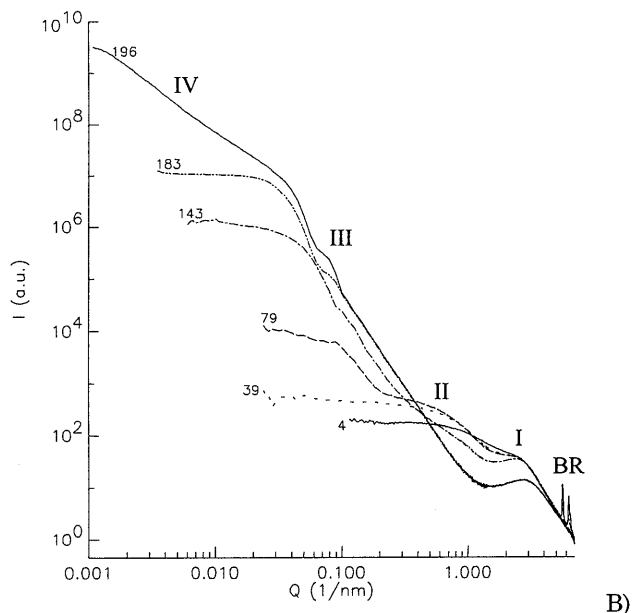
6.3 The mechanism of organic-mediated zeolite crystallization

The first event in the assembly of Si-TPA-MFI from a clear solution of TPAOH, SiO₂, NaOH and H₂O is formation of particles with an average diameter of 2.8 nm (see Figure 1). These species, hereafter referred to as the primary particles, were monitored by *in situ* SAXS-WAXS and USAXS. A description of the X-ray scattering equipment is given in chapter 2. The existence of primary particles of this size has been previously reported by Schoeman⁵, but here for the first time the specific time-resolved role of these particles in the assembly of long-range ordered materials is elucidated. IR spectra of these composite species were obtained *ex situ* and showed a band at 560 cm⁻¹ which is interpreted to be indicative of silicate 5-membered rings (also seen in Si-MFI zeolites); the samples were prepared by quenching the reaction mixture that contains only the 2.8 nm particles in liquid N₂ and freeze-drying or extracting the composite particles into an immiscible organic phase with subsequent evaporation of the solvent. This indicates that the TPA molecules and silica are interacting in the primary

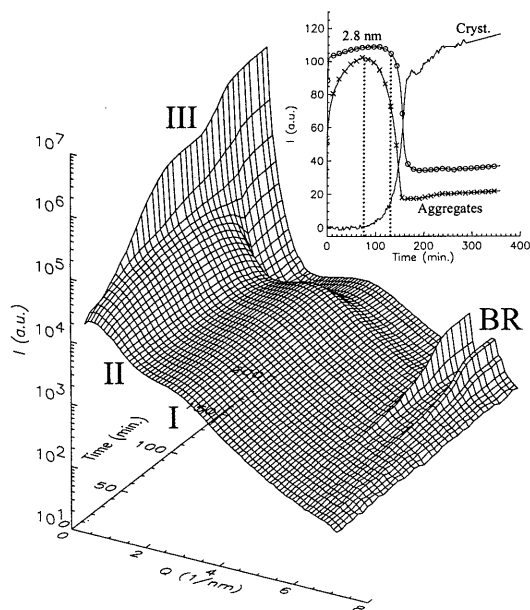


A)

Figure 1: A and A': Time dependent scattering curves for $\text{Si}/\text{OH}=2.42$. The inset in figure A' shows the scattering intensity from the different particle populations and the crystallinity. Scattering particle types: I=primary units, III=crystals, IV=crystal aggregates, BR=Bragg reflections. The patterns at short reaction times do not extend to (very) small angles since no (very) large structures are present in the sample, resulting in no excess scattering intensity above the background.

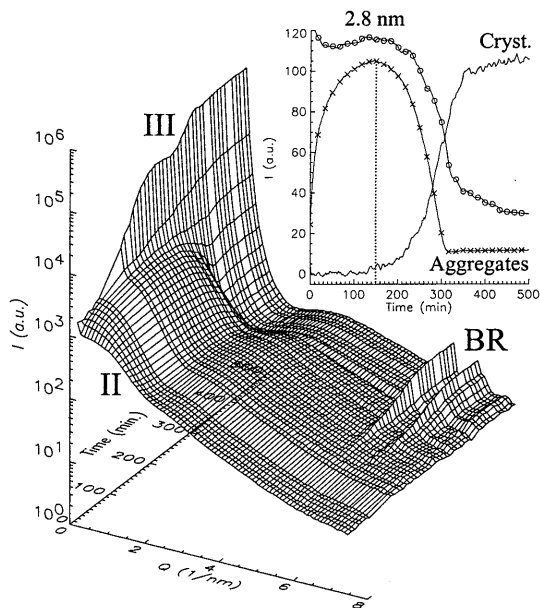
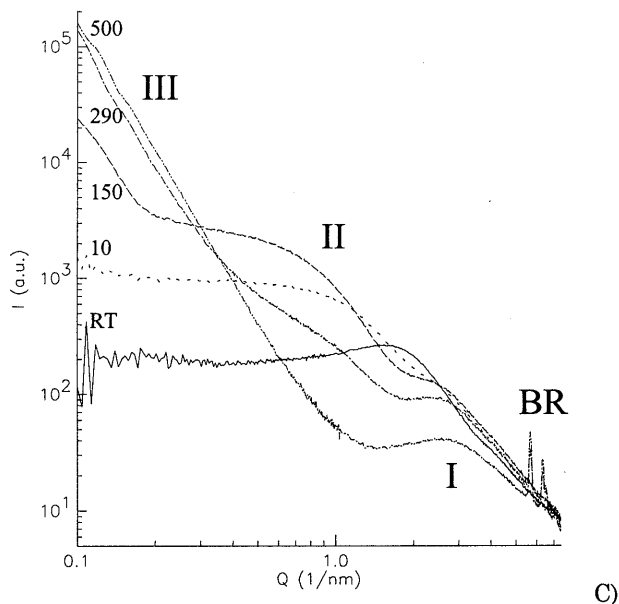


B)



B')

Figure 1: B and B': Time dependent scattering curves for $\text{Si}/\text{OH}=3.02$. The inset in figure B' shows the scattering intensity from the different particle populations and the crystallinity. Scattering particle types: I=primary units, II=aggregates, III=crystals, IV=crystal aggregates, BR=Bragg reflections. The patterns at short reaction times do not extend to (very) small angles since no (very) large structures are present in the sample, resulting in no excess scattering intensity above the background.



C')

Figure 1: C and C': Time dependent scattering curves for the synthesis using TEOS as silica source (Schoeman synthesis) with $\text{Si}/\text{OH}=2.78$. The inset in figure B' shows the scattering intensity from the different particle populations and the crystallinity. Scattering particle types: I=primary units, II=aggregates, III=crystals, IV=crystal aggregates, BR=Bragg reflections. The patterns in C do not extend to very small angles since no USAXS data is available for this system.

particles and that TPA affects the short-range ordering of the silicon atoms. Previously, Burkett and Davis showed by NMR that silicate species are in contact with TPA molecules prior to the detection of long-range order by diffraction^{6,7} (synthesis conditions were slightly different). ¹³C NMR chemical shifts of composite species trapped by silylation were different from both free TPA in solution and TPA occluded in Si-MFI; this agrees with the data presented here in that the primary species are composites of TPA molecules and silicates that have not yet adopted the long-range order of Si-TPA-MFI. Finally, TPA has clearly been identified as being present in these primary particles^{5,8} (schematic representation in Figure 2).

The ability to simultaneously monitor a broad range of length scales shows that primary units are converted into longer-scale entities in the nucleation process. The nucleation of Si-TPA-MFI is a two-step process: first nutrients must assemble into composite species, after which reorganisation and condensation reactions can form viable nuclei (we have observed crystals having the MFI structure of size 8-10 nm by electron microscopy). The importance of the first step is shown by a series of experiments in which the formation of aggregates of primary units has been changed by varying the alkalinity of the synthesis mixture (Chapter 2). In case of a relatively low alkalinity (Si/OH=3.02) the formation of aggregates with a size of approximately 10 nm is facilitated (Figure 1A). At increasing alkalinity the ability of the synthesis mixture to form such structures decreases, while no indication of particles larger than the 2.8 nm primary units are present at high alkalinities (Si/OH<2.65)⁹. Our time-resolved results show the correlation between the presence of precursors and the crystallization behaviour. In the situation where the primary units are the only precursors present, the onset of crystallization coincides with the onset of the consumption of the primary units (Figure 1A', inset vertical dotted line). However, in the case that aggregates are present (low alkalinity), the consumption of these aggregates coincides with the onset of the crystallization process, while the effective consumption of the primary units starts significantly later (Figure 1B').

The growth curves of the crystals can be obtained from the scattering from the crystal surface that is observed at very small angles¹⁰, and show that the final size of the crystals is smaller in the case of the lower alkalinity (Si/OH=3.02) while the crystal growth rate is independent of the alkalinity (Chapter 4, figure 8). Therefore, the faster crystallization as observed from the area of the Bragg reflections (Chapter 4, figure 6A) is due to a higher rate of nucleation in the case that the 10 nm aggregates are clearly present (Si/OH=3.02). At high alkalinities (Si/OH=2.42) the number of aggregates is sufficiently low that they cannot be identified from the scattering patterns, which is in agreement with the formation of a low number of viable nuclei and large crystals. At even higher alkalinities (Si/OH=2.12) the rate of nucleation is extremely low and the primary units are the only precursors observable. Adding a small amount of Si-TPA-MFI crystals as seeds (mean diameter 68 nm) results in normal crystal growth and shows that entities for growth are present in the synthesis mixture even when

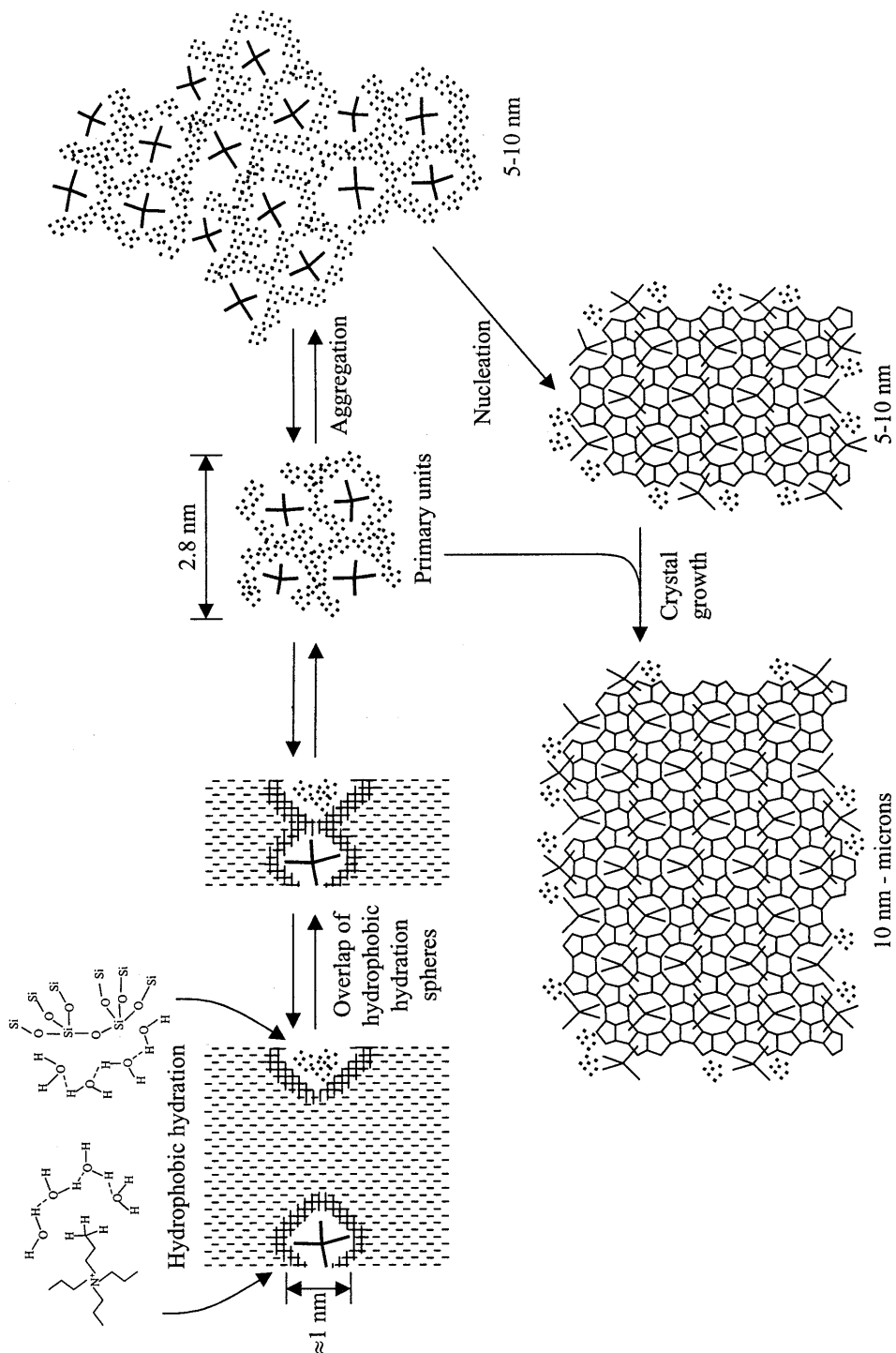


Figure 2: Scheme for the crystallization mechanism of Si-TPA-MFI.

nucleation is almost impossible. The correlation between the presence of aggregates of primary units and the rate of nucleation shows that the aggregation of primary units is an essential step in the nucleation process (see figure 2), and that the formation of viable nuclei does not occur via the growth of the primary units by addition of ions from solution. In the situation where large numbers of aggregates are present ($\text{Si}/\text{OH}=3.02$), a small fraction of these will transform into viable nuclei, while the remaining ones will dissolve due to changing conditions brought on by the crystal growth process.

Schoeman⁵ monitored the early stages of Si-TPA-MFI formation using DLS. Three major differences in the reaction mixture compositions used by Schoeman and those reported here are that tetraorthosilicate was the silica source, ethanol was present in significant concentrations and no sodium cations were present. In order to make a direct comparison to Schoeman's previous results, the exact synthesis mixture was investigated here (Figure 1C). A higher reaction temperature of 125°C was employed to increase the rate of formation due to the limited, assigned synchrotron beamtime. The scattering pattern at room temperature shows 4 nm sized particles, that after heating convert into two different particle populations of 2.8 nm and ≈ 5 nm, respectively. For up to 150 minutes of heating, the 2.8 nm sized particles remain present, and the ≈ 5 nm particles increase in size to ≈ 8 nm. These observations are in agreement with Schoeman's DLS results. From this point forward, our data reveal that the situation is more complicated and show a strong resemblance to our synthesis using silicic acid at $\text{Si}/\text{OH}=3.02$ (Figure 1B). These results clearly show the importance of following *in situ* the full assembly process and that our proposed mechanistic picture does in fact extend to the system investigated by Schoeman.

After the formation of the nanometer sized viable nuclei, growth of crystals up to the micrometer range occurs (Figure 2). The scattering experiments show that the aggregates of the primary units do not participate directly in the growth process since the linear crystal growth rate is independent of their presence (chapter 2). These data strongly suggest that the growth units are in fact the primary units. Thus, when aggregates of primary units are present they can dissolve back to smaller precursor particles and keep the concentration of the latter almost constant. This results in an almost constant scattering from the primary units in the case of low alkalinity until no scattering intensity from the 10 nm particles is observed.

When the linear growth of the Si-TPA-MFI crystals finishes, a sudden aggregation of the discrete crystals to structures larger than $6\mu\text{m}$ occurs, which gives rise to the increase in scattering intensity at Q values lower than 0.02 nm^{-1} (see figure 1A' and B'). The mass fractal dimension of 1.8 of these micrometer scaled aggregates agrees with a diffusion limited aggregation process. Using *ex situ* techniques like TEM these structures have never been observed, due to their vulnerability and the required sample treatment.

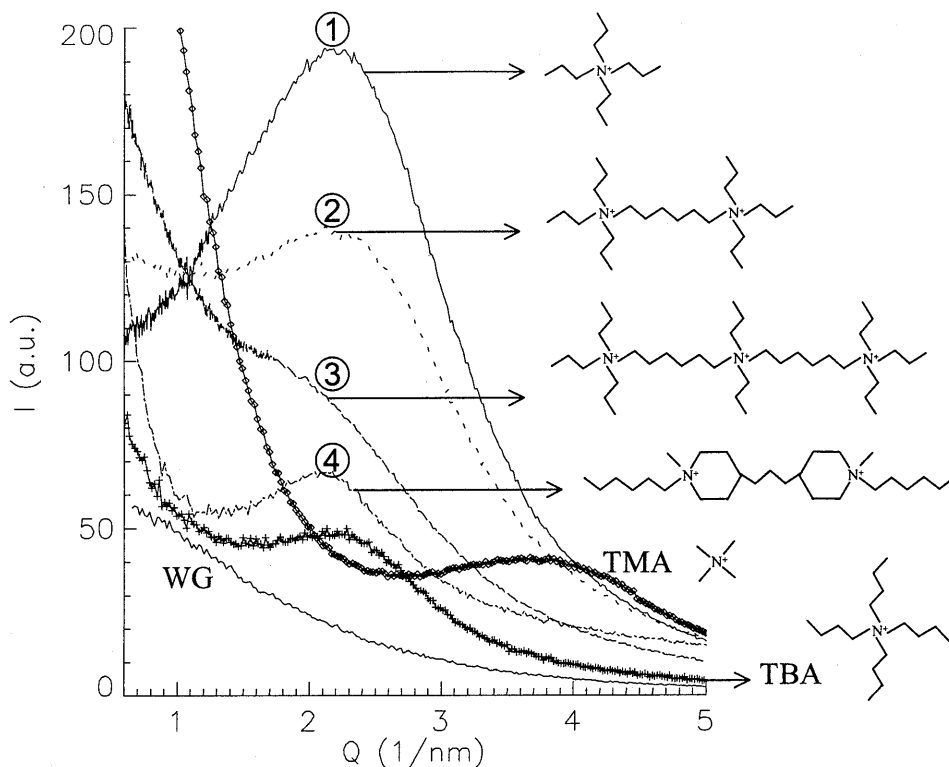


Figure 3: Scattering patterns for zeolite synthesis mixtures with different structure-directing agents (shifted vertically for comparison): ①=TPA, ②= bis-(tripropylammonium) hexamethylene, 'dimer' of TPA, ③= bis-(tripropylammonium-*N,N'*-hexamethylene)*N,N'* dipropylammonium, 'trimer' of TPA, ④= trimethylene-bis(*N*-hexyl, *N*-methyl-piperidinium), WG=water glass, no organic molecules, TBA= Tetrabutylammonium, TMA=Tetramethylammonium. The diameter, d , of the particles can be determined from the peak maximum using $d=2\pi/Q$.

To demonstrate the specificity of the primary units for the crystalline structure formed, we used several organic molecules directing the synthesis to the same crystalline structure MFI (unit cell: $2.0 \times 2.0 \times 1.3$ nm). Syntheses using TPA, a 'dimer' of TPA and a 'trimer' of TPA were all performed from clear solutions with the same composition using silicic acid as a silica source. Primary units with a size of 2.8 nm were found in all syntheses (Figure 3). The same precursor size was found when TBA was used, directing the synthesis to MFI/MEL intergrowth (unit cell: $2.0 \times 2.0 \times 1.3$ nm). A completely different synthesis procedure where a heterogeneous gel phase is present, using tetraethyl-orthosilicate as a silica source and a bis-piperidinium compound as a structure-directing agent known to produce MFI⁴, also showed the presence of 2.8 nm size primary units (Chapter 5, figure 1). These data show that the formation of the primary units in these organic-mediated syntheses of MFI is independent of the structure-directing agent, alkalinity and preparation method. Contrary, the crystal shape is strongly

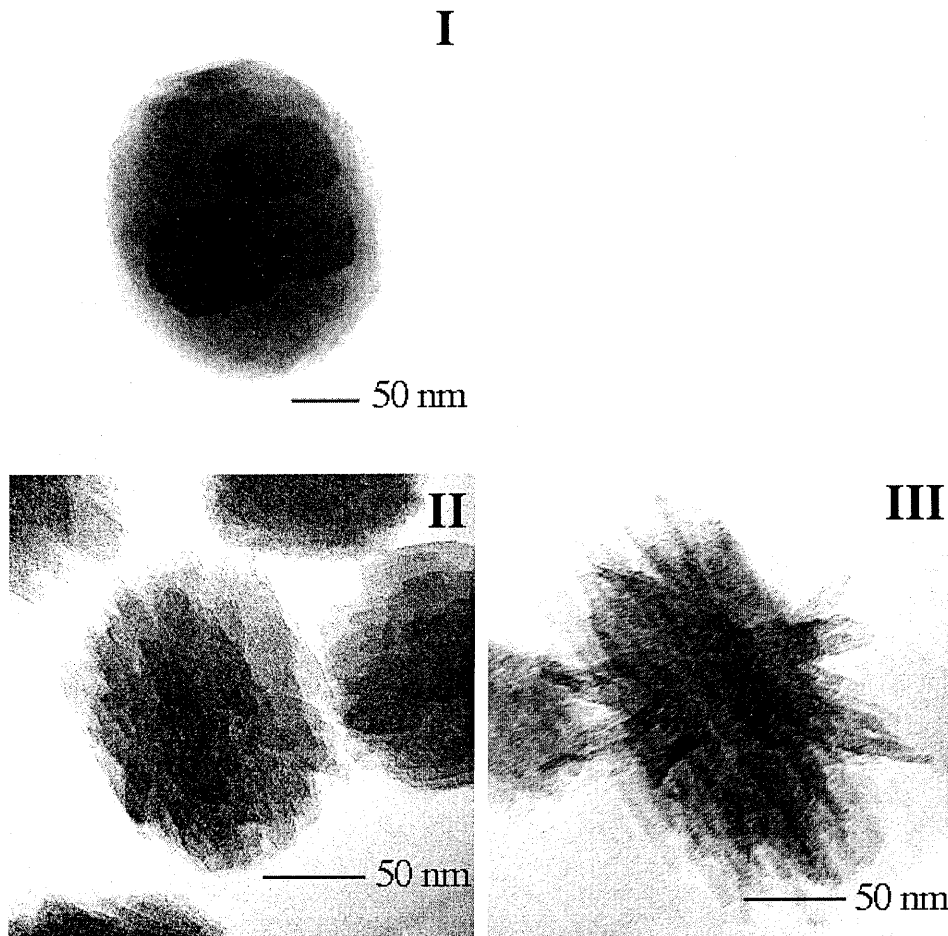


Figure 4: TEM images of Si-MFI crystals prepared from synthesis mixtures containing I: TPA, II: the 'dimer' of TPA and III: the 'trimer' of TPA. The images are provided by Larry Beck, department of Chemical Engineering, California Institute of Technology.

influenced by the structure-directing agent. This is illustrated in figure 4 for MFI crystals obtained from synthesis mixtures containing TPA, the 'dimer' of TPA, or the 'trimer' of TPA.

Using the same reaction mixture that produces the heterogeneous gel phase for MFI, the organic additive trimethylene-bis(N-benzyl, N-methyl-piperidinium) gives either pure-silica zeolite beta or pure-silica zeolite ZSM-12⁴. The *in situ* scattering data for these syntheses show that the primary particle size for beta is 2.6 nm (unit cell 1.3×1.3×2.4 nm) and 1.5 nm for Si-ZSM-12 (unit cell 2.5×0.5×2.5 nm) (Chapter 5, figure 6). In another experiment we synthesized zeolite SOD (unit cell: 0.9×0.9×0.9 nm) using tetramethylammonium as a structure-directing agent in the presence of aluminum. For this case the size of the precursors is 1.6 nm (apparent from the different position of the maximum in the scattering curves in figure 3). Although the scaling between the unit cell size

and the primary particle size is not perfect, there is clearly a correlation between the zeolite crystal structure and the dimensions of the primary particle. The scattering from a solution containing no organic molecules (no crystalline product) shows no formation of such precursors. These results lead to the conclusion that the primary units observed are indeed the entities that contain the order on a sub-nanometer scale needed for the construction of nanometer scale order, i.e. viable nuclei.

In this thesis, we have provided the first complete image of the assembly process of an organic-mediated synthesis of a pure-silica zeolite. By monitoring a very large range of length-scales simultaneously, the pathway by which organization is extended from the molecular length-scale to the crystal length-scales is elucidated. We believe that these mechanisms are not unique to the TPA-MFI system but rather provide insight to how other complex systems may assemble.

References

- ¹ Fratzl, P.; Jakob, H.F.; Rinnerthaler, S.; Roschger, P.; Klaushofer, K. *J. Appl. Cryst.*, 1997, **30**, 765-769
- ² Zemb, T.N. *Colloids and Surfaces A*, 1997, **129-130**, 435-454
- ³ Sequeira, A.D.; Kistorz, G.; Pedersen, J.S. *J. Appl. Cryst.* 1997, **30**, 575-579
- ⁴ Tsuji, K.; Davis, M.E. *Microporous Mater.*, 1997, **11**, 53-64
- ⁵ Schoeman, B.J. In: *Progress in zeolite and microporous materials* Ed.: Chon, H.; Ihm, S.-K.; Uh, Y.S., Studies in surface science and catalysis, Elsevier Science B.V., 1997, **105**, 647-654, and Schoeman, B.J. *Zeolites* 1997, **18**, 97-105
- ⁶ Burkett, S.L.; Davis, M.E. *J. Phys. Chem.* 1994, **98**, 4647-4653
- ⁷ Burkett, S.L.; Davis, M.E. *Chem. Mater.* 1995, **7**, 920-928
- ⁸ Watson, J.N.; Iton, L.E.; Keir, R.I.; Thomas, J.C.; Dowling, T.L.; White, J.W. *J. Phys. Chem. B* 1997, **101**, 10094-10104
- ⁹ De Moor, P.-P.E.A.; Beelen, T.P.M.; Van Santen, R.A. *Microporous Mater.* 1997, **9**, 117-130
- ¹⁰ De Moor, P.-P.E.A.; Beelen, T.P.M.; Komanschek, B.U.; Diat, O.; Van Santen, R.A. *J. Phys. Chem. B* 1997, **101**, 11077-11086

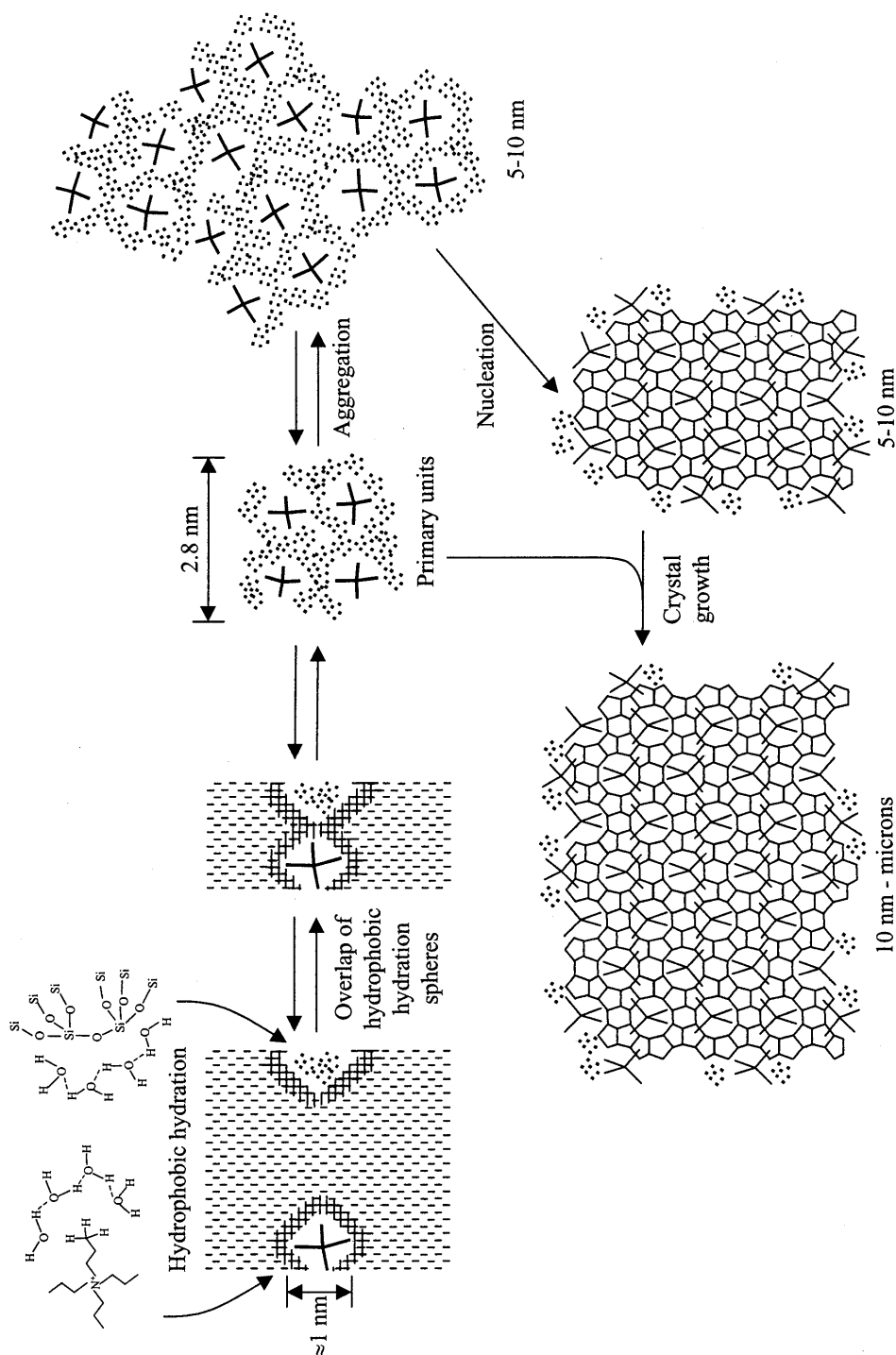
Summary

The mechanisms by which complicated structures assemble from atoms and/or molecules to macroscale entities are far from being understood. Clear insights into the rules concerning complete assembly processes, whether they be organic, inorganic, or hybrid organic-inorganic, are of general use. In this thesis the self-assembly process of zeolites is discussed, using an organic molecule as structure-directing agent to build these porous crystals from silica monomers.

In order to be able to 'image' the transformations during the complete course of an assembly process, i.e. starting with molecules and up to macroscopic crystals, a (combination of) technique(s) should be applied to cover the whole range of relevant length scales. Moreover, the intermediates can be very fragile, which can only be studied effectively using non-invasive, *in situ* techniques. In this project, these problems have been solved applying a combination of wide- and small-angle X-ray scattering techniques using high-brilliance synchrotron radiation. This allowed time-resolved, *in situ* observations over a unique range of length scales spanning over four orders of magnitude (0.17-6000 nm), during the complete course of the zeolite assembly process. This range of length scales covers the dimensions of all precursors and products present in the synthesis mixtures.

During the clear-solution synthesis of pure-silica zeolite ZSM-5 (MFI) using the tetrapropylammonium-ion (TPA) as template, three particle populations are observed: primary units (2.8 nm), their aggregates (≈ 10 nm), and the crystals. Both the primary units and their aggregates are precursors and are consumed during the formation of the crystalline product (Chapter 4). The role of each of the precursors in the crystallization process has been clarified by investigating the influence of the synthesis conditions on the formation and consumption of these particles.

The formation of the 10 nm sized aggregates of primary units can be controlled by the alkalinity of the synthesis mixture, while the 2.8 nm primary units appeared to be omnipresent. The experiments with variation of the alkalinity and the effect of the addition of seed crystals (Chapter 2 and 4) showed that the formation of aggregates of primary units is an essential step in the nucleation process.



Schematic representation of the assembly mechanism during organic-mediated zeolite crystallization.

Experiments with varying concentration of the reactants (Chapter 3) and different reaction temperatures (Chapter 4) revealed that the crystal growth process is reaction controlled (apparent activation energy for crystal growth is 83 kJ/mol). Crystal growth therefore is believed to be the reaction controlled integration of primary units at the surface to the crystal. A schematic representation of the proposed zeolite assembly process is shown on previous page.

The generality of the proposed mechanism has been tested by comparing the results for the synthesis of Si-TPA-MFI from a clear solution with a large variety of other zeolite crystallizations. For the crystallization of zeolites Si-MFI, Si-BEA, and Si-MTW from gelling systems (Chapter 5), for MFI/MEL intergrowth, and for the crystallization of sodalite (SOD) in the presence of aluminum, in all cases the formation of nanometer scale primary units was observed. The scaling between the size of the primary units and the unit cell dimensions of the zeolite topology formed, strongly suggests that the observed precursors are in fact specific for the zeolite formed. This is confirmed by the observation that primary units with the same size are present for the synthesis of Si-MFI using four different structure-directing agents (TPA, a 'dimer' of TPA, a 'trimer' of TPA, and trimethylene-bis(N-hexyl, N-methyl-piperidinium)). Moreover, the crystallization of Si-BEA and Si-MTW using the same organic molecule, showed the presence of primary units with different sizes for each synthesis. The results show that the proposed mechanism extends to organic-mediated zeolite synthesis under a broad range of conditions.

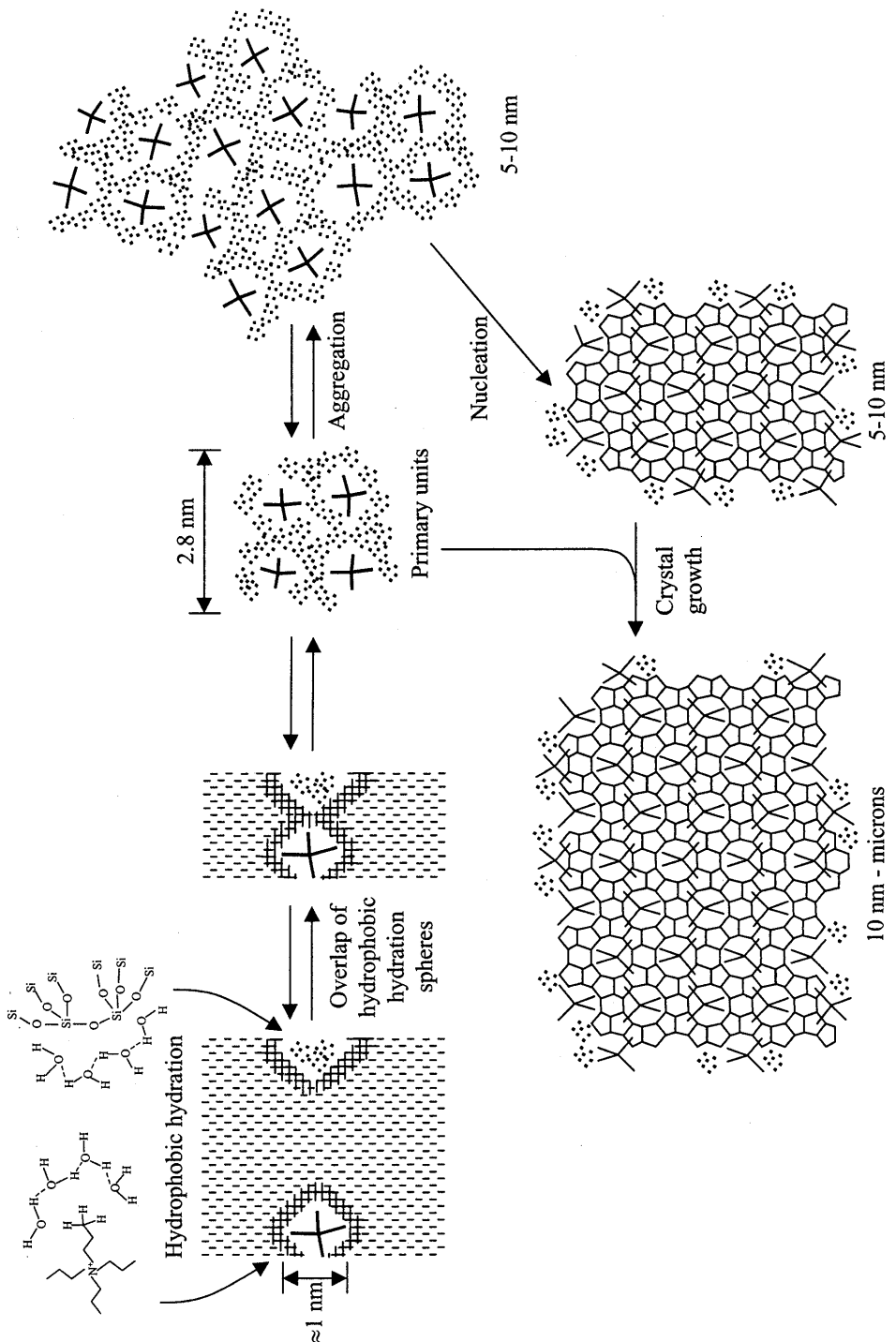
In conclusion, for the first time the nanometer-scale precursors during zeolite synthesis have been identified, and their formation and consumption has been monitored during the complete course of the crystallization process covering extended length scales. Based on a broad range of zeolite crystallizations, an assembly mechanism has been proposed which involves the sequential formation of order from small (primary units), via medium (nuclei), to large scale (crystals). This mechanism probably is a general one for organic-mediated zeolite synthesis.

Samenvatting

De mechanismen tijdens de opbouw van gecompliceerde structuren vanuit atomen en/of moleculen zijn veelal nog onbekend. Duidelijk inzicht in de regels betreffende de complete zelforganisatie processen van zowel anorganische, organische als hybride organische/anorganische materialen, is van algemeen belang. In dit proefschrift wordt de zelforganisatie van zeolieten behandeld, waarbij een organisch molecuul wordt gebruikt als structuur-bepalende component om deze poreuze kristallijne materialen op te bouwen uit silica monomeren.

Om de transformaties tijdens de gehele duur van een zelforganisatieproces van moleculen tot macroscopische kristallen te kunnen volgen, moet een (combinatie van) techniek(en) worden gebruikt die het gehele gebied van lengteschalen bestrijkt. Bovendien kunnen de intermediären zeer kwetsbaar zijn, waardoor ze alleen effectief bestudeerd kunnen worden met behulp van niet-verstorende, *in situ* technieken. In dit project zijn deze problemen opgelost door gebruik te maken van een combinatie van grote- en kleine-hoekverstrooiing van röntgenstraling met een hoge intensiteit, verkregen met behulp van een synchrotron. Hierdoor waren tijdsopgeloste, *in situ* metingen mogelijk over een uniek spectrum van lengteschalen dat meer dan vier decaden bestrijkt (0.17-6000 nm), en wel tijdens de gehele duur van het kristallisatieproces. Dit spectrum van lengteschalen bevat de afmetingen van alle intermediären en produkten die aanwezig zijn in de synthesesmengsels.

Tijdens de synthese van puur silica zeoliet ZSM-5 (MFI) vanuit een heldere oplossing met het tetrapropylammonium-ion (TPA) als template, zijn drie populaties van drie typen deeltjes waargenomen: primaire eenheden (2.8 nm), aggregaten daarvan (≈ 10 nm) en kristallen. De primaire eenheden en hun aggregaten zijn intermediären die omgezet worden in het kristallijne produkt (Hoofdstuk 4). De rol van elk van de intermediären in het kristallisatieproces is opgehelderd door de invloed van de synthesecondities op de vorming en consumptie van deze deeltjes te bestuderen.



Schematische voorstelling van het zelforganisatiemechanisme tijdens zeolietkristallisatie met behulp van een organische structuurbepalend molecuul.

De vorming van de 10 nm grote aggregaten van primaire eenheden kan worden gestuurd met behulp van de alkaliniteit van het synthesemengsel, terwijl de 2.8 nm primaire eenheden ten allen tijde aanwezig zijn. De experimenten met variatie van de alkaliniteit en het effect van het toevoegen van entkristallen (Hoofdstukken 2 en 4) lieten zien dat de vorming van aggregaten van primaire eenheden een essentiële stap is in het nucleatieproces.

Experimenten met verschillende concentraties van de reactanten (Hoofdstuk 3) en kristallisaties bij diverse temperaturen (Hoofdstuk 4) toonden aan dat het proces van kristalgroei reactie gecontroleerd verloopt (ogenschijnlijke activerings-energie voor kristalgroei is 83 kJ/mol). De kristalgroei is waarschijnlijk de reactie-bepaalde integratie van primaire eenheden aan het oppervlak van het kristal. Een schematische voorstelling van het voorgestelde zelforganisatiemechanisme van zeolieten is geschetst op de vorige pagina.

De algemene geldigheid van het voorgestelde mechanisme is getest door de resultaten voor de synthese van Si-TPA-MFI vanuit een heldere oplossing te vergelijken met een groot aantal andere zeolietkristallisaties. Tijdens de kristallisatie van Si-MFI, Si-BEA en Si-MTW vanuit geleerde systemen (Hoofdstuk 5), voor MFI/MEL mengkristallen, en voor de kristallisatie van sodaliet (SOD) in de aanwezigheid van aluminium, is in alle gevallen de vorming van primaire eenheden op nanometer schaal gevonden. De schaling tussen de grootte van de primaire eenheden en de dimensie van de eenheidscel van de gevormde kristalstructuur, is een sterke aanwijzing dat de waargenomen intermediären daadwerkelijk specifiek zijn voor de gevormde zeolieten. Dit wordt bevestigd door de waarneming van primaire eenheden van dezelfde grootte tijdens de synthese van Si-MFI met behulp van vier verschillende structuurbepalende organische moleculen (TPA, 'dimeer' van TPA, 'trimeer' van TPA en trimethylene-bis(N-hexyl, N-methyl-piperidinium)). Bovendien waren tijdens de kristallisatie van Si-BEA en Si-MTW met behulp van hetzelfde organisch molecuul primaire deeltjes aanwezig met verschillende grootte. De resultaten laten zien dat het voorgestelde mechanisme geldig is voor zeolietkristallisaties met behulp van een organisch molecuul onder een breed scala aan omstandigheden.

Concluderend: voor het eerst zijn nanometer-schaal intermediären tijdens de synthese van zeolieten geïdentificeerd, en is hun vorming en omzetting gevolgd tijdens de gehele duur van het kristallisatieproces door metingen over een breed gebied van lengteschalen. Gebaseerd op een grote variatie aan zeolietkristallisaties is een zelforganisatiemechanisme voorgesteld met de achtereenvolgende vorming van organisatie op kleine (primaire eenheden), grotere (kiemen) en macroscopische schaal (kristallen). Dit mechanisme is waarschijnlijk algemeen voor kristallisatie van zeolieten met behulp van een organisch structuur-bepalend molecuul.

Publications

De Moor, P.-P.E.A., Beelen, T.P.M., Komanschek, B.U., Beck, L.W., Davis, M.E., Van Santen, R.A., Imaging the Assembly Process of the Organic-Mediated Synthesis of a Zeolite, Submitted for publication to *Chemistry - A European Journal*.

De Moor, P.-P.E.A., Beelen, T.P.M., Van Santen, R.A., Si-MFI nucleation and growth mechanisms studied with small-angle X-ray scattering, submitted for publication in proceedings of 12th International Zeolite Conference, Baltimore, July 1998

De Moor, P.-P.E.A., Beelen, T.P.M., Van Santen, R.A., *In situ* observation of nucleation and crystal growth in zeolite synthesis. A small-angle X-ray scattering investigation on Si-TPA-MFI, submitted for publication in *J. Phys. Chem. B*.

De Moor, P.-P.E.A., Beelen, T.P.M., Van Santen, R.A., Tsuji, K., Davis, M.E., SAXS investigation on nanometer scaled precursors in organic mediated zeolite crystallization from gelating systems, Submitted for publication in *Chemistry of Materials*

De Moor, P.-P.E.A., Beelen, T.P.M., Komanschek, B.U., Van Santen, R.A., *Microporous and Mesoporous Materials*, in press, 1998

P.-P.E.A. de Moor, T.P.M. Beelen, R.A. van Santen, O. Diat, Imaging the assembly process of organic-mediated zeolite crystallization, submitted for publication as Scientific Highlight in ESRF Newsletter, 1998

P.-P.E.A. de Moor, T.P.M. Beelen, R.A. van Santen, B.U. Komanschek, E. Pantos, Imaging the Assembly Process of hybrid organic/inorganic molecular sieves, submitted for publication as Science Highlight in Daresbury Annual Report and Scientific Reports, 1998

De Moor, P.-P.E.A., Beelen, T.P.M., Komanschek, B.U., Diat, O., Van Santen, R.A. *In situ* investigation of Si-TPA-MFI crystallization using (ultra)-small and wide-angle X-ray scattering, *J. Phys. Chem. B*, **101** (1997) 11077-11086

De Moor, P.-P.E.A., Beelen, T.P.M., Van Santen, R.A., Influence of aging and dilution on the crystallization of silicalite-1, *J. Appl. Cryst.*, **30** (1997) 675-679

Diat, O., Bösecke, P., Lambard, J., De Moor, P.-P.E.A., High-angular-resolution camera coupled with an undulator source at the European Synchrotron Radiation Facility High-Brightness Beamline, *J. Appl. Cryst.*, **30** (1997) 862-866

De Moor, P.-P.E.A., Beelen, T.P.M., Van Santen, R.A., SAXS/WAXS study on the formation of precursors and crystallization of silicalite, *Microporous Mater.*, **9** (1997) 117-130

De Moor, P.-P.E.A., Beelen, T.P.M., Van Santen, R.A., Komanschek, B.U., An *in situ* X-ray study of the crystallization of silicalite, Daresbury Annual Report and Scientific Reports 1996-97, 255

Beelen, T.P.M., De Moor, P.-P.E.A., Van Santen, R.A., The influence of reaction parameters on the crystallization of silicalite. An in situ SAXS-WAXS study, Daresbury Annual Report, 1995/1996, 75-76

Beelen, T.P.M., De Moor, P.-P.E.A., Van Santen, R.A., Time-resolved SAXS-WAXS investigations on the crystallization of zeolites, Daresbury Annual Report, 1995/1996, 77

Acknowledgement

The results of this project, as described in this thesis, could never have been obtained without the help and support of many people. The excellent framework in which I could do this research was created by my direct supervisors. Rutger and Theo, thank you very much for the many, stimulating discussions, your good ideas, your critical filter of my ideas, and the continuous support. Also your pragmatic approach was very helpful in solving many experimental and logistic problems. Thank you for giving me as much freedom in my work as I wanted, but at the same time always being present to help. I also thank both of you for the high degree of geographic freedom. During my travels I made new contacts, resulting in many useful ideas, collaborations, and new friends.

Many aspects of my work involved collaborations with organisations all over the world. The insight in the mechanism of organic-mediated zeolite crystallization as described in this thesis, would never have been obtained without the contribution of the group of Mark Davis. Mark, the invaluable discussions we had were essential in understanding the correlation between my results and those obtained by complementary techniques. Thank you also for introducing me to your fellow workers, who gave a substantial experimental support. Larry Beck and Katsuyuki Tsuji, thank you very much for preparing the structure directing agents, and testing many zeolite crystallizations, often under time pressure. I am indebted to Paul Wagner, for taking state of the art transmission electron microscopy images of my samples. Patrick Piccione, thank you very much for providing the IR spectra of the extracted synthesis mixtures.

Important support was provided by prof. Wilfried Mortier, Machteld Mertens, and the late Hans Verduijn, from Exxon Chemical. Thank you for proposing many new ideas and recipes, and your hospitality for testing syntheses. I thank all other fellow workers at Exxon in Machelen for critically evaluating my data and interpretation during my presentations in your laboratory.

I thank prof. Haydn Chen and UOP for the interest they showed in our sample cells. Bob Broach, thank you for the lively discussions, which were not limited to the scattering experiments but also involved other serious subjects of common interest like guitar music and brewing beer.

Electron microscopy proved to be an informative complementary technique for the X-ray scattering experiments. I am indebted to Patricia Kooyman of the national centre for high resolution transmission electron microscopy in Delft for taking images of the many samples I produced. Prof. Tatsuya Okubo, thank you very much for taking the field-emission scanning electron micrographs and your hospitality in Tokyo. I thank Peter Frederik and Paul Bomans for their efforts to image the aqueous synthesis mixtures with transmission electron microscopy under cryogenic conditions.

All the X-ray scattering experiments were performed at the Synchrotron Radiation Source in Daresbury (United Kingdom), and the European Synchrotron Radiation Facility in Grenoble (France) under European Union and EPSRC grants. At this point I would like to acknowledge the use of beamtime. I thank Ernie Komanschek, Peter Bösecke, and Olivier Diat for setting up the X-ray scattering equipment and the excellent help with all synchrotron related problems. I thank Manolis Pantos for the stimulating discussions on the interpretation of the scattering patterns.

The organisation of the work at the synchrotrons makes it impossible to run all experiments by yourself. With this I had a lot of help from colleagues. Theo Beelen, Simon Krijnen, Willy van Well, Mark Vorstenbosch, Engel Vrieling, Ernie Komanschek, Barbara Mojet, and Fulya Gümüşburun, thank you very much!!

Special thanks are for Wout van Herpen, who had a big hand in developing the experimentally perfect and also commercially interesting sample cells. I acknowledge Jos van Wolput for the fast action in the IR experiments. I thank Mart Mennen for solving the sometimes awkward work station related problems with a big smile. Hardcopies of my posters and transparencies for presentations were made by Anja Huijgen, thank you. Furthermore I would like to express my appreciation to all colleagues who served me with sometimes very welcome distraction from the work in the form of coffee, lunch, and, last but not least, beers!!

Finally, I want to thank my father and mother for the unconditional support they always gave me. Fulya, I thank you for being the sunflower in my life, and being patient during the long periods of my absence.

Curriculum Vitae

Peter-Paul Eugène Andrea de Moor was born on January 31st, 1970, in Hulst, The Netherlands. In 1982 he started his secondary school at the Jansenius Scholengemeenschap in Hulst, where he got his Atheneum B diploma in 1988. Subsequently he started his study in Chemical Engineering at Eindhoven University of Technology. In 1993 he did a traineeship with DSM-Resins in Zwolle, The Netherlands. His final project he did in 1994 at the laboratory of chemical engineering, where he modelled two phase flow in a spray drier with Computational Fluid Dynamics. He received his engineer diploma in October 1994. From October 1994 until February 1995 he worked as a consultant for laboratory of chemical engineering at Eindhoven University of Technology on the implementation of drying and thermal degradation kinetics in the modelling two phase flow in spray driers using Computational Fluid Dynamics. On February 15th 1995 he started a research project to prepare his PhD thesis in the laboratory of Inorganic Chemistry and Catalysis at Eindhoven University. Under supervision of prof.dr. R.A. van Santen and dr. T.P.M. Beelen investigations were performed on the organic-mediated assembly of zeolites. The most important results are described in this thesis and in several publications.

